

---

# Interactions-induced dephasing in AC-driven disordered normal metals

Martin Schäffer

---



Munich, 2012



---

# Interactions-induced dephasing in AC-driven disordered normal metals

Martin Schäffer

---

Master Thesis  
Faculty of Physics  
Ludwig-Maximilians-Universität  
Munich

submitted by  
Martin Schäffer  
Darmstadt

under the supervision of  
Prof. Jan von Delft/ Dr. Oleg Yevtushenko

Munich, May 4th 2012



# Contents

<b>Introduction and structure</b>	<b>xi</b>
<b>1 Quantum transport in weakly disordered metals</b>	<b>1</b>
1.1 Electron propagation in weakly disordered metals . . . . .	1
1.1.1 Weak disorder limit . . . . .	2
1.1.2 Diffusive regime . . . . .	2
1.1.3 Scattering sequences and amplitudes . . . . .	3
1.1.4 Disorder average . . . . .	4
1.1.5 Quantum crossings and loop-expansion . . . . .	4
1.2 Quantum diffusion in disordered systems . . . . .	6
1.2.1 Disorder and impurity model . . . . .	7
1.2.2 Drude-Boltzmann approximation . . . . .	7
1.2.3 Diffusion ladder summation . . . . .	9
1.2.4 Cooperon ladder summation . . . . .	10
<b>2 Keldysh diagrammatic perturbation theory</b>	<b>13</b>
2.1 Green's functions . . . . .	13
2.2 Contour-ordered Green's function . . . . .	14
2.2.1 Matrix structure . . . . .	14
2.2.2 Keldysh formalism for scalar fields . . . . .	15
2.2.3 Particle-particle interactions . . . . .	16
2.2.4 Upper-triangular representation . . . . .	17
2.2.5 Feynman rules in upper-triangular basis . . . . .	19
2.3 Discussion on instructive interaction diagrams . . . . .	20
2.3.1 Self-energy type diagram . . . . .	20
2.3.2 Vertex type diagram . . . . .	22
<b>3 Disorder-averaged AC-conductivity of disordered normal metals</b>	<b>25</b>
3.1 AC-conductivity of normal metals . . . . .	25
3.1.1 Quantum-mechanical current operator in spatial representation . . . . .	25
3.1.2 Current expectation value . . . . .	26
3.1.3 Linear response and Keldysh technique . . . . .	27
3.2 Disorder averaged conductivity . . . . .	29

3.2.1	Drude limit . . . . .	29
3.2.2	Weak localization . . . . .	30
<b>4</b>	<b>Bethe-Salpeter equation for interacting Cooperon</b>	<b>33</b>
4.1	Bethe-Salpeter equation for the Cooperon . . . . .	33
4.1.1	Bethe-Salpeter equation . . . . .	33
4.1.2	Interaction propagators . . . . .	34
4.1.3	Cooperon self-energy . . . . .	35
4.2	Linearization of Bethe-Salpeter equation . . . . .	35
4.2.1	Linearization . . . . .	35
4.2.2	First-order diagrams . . . . .	36
4.2.3	Linearized version of the Bethe-Salpeter equation . . . . .	40
4.2.4	SEO-approximation and Dyson summation . . . . .	40
4.2.5	Neglect of vertex terms and infrared divergence . . . . .	41
4.3	Cooperon self-energy in SEO-approximation . . . . .	42
4.3.1	Electronic energy averaging . . . . .	43
4.3.2	Energy-averaged dephasing rate . . . . .	44
4.3.3	Energy-averaged spectrum . . . . .	45
4.3.4	Self-consistent infrared cut-off treatment . . . . .	46
<b>5</b>	<b>Dephasing in large system-size limit</b>	<b>47</b>
5.1	Large system-size limit and regimes . . . . .	47
5.1.1	Quasi-infinite limit . . . . .	47
5.1.2	Energy scales and regimes . . . . .	47
5.2	Calculation of the dephasing rate . . . . .	48
5.2.1	Prerequisites . . . . .	48
5.2.2	Dephasing in the high-temperature regime . . . . .	49
5.2.3	Dephasing in the AC-regime $\omega \gg T$ . . . . .	52
<b>6</b>	<b>Discussion of the results</b>	<b>55</b>
6.1	The high-temperature regime $\omega \ll 1/\tau_\phi \ll T$ . . . . .	55
6.1.1	Quasi-one-dimensional systems . . . . .	55
6.1.2	Quasi-two-dimensional systems . . . . .	56
6.1.3	Quasi-three-dimensional systems . . . . .	56
6.1.4	Conclusion . . . . .	58
6.2	The high-temperature regime $1/\tau_\phi \ll \omega \ll T$ . . . . .	58
6.2.1	Quasi-one-dimensional systems . . . . .	59
6.2.2	Quasi-two-dimensional case . . . . .	60
6.2.3	Quasi-three-dimensional case . . . . .	60
6.2.4	Conclusion . . . . .	60
6.3	The AC regime $1/\tau_\phi \ll T \ll \omega$ . . . . .	62
6.3.1	Quasi-one-dimensional systems . . . . .	62
6.3.2	Quasi-two-dimensional systems . . . . .	62

---

6.3.3	Quasi-three-dimensional systems . . . . .	63
6.3.4	Conclusion . . . . .	63
<b>Conclusion</b>		<b>65</b>
<b>A Diagrammatic disorder average</b>		<b>67</b>
A.1	Self-energy . . . . .	68
A.2	Density of states and convenient definitions . . . . .	69
A.3	Transport time . . . . .	70
<b>B Time evolution in Quantum mechanics</b>		<b>71</b>
B.1	General remarks . . . . .	71
B.2	Schrödinger representation . . . . .	71
B.3	Heisenberg representation . . . . .	72
B.4	Interaction representation . . . . .	73
<b>C Derivation of the conductivity</b>		<b>75</b>
C.1	Fourier transform of the electric current . . . . .	75
C.2	Cancellation of the diamagnetic term . . . . .	76
<b>D Electron energy averaging</b>		<b>79</b>
<b>E Useful integrals</b>		<b>81</b>
<b>F Integration over internal momenta in infinite system size approximation</b>		<b>83</b>
<b>G Asymptotic analysis in the high-temperature regime</b>		<b>85</b>
<b>H Hikami calculus</b>		<b>87</b>
<b>Acknowledgements</b>		<b>91</b>
<b>Statutory declaration</b>		<b>92</b>



# List of Figures

1.1	Illustration of a disordered system. . . . .	1
1.2	Scattering sequences in disordered systems. . . . .	3
1.3	a) Pairing of arbitrary paths. b) Classical diffusion. c) One-loop contribution. . . . .	5
1.4	Drude-Boltzmann contribution. . . . .	7
1.5	Diffusion ladder. . . . .	9
1.6	Maximally crossed diagram. . . . .	10
1.7	Diagrammatic definition of the cooperon. $\mathbf{Q} = \mathbf{k} + \mathbf{k}'$ . . . . .	11
2.1	Definition of contour-ordering. . . . .	14
2.2	Expansion of $G_C$ in powers of $W$ . . . . .	15
2.3	First-order contribution to particle-particle interaction. . . . .	16
2.4	Feynman rules in Keldysh space for upper-triangular representation. . . . .	19
2.5	a) self-energy type diagram. b) vertex type diagram. . . . .	20
2.6	Propagator combinations contributing to self-energy type diagrams. . . . .	22
2.7	Propagator combinations contributing to vertex type diagrams. . . . .	23
3.1	Classical conductivity diagram. . . . .	30
3.2	Weak localization correction to the AC-conductivity. $\mathbf{Q} = \mathbf{k} + \mathbf{k}'$ . . . . .	31
4.1	Bethe-Salpeter equation for the Cooperon. . . . .	34
4.2	Self-energy vs. vertex type diagrams. . . . .	36
4.3	Diagrams contributing to the bare self-energy. . . . .	38
4.4	Ingredients of self-energy diagrams. . . . .	39
4.5	Spectrum $W(T, \omega, \bar{\omega})$ . . . . .	46
5.1	Phase diagram for the dephasing rate $1/\tau_\phi$ as a function of $(\omega, T)$ . . . . .	48
6.1	$\omega(T)_{r=1}$ . $g_1 = 50$ . . . . .	56
6.2	$\tau_\phi$ in quasi-1d systems. $\omega \ll 1/\tau_\phi \ll T$ . $g_1 = 50$ . . . . .	57
6.3	$\tau_\phi$ in quasi-2d systems. $\omega \ll 1/\tau_\phi \ll T$ . $g_2 = 50$ . . . . .	57
6.4	$\tau_\phi$ in quasi-3d systems. $\omega \ll 1/\tau_\phi \ll T$ . $g_3 = 50$ . . . . .	58
6.5	$\omega_{r=1}(T)$ . $g_1 = 50$ . . . . .	59
6.6	$\tau_\phi$ in quasi-1d systems. $1/\tau_\phi \ll \omega \ll T$ . $g_1 = 100$ . . . . .	60
6.7	$\tau_\phi$ in quasi-2d systems. $1/\tau_\phi \ll \omega \ll T$ . $g_2 = 100$ . . . . .	61

---

6.8	$\tau_\phi$ in quasi-3d systems. $1/\tau_\phi \ll \omega \ll T$ . $g_3 = 100$ . . . . .	61
6.9	$\tau_\phi$ in quasi-1d systems. $1/\tau_\phi \ll T \ll \omega$ . $g_3 = 100$ . . . . .	63
6.10	$\tau_\phi$ in quasi-2d systems. $1/\tau_\phi \ll T \ll \omega$ . $g_3 = 100$ . . . . .	64
6.11	$\tau_\phi$ in quasi-3d systems. $1/\tau_\phi \ll T \ll \omega$ . $g_3 = 100$ . . . . .	64
A.1	Green's function before disorder-averaging. . . . .	68
A.2	Green's function after disorder-averaging. . . . .	68
A.3	Self-energy diagrams. . . . .	69
H.1	Definition of the Hikami box. . . . .	87

# Summary

In weakly disordered metals, quantum interference of the electron wave-functions leads to a negative contribution to the conductivity, reducing its classical (Drude) value. In a semi-classical picture, it can be explained by contributions of pairs of coherent, time-reversed electron trajectories propagating through the disorder landscape. This effect is called weak localization and the amplitude of the interfering time-reversed trajectories is described by the so-called Cooperon propagator. At low temperatures, when phonons are frozen out, and in the absence of magnetic fields, electron-electron interactions provide the predominant cause for decoherence in weak localization and determine the temperature dependence of its contribution to the conductivity.

In this thesis, we calculate the so-called dephasing time  $\tau_\phi$ , which is the time scale associated with interactions-induced dephasing, in the presence of a finite external AC-frequency. Extensive studies on  $\tau_\phi$  have been carried out in the past [3, 8, 10, 11]. In particular, diagrammatic methods for the calculation of  $\tau_\phi$  have been developed [11] and its temperature dependence is well-understood in the DC-limit. However, the interplay between interactions and a finite external AC-frequency  $\omega$  has not been studied in detail so far. Here, we will repeat the diagrammatic calculation for the Cooperon in the presence of interactions, developed by Jan von Delft et al. and published in 2007 [11], where the authors set up a Bethe-Salpeter equation for the Cooperon. Due to the complicated structure of this equation, no exact solution has been found. Instead, von Delft et al. solved the linearized (first-order-in-interaction) equation approximately, using an exponential ansatz in the time domain, and found results for  $\tau_\phi$  in effective dimensions  $d = 1, 2, 3$ . Here, we will keep the full dependence on the external frequency in the calculation and stay in the frequency domain for clarity. To this end, we will reduce the linearized Bethe-Salpeter equation to a Dyson equation, which is accomplished by omitting a subset of the self-energy diagrams, the so-called vertex type diagrams, and solve the self-energy integral self-consistently.

We find closed expressions for  $\tau_\phi(\omega)$  in all dimensions and analyze their asymptotic behavior. Particularly, we identify three regimes, depending on the relative magnitude of  $\omega$  with respect to  $T$  and  $1/\tau_\phi$ . The different scaling of  $\tau_\phi$  in  $T$  and  $\omega$  in these regimes is discussed in detail. A summary of the regimes is given in the conclusion at the end of this thesis.



# Chapter 1

## Quantum transport in weakly disordered metals

In this thesis, we will consider disordered metals. The disorder is due to vacancies, dislocations, substitutional impurities etc., which perturb the periodic atomic lattice and scatter the electrons in the metal. In principle, the impurities can also attract bound states, which we will not discuss. The impurities can be described by adding a random and time-independent potential  $V(\mathbf{x})$  to the Hamiltonian. This disorder potential is described by a distribution functional  $P[V(\mathbf{x})]$ , such that  $P[V(\mathbf{x})]dV(\mathbf{x})$  defines the probability, that the value of the potential at point  $\mathbf{x}$  lies in the range  $dV(\mathbf{x})$ . In Fig.1.1, we depict schematically a particular configuration of impurities. In the following, we will discuss electron propagation in the metal in the presence of weak disorder, where a criterion for weak disorder will be given in the next section.

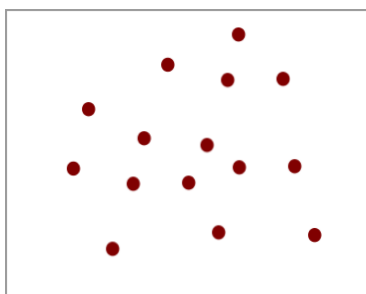


Figure 1.1: Illustration of a disordered system.

### 1.1 Electron propagation in weakly disordered metals

In this section, we will specify the weak disorder limit and introduce the diffusive regime, which defines the time and length scales at which we will work throughout this thesis.

Thereafter, we will give a brief introduction to electron propagation in weakly disordered metals.

### 1.1.1 Weak disorder limit

Disorder in a given metallic sample is called weak, if the mean free path  $l_e$ , the average distance between the locations of subsequent electron-impurity collisions, is much larger than the de-Broglie wavelength  $\lambda$ . We assume that the electron energy  $E$  lies close to the Fermi energy  $E_F$ , and since  $\lambda = 2\pi/k$  with  $k$  the momentum of the electron<sup>1</sup>, a criterion for weak disorder can be given as follows:

$$k_F l_e \gg 1. \quad (1.1)$$

In this limit, it is reasonable to assume that the electron travels ballistically, i.e. on a straight line, between two subsequent collisions. Further, for time-independent disorder potentials  $V(\mathbf{x})$ , the electron-impurity scattering is always elastic. For later use, we introduce the transport time  $\tau$  via  $l_e = v_F \tau$ , where  $v_F$  is the Fermi velocity.  $\tau$  gives the average time between two subsequent collisions.

### 1.1.2 Diffusive regime

The diffusive regime is reached on length scales  $l \gg l_e$ , and hence on time scales  $t \gg \tau$ . It is equivalent to say that we consider only small excitations with momentum and energy  $(\mathbf{q}, \omega)$ :

$$\begin{aligned} \omega \tau &\ll 1 \\ ql_e &\ll 1. \end{aligned} \quad (1.2)$$

In the diffusive regime, the probability  $P(\mathbf{r}, \mathbf{r}', t)$  satisfies a diffusion equation:

$$\left( \frac{\partial}{\partial t} - D \Delta_{\mathbf{r}'} \right) P(\mathbf{r}, \mathbf{r}', t) = \delta(\mathbf{r} - \mathbf{r}') \quad (1.3)$$

with diffusion constant  $D = v_F^2 \tau / d$  and  $d$  the space dimension. For infinite systems, the solution to Eq.(1.3) is of the following form:

$$P(\mathbf{r}, \mathbf{r}', t) \propto \frac{1}{\sqrt{Dt}} e^{-|\mathbf{r} - \mathbf{r}'|^2 / Dt}, \quad (1.4)$$

and corresponds to a Gaussian which spreads out as time evolves. At time  $t$ , the diffusion has covered a distance  $x$  of order  $x \sim \sqrt{Dt}$ . In this work, we neglect finite-size effects. The neglect of the latter is only justified on time scales which are smaller than the typical time

<sup>1</sup>In this thesis throughout, we set  $c = 1, \hbar = 1$ . They can be reinstated by dimensional analysis.

it takes the electron to reach the boundaries of the metal. This time is called Thouless time. For  $d$ -dimensional samples of volume  $L^d$ , it is given as follows:

$$\tau_{\text{th}} = \frac{L^2}{D}. \quad (1.5)$$

In this thesis, we will thus work on time scales satisfying  $\tau \ll t \ll t_{\text{th}}$ , which is equivalent to length scales which obey  $l_e \ll l \ll L$ . On the contrary, on scales much larger than the Thouless time, the particle will have encountered the boundaries many times and in the limit  $t \rightarrow \infty$ , the probability to find the electron at some point in the system becomes uniform throughout the system.

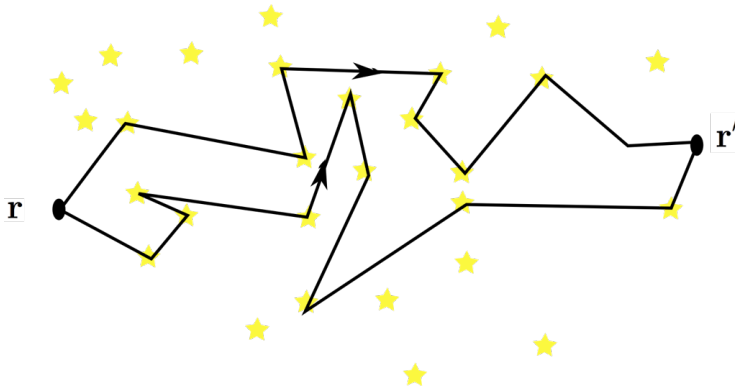


Figure 1.2: Scattering sequences in disordered systems.

### 1.1.3 Scattering sequences and amplitudes

Following the idea of Feynman path integration [16], the probability amplitude for the electron to travel between  $\mathbf{r}$  and  $\mathbf{r}'$  is given by the sum over the amplitudes associated with all possible classical paths which connect those points [17]. Since propagation is assumed ballistic between scattering events, these paths correspond to sequences of impurity collisions. We denote by  $a_j(\mathbf{r}, \mathbf{r}')$  the amplitude associated with the  $j$ th classical path, and schematically show two typical paths in Fig.1.2. The total probability is the square modulus of the sum over all  $a_j(\mathbf{r}, \mathbf{r}')$ :

$$P(\mathbf{r}, \mathbf{r}') = \left| \sum_j a_j(\mathbf{r}, \mathbf{r}') \right|^2, \quad (1.6)$$

We write  $a_j(\mathbf{r}, \mathbf{r}') = |a_j(\mathbf{r}, \mathbf{r}')| e^{i\delta_j}$ . The meaning of the phase  $\delta_j$  is specified as follows: We assume that the electrons travel along straight lines between subsequent collisions. We further assume the collisions to be approximately point-like in space and neglect interactions for the moment. In this limit, the phase  $\delta_j$  can be taken proportional to the length of the

corresponding trajectory. We rewrite Eq.(1.6) as follows:

$$P(\mathbf{r}, \mathbf{r}') = \sum_i |a_i(\mathbf{r}, \mathbf{r}')|^2 + \sum_{i \neq j} |a_j(\mathbf{r}, \mathbf{r}')| |a_i(\mathbf{r}, \mathbf{r}')| e^{i(\delta_i - \delta_j)}. \quad (1.7)$$

This separation is instructive as it explains the difference between classical and quantum contributions to  $P(\mathbf{r}, \mathbf{r}')$ . The first sum on the r.h.s of Eq.(1.7) contains no interference between the trajectories, and hence corresponds to the classical result. On the contrary, the second sum describes mutual interference between the trajectories and hence is inherently quantum-mechanical.

### 1.1.4 Disorder average

In many situations, it is appropriate to consider a disorder average of quantities like the transport probability  $P(\mathbf{r}, \mathbf{r}')$  introduced above. The disorder average corresponds to an average over all possible spatial distributions of the impurities. In general, contributions to  $P(\mathbf{r}, \mathbf{r}')$  from the pairing of arbitrary trajectories, c.f. Fig.1.3a), vanish after disorder average. Since the phase difference associated with the pairing of those trajectories can be very different for different configurations of the impurities, the phase factor averages to zero when averaging over all possible configurations. On the contrary, the phase-independent first sum in Eq.(1.7) survives disorder averaging. This contribution is related to the pairing of identical trajectories, as indicated in Fig.1.3b), and we will call it a classical diffusion, as it corresponds to the classical result for  $P(\mathbf{r}, \mathbf{r}')$ . One might expect, that the second sum in Eq.(1.7) vanishes after disorder averaging, as the terms in this sum depend on the phase differences. However, the sum does not vanish identically. Consider Fig.1.3c). The picture shows a pairing of two trajectories, which form a loop. The trajectories are identical before and after the loop, and traverse the loop in exactly opposite direction. Thus, outside the loop, the phase difference is identically zero. This part obviously corresponds to the contribution in Fig.1.3b), which has already been discussed, and hence we focus on the loop part. Such a loop corresponds to the pairing of closed time-reversed trajectories. For the loop, the phase difference is exactly zero if and only if the system is time-reversal invariant. If time-reversal symmetry holds, the loops thus give a quantum-mechanical correction to the disorder averaged electron propagation probability. They correspond to the so-called Cooperon, and lead to a reduction of the conductivity. The latter effect is called weak localization and will be calculated in Ch.3.

### 1.1.5 Quantum crossings and loop-expansion

In the last subsection, we have seen that pairings of closed time-reversed trajectories(loops) survive disorder averaging if time-reversal symmetry holds. In this subsection, we will give an estimate for the probability of such a loop to occur. The estimate is built on the following consideration: Given a metallic sample of volume  $L^3$ , which is coupled to leads, such that the electron can escape the sample. We ask for the probability  $p_\times$ , that two

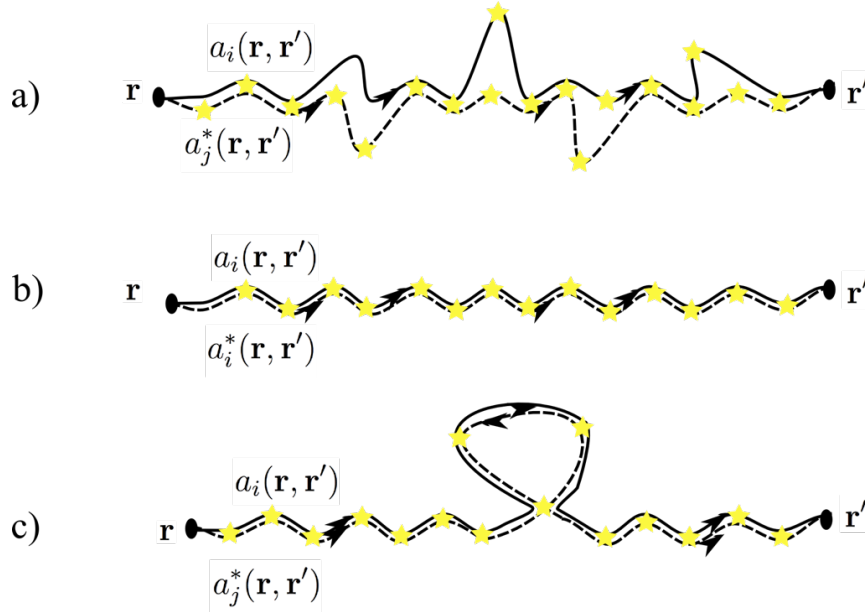


Figure 1.3: a) Pairing of arbitrary paths. b) Classical diffusion. c) One-loop contribution.

diffusions, c.f. Fig.1.3b), intersect. We assign a length  $dl = vdt$  to the diffusion, where  $v$  is the group velocity of the electron wave packets and is of order  $v_F$ . Further, we assign a finite cross section  $A$  to the diffusion, where  $A$  is of order of  $\lambda^2 \propto 1/k_F^2$ . Thus,  $dp_\times$  can be written as follows:

$$dp_\times(t) \sim \frac{A \times dl}{V} \sim \frac{dt}{k_F V}, \quad (1.8)$$

with  $V$  the volume of the system. We have  $V \sim L^3$ . With  $\tau_{\text{th}} = L^2/D$  from Eq.(1.5), Eq.(1.8) leads to:

$$dp_\times(t) \sim \frac{1}{k_F D L} \frac{dt}{\tau_{\text{th}}}. \quad (1.9)$$

Further,  $D = v_F l_e / d$  yields

$$dp_\times(t) \sim \frac{1}{(k_F l_e)(k_F L)} \frac{dt}{\tau_{\text{th}}}. \quad (1.10)$$

The electron escapes from the sample after a time of the order of  $t_{\text{th}}$ . Hence, the crossing can only appear at a time  $t < t_{\text{th}}$ , and to find the probability  $p$ , we should integrate Eq.(1.10) from  $t = 0$  to  $t = \tau_{\text{th}}$ . Hence we find:

$$p_\times \sim \frac{1}{(k_F l_e)(k_F L)}. \quad (1.11)$$

The dimensionless conductance  $g$  is defined in terms of the conductance  $G$  as follows:

$$g = \left( \frac{2\pi}{e^2} \right) G, \quad (1.12)$$

and can be rewritten by use of Ohm's law, for  $d = 3$ : [5, pp.274,275]:

$$g \propto (k_F l_e)(k_F L). \quad (1.13)$$

Hence we obtain from Eq.(1.11)

$$p_\times \sim \frac{1}{g}. \quad (1.14)$$

Normal metals are good conductors,  $g \gg 1$ . Thus, the one-loop contribution depicted in Fig.1.3c) yields a parametrically small correction to the classical diffusion. Further we infer that for  $g \gg 1$ , pairings of trajectories forming two or more loops are negligible and it is sufficiently accurate to include only the one-loop corrections.

## 1.2 Quantum diffusion in disordered systems

We consider electrons in a disordered metal, governed by the following Hamiltonian:

$$H = -\frac{1}{2m}\Delta + V(\mathbf{x}). \quad (1.15)$$

In the following, we will discuss the disorder averaged probability  $\overline{P(\mathbf{r}, \mathbf{r}', \omega)}$ , that an electron of given energy  $\epsilon$  propagates from  $\mathbf{r}$  to  $\mathbf{r}'$ . We assume that the electron can be described by a Gaussian wave packet of width much smaller than  $\omega$ . In this limit,  $\overline{P(\mathbf{r}, \mathbf{r}', \omega)}$  to good accuracy does not depend on the electronic energy [5].  $\overline{P(\mathbf{r}, \mathbf{r}', \omega)}$  can be expressed in terms of retarded and advanced disorder-averaged propagators [5, Eq.4.9]:

$$\overline{P(\mathbf{r}, \mathbf{r}', \omega)} = \frac{1}{2\pi\rho} \overline{G_\epsilon^R(\mathbf{r}, \mathbf{r}')G_{\epsilon-\omega}^A(\mathbf{r}', \mathbf{r})}. \quad (1.16)$$

The Green's functions introduced above are solutions to the following differential equation [5, Eq.3.17]:

$$(\epsilon - H \pm i0)G_\epsilon^{R/A}(\mathbf{r}, \mathbf{r}') = \delta(\mathbf{r}' - \mathbf{r}), \quad (1.17)$$

where  $H$  is given by Eq.(1.15).

### 1.2.1 Disorder and impurity model

In this thesis, we will adopt the following time-independent Gaussian disorder potential [5, Ch.2.2], which is entirely defined by

$$\begin{aligned} \overline{V(\mathbf{x})} &= 0 \\ \overline{V(\mathbf{x})V(\mathbf{x}')} &= \gamma\delta(\mathbf{x} - \mathbf{x}'), \end{aligned} \quad (1.18)$$

all other cumulants of the distribution being zero. Note that all even moments of this model are non-zero. However, in this thesis we consider low impurity concentrations, and we will neglect moments higher than the second. The model describes isotropic scatterers, as it does not depend on the incoming and outgoing momenta. In Eq.(1.18), we have introduced the disorder average  $\overline{(\dots)^2}$  and  $\gamma$ , the measure of strength of a single impurity.

### 1.2.2 Drude-Boltzmann approximation

As a first step towards the calculation of  $\overline{P(\mathbf{r}, \mathbf{r}', \omega)}$ , one neglects correlations between the Green's functions and replaces the average of the product with the product of the averages. This approximation amounts to the pairing of two disorder-averaged propagators and is commonly called the Drude-Boltzmann approximation. It can be interpreted as the pairing of two electron propagators, which scatter off the disorder potential independently. As for all calculations in this section, we work in momentum space, i.e. we find contributions to  $\overline{P(\mathbf{q}, \omega)}$ , which depends only on one momentum, since disorder average is well-known to restore translational symmetry, as shown explicitly in Appendix A. The Drude-Boltzmann contribution is represented by the diagram in Fig.1.4<sup>3</sup>, and is written as follows [5, eq.4.68]:

$$P_0(\mathbf{q}, \omega) = \frac{1}{2\pi\rho V} \sum_{\mathbf{k}} \overline{G}_{\epsilon}^R(\mathbf{k}) \overline{G}_{\epsilon-\omega}^A(\mathbf{k} - \mathbf{q}). \quad (1.19)$$

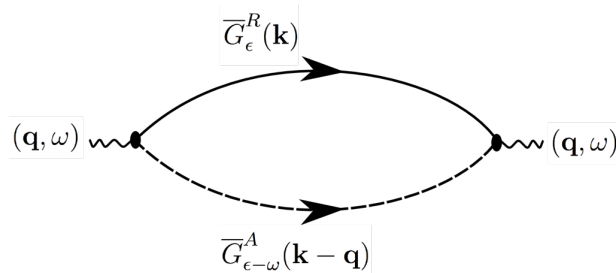


Figure 1.4: Drude-Boltzmann contribution.

<sup>2</sup>It is convenient to perform the disorder average diagrammatically [5], and we will demonstrate this procedure in Appendix A, where we calculate the disorder average of the electronic Green's function.

<sup>3</sup>In this thesis throughout, we will represent retarded/advanced electron propagators by solid/dashed lines.

The disorder-averaged propagators  $\overline{G}_\epsilon^{R/A}(\mathbf{k})$  are calculated in Appendix A, with the following result:

$$\overline{G}_\epsilon^{R/A}(\mathbf{k}) = \frac{1}{\epsilon - \epsilon(\mathbf{k}) \pm \frac{i}{2\tau}}, \quad (1.20)$$

where  $\tau = 1/2\pi\rho\gamma$  is the transport time.  $\tau$  can be interpreted as the finite life-time of momentum eigenstates: An electron changes the direction of its momentum after time  $\tau$ , the average time between two subsequent electron-impurity collisions. Substituting Eq.(1.20) into Eq.(1.19), we find:

$$P_0(\mathbf{q}, \omega) = \frac{1}{2\pi\rho V} \sum_{\mathbf{k}} \frac{1}{\left(\epsilon - \epsilon(\mathbf{k}) + \frac{i}{2\tau}\right)} \frac{1}{\left(\epsilon - \omega - \epsilon(\mathbf{k} - \mathbf{q}) - \frac{i}{2\tau}\right)}. \quad (1.21)$$

In the diffusive regime, we expand  $\epsilon(\mathbf{k} - \mathbf{q}) \approx \epsilon(\mathbf{k}) - \mathbf{v} \cdot \mathbf{q}$ , where  $\mathbf{v} = \nabla_{\mathbf{k}}\epsilon(\mathbf{k})$  is the group velocity of the electronic wave packet. Further we convert the sum over  $\mathbf{k}$  into an integral over  $\epsilon$  via

$$\frac{1}{V} \sum_{\mathbf{k}} g(\mathbf{k}) \rightarrow \int d\xi \rho(\xi) \int d\bar{\omega} g(\bar{\omega}, \xi), \quad (1.22)$$

where  $\bar{\omega}$  is the normalized solid angle.  $\epsilon$  and  $\mathbf{k}$  are related via the dispersion relation, and instead of summing  $g(\mathbf{k})$  over all momentum eigenvectors, we can as well sum over all energies. We need the density of states  $\rho(\epsilon)$  and the solid angle to take into account all momentum states corresponding to a given energy. We obtain the following expression:

$$P_0(\mathbf{q}, \omega) = \frac{1}{2\pi\rho} \iint \rho(\xi) d\xi d\bar{\omega} \frac{1}{\left(\epsilon - \xi + \frac{i}{2\tau}\right)} \frac{1}{\left(\epsilon - \omega - \xi + \mathbf{v} \cdot \mathbf{q} - \frac{i}{2\tau}\right)}. \quad (1.23)$$

We perform the energy integral using the method of residuals, tacitly assuming that the density of states does not vary greatly around  $E_F$ ,  $\rho(\epsilon) \equiv \rho$ . Finally, we find:

$$P_0(\mathbf{q}, \omega) = \tau \int \frac{d\bar{\omega}}{1 - i\omega\tau + i\tau\mathbf{v} \cdot \mathbf{q}}. \quad (1.24)$$

This integral yields in the limit  $\mathbf{q} = 0$  the following result:

$$P_0(0, \omega) = \frac{\tau}{1 - i\omega\tau}, \quad (1.25)$$

which is directly related to the Drude result for AC-conductivity, as we will see in Ch.3. For finite  $\mathbf{q}$ , we obtain in the diffusive regime:

$$P_0(\mathbf{q}, \omega) = \tau \left[ 1 + i\omega\tau - D\mathbf{q}^2\tau + \mathcal{O}((ql_e)^4, (\omega\tau)^2) \right]. \quad (1.26)$$

### 1.2.3 Diffusion ladder summation

In the Drude-Boltzmann approximation, we have paired two independent disorder-averaged propagators. We obtain classical contributions beyond the Drude-Boltzmann approximation, if we take into account pairings of the type in Fig.1.3b), which correspond to the diagrammatic equations displayed in Fig.1.5. The diagrams on the l.h.s. of the first diagrammatic equation are obtained from Fig.1.4 by inserting additional impurity lines to obtain the so-called diffusion ladder [5, pp.97-101]. This ladder corresponds to sequences of independent scattering events. Pictorially, we arrive at the diffusion ladder, if we start from the Drude-Boltzmann approximation and take into account, that the electronic propagators can also scatter off the same impurity simultaneously, and scatter independently of each other before and after this event. Building sequences of such type gives the diffusion ladder. We denote the contribution of the ladder by  $P_d(\mathbf{q}, \omega)$ .

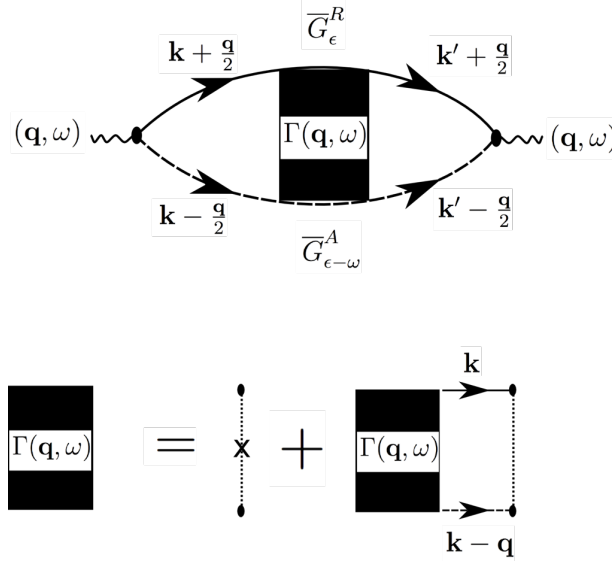


Figure 1.5: Diffusion ladder.

From the upper diagram in Fig.1.5, one infers

$$P_d(\mathbf{q}, \omega) = \frac{1}{2\pi\rho V^2} \sum_{\mathbf{k}, \mathbf{k}'} \bar{G}_\epsilon^R(\mathbf{k} + \frac{\mathbf{q}}{2}) \bar{G}_{\epsilon-\omega}^A(\mathbf{k} - \frac{\mathbf{q}}{2}) \Gamma(\mathbf{q}, \omega) \bar{G}_\epsilon^R(\mathbf{k}' + \frac{\mathbf{q}}{2}) \bar{G}_{\epsilon-\omega}^A(\mathbf{k}' - \frac{\mathbf{q}}{2}). \quad (1.27)$$

and from the iteration for the so-called structure factor  $\Gamma(\mathbf{q}, \omega)$ , which describes the impurity ladder, we have, see the lower diagram of Fig.1.5:

$$\Gamma(\mathbf{q}, \omega) = \gamma + \frac{\gamma}{V} \sum_{\mathbf{k}} \Gamma(\mathbf{q}, \omega) \bar{G}_\epsilon^R(\mathbf{k}) \bar{G}_{\epsilon-\omega}^A(\mathbf{k} - \mathbf{q}), \quad (1.28)$$

which factorizes to give

$$\Gamma(\mathbf{q}, \omega) = \gamma + \frac{\gamma \Gamma(\mathbf{q}, \omega)}{V} \sum_{\mathbf{k}} \bar{G}_\epsilon^R(\mathbf{k}) \bar{G}_{\epsilon-\omega}^A(\mathbf{k} - \mathbf{q}) = \gamma + \frac{\Gamma(\mathbf{q}, \omega)}{\tau} P_0(\mathbf{q}, \omega), \quad (1.29)$$

with  $P_0(\mathbf{q}, \omega)$  given by Eq.(1.19). We solve for the diffusion structure factor  $\Gamma(\mathbf{q}, \omega)$  and obtain:

$$\Gamma(\mathbf{q}, \omega) = \frac{\gamma}{1 - P_0(\mathbf{q}, \omega)/\tau}. \quad (1.30)$$

In Eq.(1.27), the structure factor also factorizes:

$$P_d(\mathbf{q}, \omega) = \frac{\Gamma_\omega(\mathbf{q}, \omega)}{2\pi\rho V^2} \sum_{\mathbf{k}, \mathbf{k}'} \bar{G}_\epsilon^R(\mathbf{k} + \frac{\mathbf{q}}{2}) \bar{G}_{\epsilon-\omega}^A(\mathbf{k} - \frac{\mathbf{q}}{2}) \bar{G}_\epsilon^R(\mathbf{k}' + \frac{\mathbf{q}}{2}) \bar{G}_{\epsilon-\omega}^A(\mathbf{k}' - \frac{\mathbf{q}}{2}). \quad (1.31)$$

which, by using Eq.(1.19), yields:

$$P_d(\mathbf{q}, \omega) = 2\pi\rho P_0(\mathbf{q}, \omega)^2 \Gamma(\mathbf{q}, \omega). \quad (1.32)$$

Together with Eq.(1.30), we find

$$P_d(\mathbf{q}, \omega) = P_0(\mathbf{q}, \omega) \frac{P_0(\mathbf{q}, \omega)}{\tau - P_0(\mathbf{q}, \omega)}. \quad (1.33)$$

In the diffusive limit, we use Eq.(1.26) and find the final result:

$$P_d(\mathbf{q}, \omega) = \frac{1}{-i\omega + D\mathbf{q}^2}. \quad (1.34)$$

We explicitly give the structure factor in the diffusive limit. From Eq.(1.30), we find

$$\Gamma(\mathbf{q}, \omega) = \frac{1}{2\pi\rho\tau^2} \frac{1}{-i\omega + D\mathbf{q}^2}. \quad (1.35)$$

It is easy to check that  $\Gamma(\mathbf{q}, \omega)$  solves the diffusion equation, c.f. Eq.(1.3).

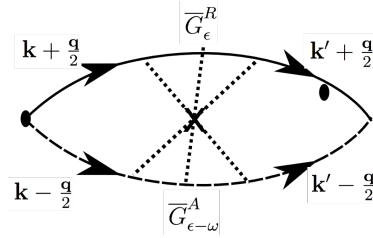


Figure 1.6: Maximally crossed diagram.

### 1.2.4 Cooperon ladder summation

In this subsection, we review the calculation of the leading quantum correction to  $\overline{P(\mathbf{q}, \omega)}$ . From Sec.1.1.5, we know that it should arise from diagrams which contain one loop. These loop diagrams correspond to the class of maximally crossed diagrams [12], one example

of the latter being depicted in Fig.1.6. To see this correspondence, reverse the advanced electron line of this exemplaric diagram, i.e. twist it to entangle the impurity lines. From this procedure we infer that the sum over all maximally crossed diagrams can be presented as in Fig.1.7, exhibiting a ladder structure similar to the diffusion, with the important difference, that the structure factor  $\Gamma'(\mathbf{Q}, \omega)$  depends on the sum of the incoming wave vectors,  $\mathbf{Q} = \mathbf{k} + \mathbf{k}'$ , rather than on their difference. The contribution from the maximally crossed diagrams is called Cooperon.

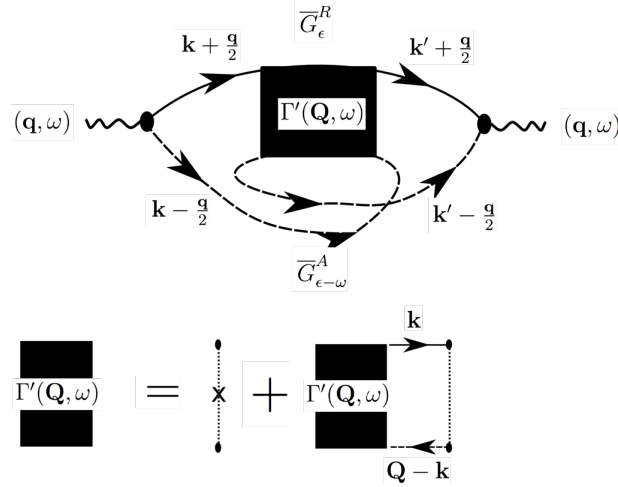


Figure 1.7: Diagrammatic definition of the cooperon.  $\mathbf{Q} = \mathbf{k} + \mathbf{k}'$ .

The Cooperon contribution to the propagation probability, denoted  $P_c(\mathbf{q}, \omega)$ , is calculated in a way similar to the diffusion:

$$P_c(\mathbf{q}, \omega) = \frac{1}{2\pi\rho V^2} \sum_{\mathbf{k}, \mathbf{k}'} \bar{G}_\epsilon^R(\mathbf{k} + \frac{\mathbf{q}}{2}) \bar{G}_{\epsilon-\omega}^A(\mathbf{k} - \frac{\mathbf{q}}{2}) \Gamma'(\mathbf{k} + \mathbf{k}', \omega) \bar{G}_\epsilon^R(\mathbf{k}' + \frac{\mathbf{q}}{2}) \bar{G}_{\epsilon-\omega}^A(\mathbf{k}' - \frac{\mathbf{q}}{2}), \quad (1.36)$$

which can be rewritten by the transformation  $\mathbf{k}' = \mathbf{Q} - \mathbf{k}$ :

$$P_c(\mathbf{q}, \omega) = \frac{1}{2\pi\rho V^2} \sum_{\mathbf{k}, \mathbf{Q}} \bar{G}_\epsilon^R(\mathbf{k} + \frac{\mathbf{q}}{2}) \bar{G}_{\epsilon-\omega}^A(\mathbf{k} - \frac{\mathbf{q}}{2}) \Gamma'(\mathbf{Q}, \omega) \bar{G}_\epsilon^R(\mathbf{Q} - \mathbf{k} + \frac{\mathbf{q}}{2}) \bar{G}_{\epsilon-\omega}^A(\mathbf{Q} - \mathbf{k} - \frac{\mathbf{q}}{2}). \quad (1.37)$$

The Cooperon structure factor  $\Gamma'(\mathbf{q}, \omega)$  obeys:

$$\Gamma'(\mathbf{Q}, \omega) = \gamma + \frac{\gamma}{V} \sum_{\mathbf{k}} \Gamma'(\mathbf{Q}, \omega) \bar{G}_\epsilon^R(\mathbf{k}) \bar{G}_{\epsilon-\omega}^A(\mathbf{Q} - \mathbf{k}). \quad (1.38)$$

We assume  $\bar{G}(\mathbf{Q} - \mathbf{k}) = \bar{G}(\mathbf{k} - \mathbf{Q})$ , which is true for isotropic dispersion relations. We can use Eq.(1.19) again to find

$$\Gamma'(\mathbf{Q}, \omega) = \frac{\gamma}{1 - P_0(\mathbf{Q}, \omega)/\tau}, \quad (1.39)$$

which simplifies in the diffusive limit, c.f. Eq.(1.26), to give:

$$\Gamma'(\mathbf{Q}, \omega) = \frac{1}{2\pi\rho\tau^2} \frac{1}{-i\omega + D\mathbf{Q}^2}, \quad (1.40)$$

Next, consider Eq.(1.37). In the diffusive limit, we neglect the dependence on  $(\mathbf{q}, \omega)$  in the Green's function, which would give only subleading contributions, c.f. Eq.(1.2). Further, due to the peaked structure of  $\Gamma_{\mathbf{Q}}(\omega)$  for  $\mathbf{Q} \rightarrow 0$ , we also neglect the  $\mathbf{Q}$ -dependence in the Green's functions and obtain:

$$P_c(\mathbf{q}, \omega) = \frac{1}{2\pi\rho V^2} \sum_{\mathbf{k}} [\bar{G}_\epsilon^R(\mathbf{k}) \bar{G}_\epsilon^A(\mathbf{k})]^2 \sum_{\mathbf{Q}} \frac{1}{-i\omega + D\mathbf{Q}^2}. \quad (1.41)$$

In Eq.(1.41), the sum over  $\mathbf{k}$  is calculated to give  $4\pi\rho\tau^3$  [5, Eq.3.107], and hence we obtain

$$P_c(\mathbf{q}, \omega) = \frac{\tau}{\pi\rho V} \sum_{\mathbf{Q}} \frac{1}{-i\omega + D\mathbf{Q}^2}. \quad (1.42)$$

For later use, we define

$$\Gamma_{\mathbf{Q}}^0(\omega) = \frac{1}{2\pi\rho\tau^2} \frac{1}{D\mathbf{Q}^2 - i\omega}. \quad (1.43)$$

$P_c(\mathbf{q}, \omega)$  does not depend on  $\mathbf{q}$ , hence the Cooperon is a short-ranged object. In real space,  $P_C(\mathbf{r}, \mathbf{r}') \sim \delta(\mathbf{r} - \mathbf{r}')$ . The Cooperon is built of pairs of time-reversed trajectories. If time-reversal symmetry is broken, which is accomplished by magnetic fields or electron interactions, the contribution from the Cooperon vanishes.

# Chapter 2

## Keldysh diagrammatic perturbation theory

In this thesis, we want to calculate the Cooperon self-energy due to Coulomb interactions in the presence of an external AC-frequency at finite temperature. To this end, we will use Keldysh perturbation theory, which is tailored for finite temperature situations, and for which a diagrammatic framework exists which we will work with. In this chapter, we will give a brief summary of Keldysh diagrammatic perturbation theory for the electronic Green's function in thermal equilibrium.

### 2.1 Green's functions

In the following sections, we will see that many observables, such as the electric conductivity, can be expressed in terms of the following object:

$$G^<(\mathbf{x}t, \mathbf{x}'t') = i \left\langle \hat{\Psi}^\dagger(\mathbf{x}', t') \hat{\Psi}(\mathbf{x}, t) \right\rangle, \quad (2.1)$$

which is usually called a "lesser" Green's function and defines thermal average of correlations between the quantum field operators in Heisenberg representation<sup>1</sup>,  $\hat{\Psi}^\dagger(\mathbf{x}', t')$  and  $\hat{\Psi}(\mathbf{x}, t)$ . It is convenient to define also the "greater" Green's function:

$$G^>(\mathbf{x}t, \mathbf{x}'t') = -i \left\langle \hat{\Psi}(\mathbf{x}, t) \hat{\Psi}^\dagger(\mathbf{x}', t') \right\rangle. \quad (2.2)$$

Retarded and advanced propagators can be defined in terms of  $G^<(\mathbf{x}t, \mathbf{x}'t')$  and  $G^>(\mathbf{x}t, \mathbf{x}'t')$  as follows:

$$\begin{aligned} G^R(\mathbf{x}t, \mathbf{x}'t') &= +i\theta(t-t') [G^>(\mathbf{x}t, \mathbf{x}'t') - G^<(\mathbf{x}t, \mathbf{x}'t')] , \\ G^A(\mathbf{x}t, \mathbf{x}'t') &= -i\theta(t'-t) [G^>(\mathbf{x}t, \mathbf{x}'t') - G^<(\mathbf{x}t, \mathbf{x}'t')] . \end{aligned} \quad (2.3)$$

The Green's functions introduced in this section will be heavily used in what follows.

---

<sup>1</sup>C.f. Appendix B.

## 2.2 Contour-ordered Green's function

The Keldysh formalism can be developed from the so-called contour-ordered Green's function,  $G_C$  which is defined as follows [1, 9]:

$$G_C(\mathbf{x}t, \mathbf{x}'t') = -i \langle \mathbf{T}_C \Psi(\mathbf{x}, t) \Psi^\dagger(\mathbf{x}', t') \rangle . \quad (2.4)$$

$G_C$  corresponds to a thermal average of the contour-ordered product of field operators. The contour  $C$  is defined to run from  $-\infty$  to  $+\infty$  back to  $-\infty$  and is depicted in Fig.2.1 below, together with the definition of the action of the contour-ordering  $\mathbf{T}_C$ . Note that  $t, t'$  are not real time arguments, but rather lie on the contour. The action of the contour ordering is such that  $\Psi(\mathbf{x}, t)$  is placed to the left/right of  $\Psi^\dagger(\mathbf{x}', t')$ , if  $t$  comes later/earlier on  $C$  than  $t'$ . The contour-ordering leads to a more complicated structure of the Green's function, compared to zero-temperature theory, where the field operators are ordered in real time. However,  $G_C$  can be expanded into its Feynman diagrams, as in zero-temperature theory [9]. In particular, it is possible to rewrite the contour-ordered propagator  $G_C$  in terms of real time-ordering, which we are going to explain next.

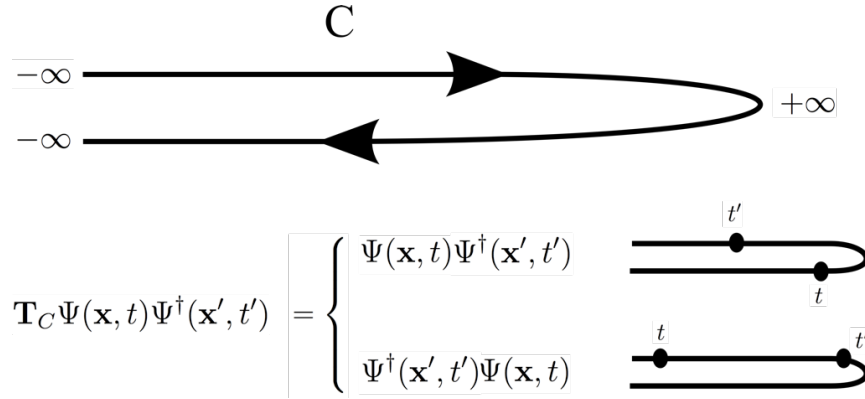


Figure 2.1: Definition of contour-ordering.

### 2.2.1 Matrix structure

Let us divide the contour  $C$  into upper(lower) branch  $C_1(C_2)$ , where  $C_1$  runs from  $-\infty$  to  $+\infty$ , and  $C_2$  runs back again. The time arguments  $t$  and  $t'$  of the Green's function can both either lie on  $C_1$  or  $C_2$ , which gives four possibilities in total.  $G_C(\mathbf{x}t, \mathbf{x}'t')$  can then be represented [9] by the  $2 \times 2$  - matrix  $\hat{G}$ , its components  $G_{ij}$  being associated with these

four possibilities:

$$\begin{aligned}
G_{11}(1, 1') &= -i \langle \mathbf{T} \Psi(1) \Psi^\dagger(1') \rangle, \\
G_{12}(1, 1') &= G^<(1, 1'), \\
G_{21}(1, 1') &= G^>(1, 1'), \\
G_{22}(1, 1') &= -i \langle \bar{\mathbf{T}} \Psi(1) \Psi^\dagger(1') \rangle,
\end{aligned} \tag{2.5}$$

where  $(j)$  is short for  $(\mathbf{x}_j, t_j)$ . The first/second index of  $\hat{G}$  is equal to 1 or 2, if the first/second time argument of  $G_C$  lies on  $C_1$  or  $C_2$ , respectively. The space of the matrices  $\hat{G}$  is called Keldysh space. In the following, we derive the Feynman rules for Keldysh diagrammatic perturbation theory, for scalar fields and particle-particle interactions.

### 2.2.2 Keldysh formalism for scalar fields

We consider a scalar field  $W(\mathbf{x}, t)$ . A generic diagrammatic expansion for the contour-ordered Green's function  $G_C(1, 1')$  in powers of this scalar field is shown in Fig.2.2<sup>2</sup>, and we will derive the rules for the coupling of particles to  $W(\mathbf{x}, t)$  from the second diagram on the right hand side of the diagrammatic equation, which corresponds to the first correction  $G_C^1(1, 1')$  to the free propagator  $G_C^0(1, 1')$ .

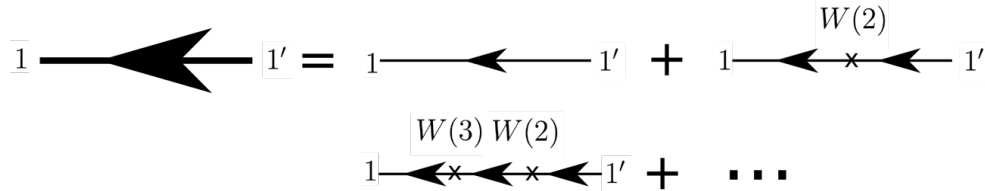


Figure 2.2: Expansion of  $G_C$  in powers of  $W$ .

This diagram represents a single scattering of a particle off the scalar potential and corresponds to the expression

$$\hat{G}_C^1(1, 1') = \int d\mathbf{x}_2 \int_C d\tau_2 \hat{G}_C^0(1, 2) W(2) \hat{G}_C^0(2, 1'). \tag{2.6}$$

$\hat{G}_C^1(1, 1')$  can be expressed in terms of an integration along the real axis in real time, rather than along the contour  $C$ . To this end, we divide the contour integration into two integrations, where the first goes along  $C_1$  and the second along  $C_2$ . We then use the definition of  $C_1$  and  $C_2$  and the notation of Eq.(2.5) to derive from Eq.(2.6) the following expressions

<sup>2</sup>In this chapter, we closely follow the steps in [9], where the Green's functions are defined to point from right to left, opposite to the electronic Green's functions in the rest of this thesis.

for the components of  $\hat{G}_C^1(1, 1')$ :

$$\begin{aligned}
G_{11}^1(1, 1') &= \int d\mathbf{x}_2 \int_{-\infty}^{\infty} dt_2 [G_{11}^0(1, 2)W(2)G_{11}^0(2, 1') - G_{12}^0(1, 2)W(2)G_{21}^0(2, 1')] \\
G_{12}^1(1, 1') &= \int d\mathbf{x}_2 \int_{-\infty}^{\infty} dt_2 [G_{11}^0(1, 2)W(2)G_{12}^0(2, 1') - G_{12}^0(1, 2)W(2)G_{22}^0(2, 1')] \\
G_{21}^1(1, 1') &= \int d\mathbf{x}_2 \int_{-\infty}^{\infty} dt_2 [G_{21}^0(1, 2)W(2)G_{11}^0(2, 1') - G_{22}^0(1, 2)W(2)G_{21}^0(2, 1')] \\
G_{22}^1(1, 1') &= \int d\mathbf{x}_2 \int_{-\infty}^{\infty} dt_2 [G_{21}^0(1, 2)W(2)G_{12}^0(2, 1') - G_{22}^0(1, 2)W(2)G_{22}^0(2, 1')] ,
\end{aligned} \tag{2.7}$$

where we took care of the fact, that contour-ordering is equivalent to anti-time-ordering in real time, if  $t_1$  and  $t'_1$  lie both on  $C_2$ , and where the integration along  $C_2$  was turned into an integration over  $C_1$ , which gives a minus sign. Eqs.(2.7) can be written as follows:

$$G_{ij}^1(1, 1') = \int d\mathbf{x}_2 \int dt_2 W(2)G_{ik}^0(1, 2)\sigma_{kl}^3 G_{lj}^0(2, 1') , \tag{2.8}$$

where  $\sigma^3$  is the 3rd Pauli matrix. Thus, we conclude that in Keldysh space, a scalar field  $W(\mathbf{x}, t)$  is represented by the following  $2 \times 2$ -matrix:

$$W(\mathbf{x}, t)_{ij} \equiv W(\mathbf{x}, t)\sigma_{ij}^3 . \tag{2.9}$$

### 2.2.3 Particle-particle interactions

Particle-particle interactions are mediated by exchange of virtual particles. The Coulomb interaction, which we will consider later in the text, is mediated by bosons, namely virtual photons. We have to define how emission and absorption of the mediators is represented in Keldysh space. Considering the diagram in Fig.2.3, which corresponds to the expansion of Green's function to linear order in the particle-particle interaction. In this thesis throughout, we will draw particle-particle interactions by wavy lines and particle propagators by straight lines.

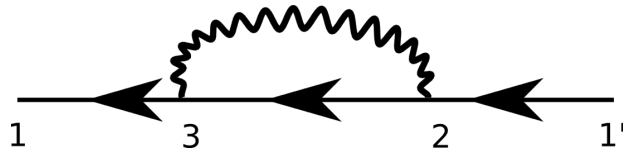


Figure 2.3: First-order contribution to particle-particle interaction.

We denote  $\hat{L}_C^0(i, j)$  the contour-ordered free interaction propagator between  $(\mathbf{x}_j, t_j)$  and  $(\mathbf{x}_i, t_i)$ . The analytic expression equivalent to the diagram in Fig.2.3 is given as follows:

$$\hat{G}_C^1(1, 1') = \int d\mathbf{x}_3 \int_C d\tau_3 \int d\mathbf{x}_2 \int_C d\tau_2 \hat{G}_C^0(1, 3) \hat{G}_C^0(3, 2) \hat{L}_C^0(3, 2) \hat{G}_C^0(2, 1'). \quad (2.10)$$

We repeat similar steps as in the discussion of the scalar fields to find the following expression for  $\hat{G}_C^1(1, 1')$  in terms of an integral over ordinary time:

$$G_{ij}^1(1, 1') = \int d\mathbf{x}_3 \int dt_3 \int d\mathbf{x}_2 \int dt_2 G_{ik}^0(1, 3) \gamma_{kl}^\mu G_{lm}^0(3, 2) L_{\mu\nu}^0(3, 2) \gamma_{mn}^\nu \hat{G}_{nj}^0(3, 1'), \quad (2.11)$$

where  $\hat{\gamma}$  is the vertex tensor which obeys:

$$\gamma_{ij}^\mu = \delta_{ij} \sigma_{j\mu}^3, \quad (2.12)$$

with no summation over  $j$  implied. In this representation, there is no distinction between emission and absorption vortices.

### 2.2.4 Upper-triangular representation

In Keldysh formalism, the Green's function has become a  $2 \times 2$  - matrix in Keldysh space. However, the four components are not linearly independent, as it is straightforward to show that the sum of the diagonal entries equals the sum of the off-diagonal ones. We can transform  $\hat{G}$  to an upper-triangular matrix, denoted by  $\underline{G}$ , to remove part of the redundancy and to simplify later calculations. To this end, we apply to  $\hat{G}$  the following linear transformation:

$$\hat{G}_{ij} \rightarrow \underline{G}_{ij} = M_{ik} \sigma_{kl}^3 G_{lm} M_{mj}^\dagger \quad (2.13)$$

$$M_{ij} \equiv \frac{1}{\sqrt{2}} (\delta_{ij} - i\sigma_{ij}^2). \quad (2.14)$$

Explicit transformation of the matrix in Eq.(2.5) yields:

$$\underline{G} = \begin{pmatrix} G^R & G^K \\ 0 & G^A \end{pmatrix}, \quad (2.15)$$

where we have defined the Keldysh Green's function,  $G^K(1, 1')$ , as follows:

$$G^K(1, 1') = G^>(1, 1') + G^<(1, 1'). \quad (2.16)$$

The explicit expressions of the matrix components can be read off from the definitions given in Eqs.(2.1), (2.2) and (2.3). Note that in thermal equilibrium, the three remaining components are not independent either. Consider fermions: From the relation in momentum space,  $G^<(\epsilon) = -e^{-\beta\epsilon} G^>(\epsilon)$ , we find [9, Eqs.2.65,2.66]

$$G^K(\epsilon) = \tanh \frac{\beta\epsilon}{2} [G^R(\epsilon) - G^A(\epsilon)]. \quad (2.17)$$

For bosons, we have a similar equation:

$$L^K(\bar{\omega}) = \coth \frac{\beta\epsilon}{2} [L^R(\bar{\omega}) - L^A(\bar{\omega})] . \quad (2.18)$$

In the rest of this thesis throughout, we will work in the just derived upper-triangular representation for the Green's function. To this end, we have to find the new coupling rules to scalar fields and particle-particle interactions.

### Scalar fields

We start from Eq.(2.6). Using the abbreviation  $\underline{\Omega}$  for the kernel of the integral on the r.h.s. and employing the transformation explicitly, we obtain

$$\underline{\Omega} = M\sigma^3\hat{G}W\sigma^3\hat{G}M^\dagger . \quad (2.19)$$

Inserting the identity  $M_{ik}M_{kj}^\dagger = \delta_{ij}$ , we find

$$\underline{\Omega} = M\sigma^3\hat{G}M^\dagger MW\sigma^3\hat{G}M^\dagger = \underline{G}W\underline{G} . \quad (2.20)$$

We conclude that the coupling to a scalar field changes in upper-triangular representation to the very simple expression

$$\underline{W}_{ij}(\mathbf{x}, t) = W(\mathbf{x}, t)\delta_{ij} . \quad (2.21)$$

### Particle-particle interactions

We label the integral kernel on the r.h.s. of Eq.(2.11) as

$$\Omega_{ij} \equiv G_{ik}\gamma_{kl}^\mu G_{lm}L_{\mu\nu}\gamma_{mn}^\nu G_{nj} , \quad (2.22)$$

and specify to put the absorption vertex to the left and the emission vertex to the right. Expressing the kernel in terms of propagators in the new basis, we find

$$\begin{aligned} \underline{\Omega}_{ij} &= M_{ik}\sigma_{kl}^3 G_{lm}\gamma_{mn}^\mu G_{no}L_{\mu\nu}\gamma_{op}^\nu G_{pq}M_{qj}^\dagger \\ &= M_{ik}\sigma_{kl}^3 G_{lm}M_{mn}^\dagger M_{no}\gamma_{op}^\mu G_{pq}L_{qr}\gamma_{rs}^\nu \sigma_{sa}^3 M_{ab}^\dagger M_{bc}\sigma_{cd}^3 G_{de}M_{ej}^\dagger \\ &= \underline{G}_{ik}M_{kl}\gamma_{lm}^\mu \underline{G}_{mn}L_{\mu\nu}\gamma_{no}^\nu \sigma_{op}^3 M_{pq}^\dagger \underline{G}_{qj} \\ &= \underline{G}_{ik}M_{kl}\gamma_{lm}^\mu \sigma_{mn}^3 M_{no}^\dagger \underline{G}_{op}M_{pq}\sigma_{\mu a}^3 M_{ab}^\dagger \underline{L}_{bc}M_{cv}\gamma_{qr}^\nu \sigma_{rs}^3 M_{sd}^\dagger \underline{G}_{dj} \\ &= \underline{G}_{ik}M_{kl}\gamma_{lm}^\mu \sigma_{mn}^3 M_{no}^\dagger \sigma_{\mu a}^3 M_{ab}^\dagger \underline{G}_{op}\underline{L}_{bc}M_{pq}M_{cv}\gamma_{qr}^\nu \sigma_{rs}^3 M_{sd}^\dagger \underline{G}_{dj} . \end{aligned}$$

In the second line we inserted twice a resolution of the identity and in the third line we marked the objects which we transform to the new basis in the fourth line. Rearrangement leads to the fifth line, from which the transformation rules for the vertex functions become apparent. The result is formally written as

$$\underline{\Omega}_{ij} = \underline{G}_{ik}\underline{\gamma}_{ko}^b \underline{G}_{op}\underline{L}_{bc}\underline{\gamma}_{pd}^c \underline{G}_{dj} , \quad (2.23)$$

where  $\underline{\gamma}_{ij}^\mu$  derive from  $\gamma_{ij}^\mu$  according to the following prescriptions:

$$\underline{\gamma}_{ko}^b = M_{kl} \gamma_{lm}^\mu \sigma_{mn}^3 M_{no}^\dagger \sigma_{\mu a}^3 M_{ab}^\dagger, \quad (2.24)$$

$$\underline{\gamma}_{pd}^c = M_{pq} M_{cv} \gamma_{qr}^\nu \sigma_{rs}^3 M_{sd}^\dagger. \quad (2.25)$$

Here, the first expression is the absorption vertex, and the second one describes emission. Explicitly plugging in the transformation, we finally obtain

$$\begin{aligned} \text{Emission vortices: } \underline{\tilde{\gamma}}_{ij}^1 &= \frac{1}{\sqrt{2}} \sigma_{ij}^1, \quad \underline{\tilde{\gamma}}_{ij}^2 = \frac{1}{\sqrt{2}} \delta_{ij} \\ \text{Absorption vortices: } \underline{\gamma}_{ij}^1 &= \frac{1}{\sqrt{2}} \delta_{ij}, \quad \underline{\gamma}_{ij}^2 = \frac{1}{\sqrt{2}} \sigma_{ij}^1. \end{aligned} \quad (2.26)$$

Thus, the vortices for absorption and emission are now different from each other.

### 2.2.5 Feynman rules in upper-triangular basis

The structure of the Feynman diagrams is summarized in Fig.2.4.

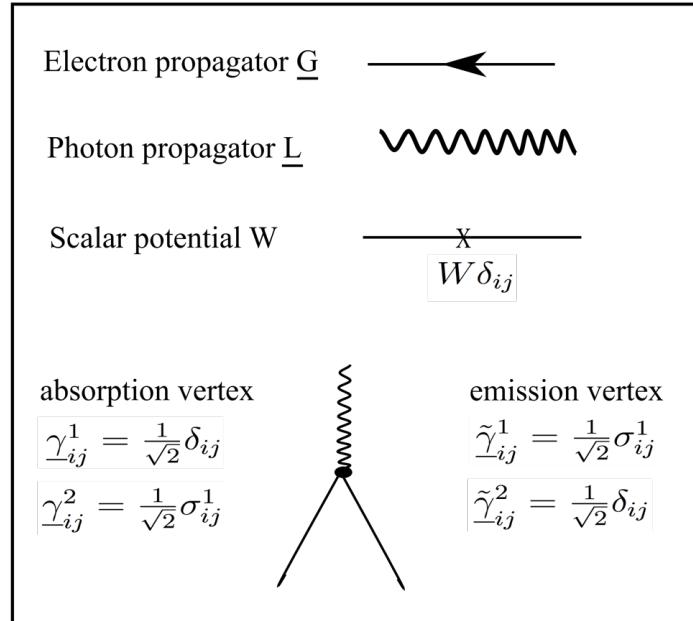


Figure 2.4: Feynman rules in Keldysh space for upper-triangular representation.

## 2.3 Discussion on instructive interaction diagrams

In this thesis, we will calculate the Cooperon self-energy in the framework of Keldysh formalism, hence it proves useful to discuss already at this stage the types of diagrams which will appear. The cooperon consists of two time-reversed electron trajectories, and the Coulomb interaction may either affect only one trajectory by energy exchange with the environment, or both via energy exchange between them. The former process, of so-called self-energy type<sup>3</sup> corresponds to diagrams of the form depicted in Fig.2.5a), while the latter, which is of so-called vertex type, corresponds to diagrams of the type depicted in Fig.2.5b). Of course, those diagrams are not a priori related to the Cooperon, but we can extract the diagrammatic rules needed for the Cooperon self-energy from this consideration. More precisely, we will find in which combinations the components of the electronic Green's functions appear in the diagrams, which will help us to draw later the diagrams contributing to the Cooperon self-energy.

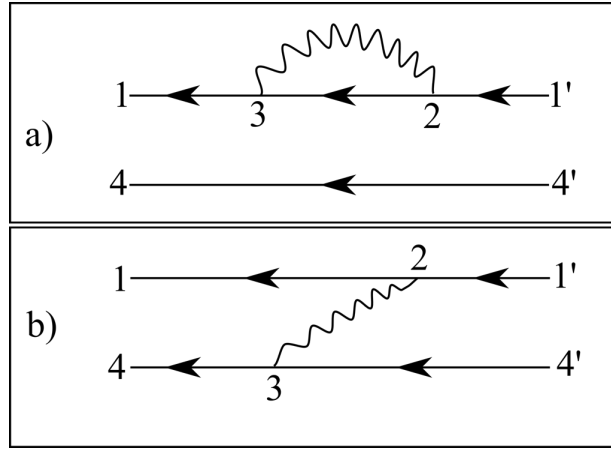


Figure 2.5: a) self-energy type diagram. b) vertex type diagram.

### 2.3.1 Self-energy type diagram

We focus on the diagram in Fig.2.5a), which we denote by  $\underline{\Sigma}_{ijpq}^S(1, 1', 4, 4')$ , and obtain from Eq.(2.11), in the basis Eq.(2.23)<sup>4</sup>

$$\underline{\Sigma}_{ijpq}^S(1, 1', 4, 4') = \int d3 \int d2 \underline{G}_{ik}(1, 3) \gamma_{kl}^\mu \underline{G}_{lm}(3, 2) \underline{L}_{\mu\nu}(3, 2) \tilde{\gamma}_{mn}^\nu \underline{G}_{nj}(3, 1') \underline{G}_{pq}(4, 4'). \quad (2.27)$$

<sup>3</sup>We adopt nomenclature by Jan von Delft in [11].

<sup>4</sup>We consider only diagrams first-order in interaction. We denote by a superscript "1" the first-order contribution to the electronic Green's function, and the free electron and interaction propagators get no subscript at all.

We carry out the  $\mu, \nu$ -sums first and find

$$\gamma_{kl}^\mu \underline{L}_{\mu\nu} \tilde{\gamma}_{mn}^\nu = \underline{L}^R \gamma_{kl}^1 \tilde{\gamma}_{mn}^1 + \underline{L}^K \gamma_{kl}^1 \tilde{\gamma}_{mn}^2 + \underline{L}^A \gamma_{kl}^2 \tilde{\gamma}_{mn}^2. \quad (2.28)$$

Inserting the vertex representations from Eq.(2.26), we get that the kernel of the integral in Eq.(2.27), denoted  $\underline{\Omega}_{ijpq}(1, 1, 4, 4')$  equals to the following expression

$$2\underline{\Omega}_{ijpq}^{11'44'} = G_{ik}^{13} G_{kl}^{32} \sigma_{lm}^1 G_{mj}^{21'} L^{R,32} G_{pq}^{44'} + G_{ik}^{13} G_{kl}^{32} G_{lj}^{21'} L^{K,32} G_{pq}^{44'} + G_{ik}^{13} \sigma_{kl}^1 G_{lm}^{32} G_{mj}^{21'} L^{A,32} G_{pq}^{44'}, \quad (2.29)$$

where we introduced the condensed notation ( $U_{ij}^{11'}$ ) to replace  $\underline{U}_{ij}(1, 1')$  for  $U = L, G, \Omega$ . From Eq.(2.29),

$$\begin{aligned} 2\underline{\Omega}^{11'} &= L^{R,32} G^{44'} \begin{pmatrix} G^{R,13} & G^{K,13} \\ 0 & G^{A,13} \end{pmatrix} \begin{pmatrix} G^{R,32} & G^{K,32} \\ 0 & G^{A,32} \end{pmatrix} \begin{pmatrix} 0 & 1 \\ 1 & 0 \end{pmatrix} \begin{pmatrix} G^{R,21'} & G^{K,21'} \\ 0 & G^{A,21'} \end{pmatrix} \\ &+ L^{K,32} G^{44'} \begin{pmatrix} G^{R,13} & G^{K,13} \\ 0 & G^{A,13} \end{pmatrix} \begin{pmatrix} G^{R,32} & G^{K,32} \\ 0 & G^{A,32} \end{pmatrix} \begin{pmatrix} G^{R,21'} & G^{K,21'} \\ 0 & G^{A,21'} \end{pmatrix} \\ &+ L^{A,32} G^{44'} \begin{pmatrix} G^{R,13} & G^{K,13} \\ 0 & G^{A,13} \end{pmatrix} \begin{pmatrix} 0 & 1 \\ 1 & 0 \end{pmatrix} \begin{pmatrix} G^{R,32} & G^{K,32} \\ 0 & G^{A,32} \end{pmatrix} \begin{pmatrix} G^{R,21'} & G^{K,21'} \\ 0 & G^{A,21'} \end{pmatrix}. \end{aligned}$$

Now we perform multiplication of pairs of neighboring matrices. Note that the matrix  $G^{44'}$  is not coupled to the other matrices. We obtain

$$\begin{aligned} 2\underline{\Omega}^{11'44'} &= L^{R,32} G^{44'} \begin{pmatrix} G^{R,13} G^{R,32} & G^{R,13} G^{K,32} + G^{K,13} G^{A,32} \\ 0 & G^{A,13} G^{A,32} \end{pmatrix} \begin{pmatrix} 0 & G^{A,21'} \\ G^{R,21'} & G^{K,21'} \end{pmatrix} \\ &+ L^{K,32} G^{44'} \begin{pmatrix} G^{R,13} G^{R,32} & G^{R,13} G^{K,32} + G^{K,13} G^{A,32} \\ 0 & G^{A,13} G^{A,32} \end{pmatrix} \begin{pmatrix} G^{R,21'} & G^{K,21'} \\ 0 & G^{A,21'} \end{pmatrix} \\ &+ L^{A,32} G^{44'} \begin{pmatrix} G^{K,13} & G^{R,13} \\ G^{A,13} & 0 \end{pmatrix} \begin{pmatrix} G^{R,32} G^{R,21'} & G^{R,32} G^{K,21'} + G^{K,32} G^{A,21'} \\ 0 & G^{A,32} G^{A,21'} \end{pmatrix}. \end{aligned}$$

We specify for later use, that the retarded/advanced component of  $\Omega^{11'44'}$  contains the advanced/retarded component of  $G^{44'}$ , respectively. Thus we find:

$$\begin{aligned} 2\underline{\Omega}^{R,11'44'} &= G^{R,13} G^{K,32} L^{R,32} G^{R,21'} G^{A,44'} + G^{K,13} \color{red}{G^{A,32} L^{R,32}} G^{R,21'} G^{A,44'} \\ &+ G^{R,13} G^{R,32} L^{K,32} G^{R,21'} G^{A,44'} + G^{K,13} \color{red}{G^{R,32} L^{A,32}} G^{R,21'} G^{A,44'} \\ 2\underline{\Omega}^{A,11'44'} &= G^{A,13} \color{red}{G^{A,32} L^{R,32}} G^{K,21'} G^{R,44'} + G^{A,13} G^{A,32} L^{K,32} G^{A,21'} G^{R,44'} \\ &+ G^{A,13} \color{red}{G^{R,32} L^{A,32}} G^{K,21'} G^{R,44'} + G^{A,13} G^{K,32} L^{A,32} G^{A,21'} G^{R,44'}. \end{aligned} \quad (2.30)$$

The combinations which are marked red in Eq.(2.30), do not contribute [9, Eq.4.39]. An intuitive argument is that retarded/advanced propagators vanish at negative/positive times, hence their product is zero. We do not explicitly show the structure of  $\Omega^{K,11'44'}$  in Eq.(2.30), since we will not need it in later considerations and since it is anyhow given in terms of

advanced/retarded components via Eq.(2.17). The non-vanishing part of retarded(R) and advanced(A) components of  $\Omega^{11'44'}$  is shown in Fig.2.6. We learn that interaction can be carried by all components of the propagator L. If the interaction is carried by the Keldysh(K) component, the retardation of the electron line is unchanged. If the interaction is carried by R/A component, the interaction changes the retardation of the electron line,  $R/A \rightarrow K$  and  $K \rightarrow R/A$ .

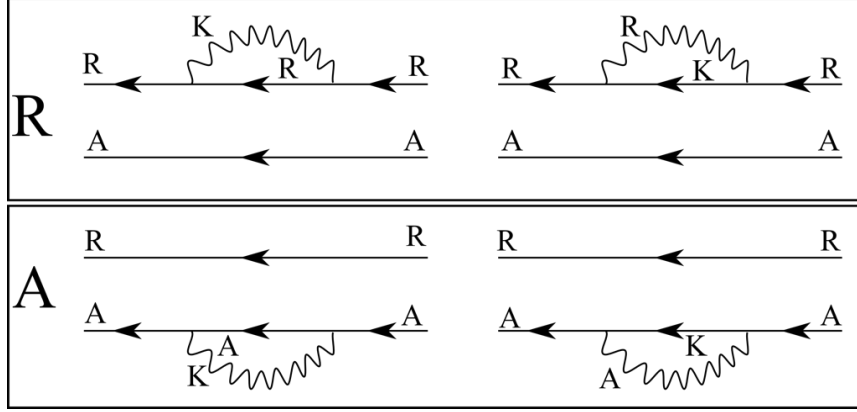


Figure 2.6: Propagator combinations contributing to self-energy type diagrams.

### 2.3.2 Vertex type diagram

We proceed with the vertex type diagram depicted in Fig.2.5b), and denote it by  $\underline{\Sigma}_{ijpq}^V(1, 1', 4, 4')$ . Adopting the notation introduced just before Eq.(2.29), we obtain:

$$\Sigma_{ijpq}^{11'44'} = \int d3 \int d2 G_{ik}(1, 2) \gamma_{kl}^\mu G_{lj}(2, 1') L_{\mu\nu}(2, 3) G_{pm}(4, 3) \tilde{\gamma}_{mn}^\nu G_{nq}(3, 4'). \quad (2.31)$$

We Eqs.(2.28),(2.26) to find for the kernel of the integral in Eq.(2.31), denoted  $\eta_{ijpq}^{11'44'}$ :

$$2\eta_{ijpq}^{11'44'} = \left[ G_{ik}^{12} G_{kj}^{21'} \right] L^{R,23} \left[ G_{pm}^{43} \sigma_{mn}^1 G_{nq}^{34'} \right] + \left[ G_{ik}^{12} G_{kj}^{21'} \right] L^{K,23} \left[ G_{pm}^{43} G_{mq}^{34'} \right] \\ + \left[ G_{ik}^{12} \sigma_{kl}^1 G_{lj}^{21'} \right] L^{A,23} \left[ G_{pm}^{43} G_{mq}^{34'} \right]. \quad (2.32)$$

The square brackets before/behind the interaction propagators correspond to the upper/lower electron line in Fig.2.5b). For later use, we keep the retarded/advanced part of the upper/lower line, and denote the emerging structure  $\Gamma^{11'44'}$ . Under this restriction and after matrix multiplications we find:

$$2\Gamma^{11'44'} = \left[ G^{R,12} G^{R,21'} \right] L^{R,23} \left[ G^{A,43} G^{K,34'} \right] + \left[ G^{R,12} G^{R,21'} \right] L^{K,23} \left[ G^{A,43} G^{A,34'} \right] \\ + \left[ G^{K,12} G^{R,21'} \right] L^{A,23} \left[ G^{A,43} G^{A,34'} \right]. \quad (2.33)$$

We display those diagrams in Fig.2.7 and conclude that all components of the interaction propagator can appear. If the interaction is carried by the Keldysh component, the retardation of upper and lower line is unchanged. If the interaction comes with retarded/advanced component, the retardation of the lower/upper line is changed. This concludes our discussion on Keldysh perturbation theory.

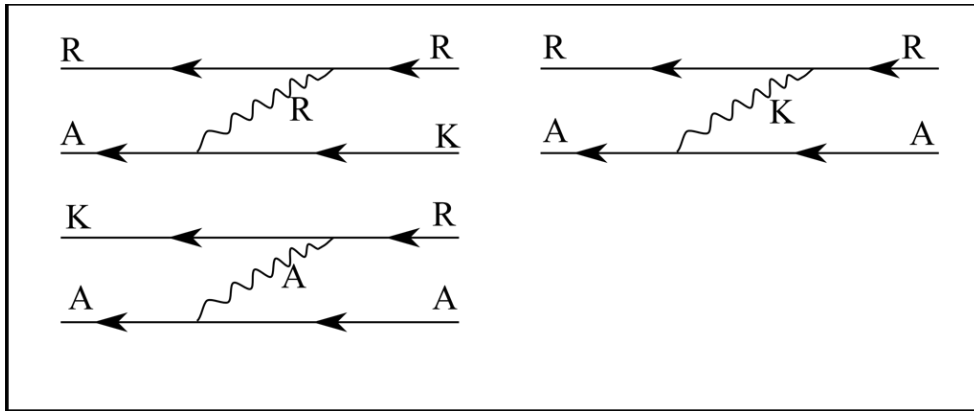


Figure 2.7: Propagator combinations contributing to vertex type diagrams.



# Chapter 3

## Disorder-averaged AC-conductivity of disordered normal metals

In this chapter, we will review how the disorder-averaged AC-conductivity can be obtained from Keldysh diagrammatic perturbation theory. More precisely, we will obtain the classical Drude result and the leading quantum contribution, i.e. the weak localization correction, from a linear response calculation using the Keldysh technique developed in Ch.2.

### 3.1 AC-conductivity of normal metals

Application of an electric field  $\mathbf{E}(\omega)$  to a metal leads to current flow  $\mathbf{j}(\omega)$  in the metal. In linear response theory, the current is related to the field via the following relation:

$$j_\alpha(\mathbf{q}, \omega) = \sigma_{\alpha\beta}(\mathbf{q}, \omega) E_\beta(\mathbf{q}, \omega), \quad (3.1)$$

which defines the conductivity tensor  $\hat{\sigma}(\omega)$ . We will assume a spatially uniform field, and we will use the gauge  $V = 0$ ,  $\mathbf{A}(\omega) = \mathbf{E}(\omega)/i\omega$ . The expression for the conductivity is obtained from a linear response calculation of the current.

#### 3.1.1 Quantum-mechanical current operator in spatial representation

Electromagnetic fields are represented in the Hamiltonian operator via minimal coupling, i.e. the momentum operator  $\hat{\mathbf{p}}$  is replaced with the generalized momentum operator:

$$\hat{\mathbf{p}} \rightarrow (\hat{\mathbf{p}} - e\mathbf{A}). \quad (3.2)$$

As a result, in spatial representation, the Hamilton operator becomes

$$\hat{H} = \frac{1}{2m} \int d^d x \hat{\Psi}^\dagger(\mathbf{x}, t) [i\nabla + e\mathbf{A}(t)]^2 \hat{\Psi}(\mathbf{x}, t). \quad (3.3)$$

From Eq.(3.3), we obtain:

$$\hat{H} = \frac{1}{2m} \int d^d x \hat{\Psi}^\dagger(\mathbf{x}, t) [-\nabla^2 + ie(\nabla \cdot \mathbf{A} + \mathbf{A} \cdot \nabla) + e^2 \mathbf{A}^2] \hat{\Psi}(\mathbf{x}, t), \quad (3.4)$$

and by integration by parts, we shift the derivative acting on  $\mathbf{A}$  onto  $\hat{\Psi}^\dagger(\mathbf{x}, t)$ . Hence we obtain

$$\hat{H} = T + W \quad (3.5)$$

where  $T$  is the kinetic energy,

$$T = -\frac{1}{2m} \int d\mathbf{x} \hat{\Psi}^\dagger(\mathbf{x}, t) \nabla^2 \hat{\Psi}(\mathbf{x}, t), \quad (3.6)$$

and  $W$  is the scalar interaction term:

$$W = \int d^d x \hat{\mathbf{j}}(\mathbf{x}, t) \cdot \mathbf{A}(t), \quad (3.7)$$

where we introduced the current operator  $\mathbf{j}(\mathbf{x}, t)$  [7]:

$$\hat{\mathbf{j}} = \hat{\mathbf{j}}_{\text{para}} + \hat{\mathbf{j}}_{\text{dia}}, \quad (3.8)$$

with the following paramagnetic and diamagnetic parts:

$$\begin{aligned} \hat{\mathbf{j}}_{\text{para}}(\mathbf{x}, t) &= \frac{e}{2mi} \left[ \left( \nabla \hat{\Psi}^\dagger(\mathbf{x}, t) \right) \hat{\Psi}(\mathbf{x}, t) - \hat{\Psi}^\dagger(\mathbf{x}, t) \left( \nabla \hat{\Psi}(\mathbf{x}, t) \right) \right], \\ \hat{\mathbf{j}}_{\text{dia}}(\mathbf{x}, t) &= \frac{e^2}{2m} \mathbf{A}(t) \hat{\Psi}^\dagger(\mathbf{x}, t) \hat{\Psi}(\mathbf{x}, t). \end{aligned} \quad (3.9)$$

### 3.1.2 Current expectation value

It is convenient to rewrite Eq.(3.9) as follows:

$$\hat{\mathbf{j}}(\mathbf{x}, t) = - \lim_{\mathbf{x} \rightarrow \mathbf{x}'} \frac{e}{m} [\nabla - \nabla' - 2ie\mathbf{A}(t)] i\hat{\Psi}^\dagger(\mathbf{x}', t') \hat{\Psi}(\mathbf{x}, t). \quad (3.10)$$

We denote the measured current by  $\mathbf{j}(\mathbf{x}, t)$ . It can be shown [7] that  $\mathbf{j}(\mathbf{x}, t)$  is given as the thermal average of the current operator  $\hat{\mathbf{j}}(\mathbf{x}, t)$ :

$$\mathbf{j}(\mathbf{x}, t) = \left\langle \hat{\mathbf{j}}(\mathbf{x}, t) \right\rangle. \quad (3.11)$$

Thus, from Eq.(3.10), we can express  $\mathbf{j}(\mathbf{x}, t)$  in terms of the Green's function  $G^<(\mathbf{x}t, \mathbf{x}'t')$  defined in Eq.(2.1):

$$\mathbf{j}(\mathbf{x}, t) = - \lim_{\mathbf{x} \rightarrow \mathbf{x}'} \frac{e}{m} (\nabla - \nabla') G^<(\mathbf{x}t, \mathbf{x}'t') - \frac{ne^2}{m} \mathbf{A}(t). \quad (3.12)$$

### 3.1.3 Linear response and Keldysh technique

We use the Keldysh technique to find the leading correction to the electronic Green's function due to the field  $\mathbf{A}(t)$ . In the representation in Keldysh space described in Sect.2.2.4, this leading correction, denoted  $\underline{G}_{ij}^1$ , is written as follows:

$$\underline{G}_{ij}^1(1, 1') = \frac{ie}{2m} \int d\mathbf{x}_2 \int dt_2 [\mathbf{A}(t_2) (\nabla_2 - \nabla_{2'}) \underline{G}_{ik}(1, 2') \underline{G}_{kj}(2, 1')]_{2=2'} , \quad (3.13)$$

c.f. Eqs.(2.6), (2.9) and (2.21). We consider linear response and hence dropped the diamagnetic term in Eq.(3.13), which gives a contribution  $\sim \mathbf{A}(t)^2$  to the current, c.f. Eqs.(3.9), (3.7). We have to keep the diamagnetic part in Eq.(3.12), though. In Eq.(3.13),  $\underline{G}_{ij}$  denotes the unperturbed electron propagator, i.e. at  $\mathbf{A} = 0$ . To write the linear response  $\mathbf{j}(1)$  from Eq.(3.12), we need  $G^<(\mathbf{x}t, \mathbf{x}'t')$ , which obeys

$$G^< = \frac{1}{2} [G^K - G^R + G^A] , \quad (3.14)$$

as verified by use of Eqs.(2.3),(2.16). With Eq.(3.14) and Eq.(2.15), it is straightforward matrix multiplication to arrive at

$$\begin{aligned} \mathbf{j}(1) + \frac{ne^2}{m} \mathbf{A}(t_1) = & -\frac{ie^2}{4m^2} \int d\mathbf{x}_2 \int dt_2 \left[ \mathbf{A}(t_2) (\nabla_2 - \nabla_{2'}) (\nabla_1 - \nabla_{1'}) \right. \\ & \times \left( G^R(1, 2') G^K(2, 1') + G^K(1, 2') G^A(2, 1') \right. \\ & \left. \left. - G^R(1, 2') G^R(2, 1') + G^A(1, 2') G^A(2, 1') \right) \right]_{1=1', 2=2'} , \end{aligned} \quad (3.15)$$

where we employed Eq.(3.12). We perform a Fourier transformation of Eq.(3.15), see Sec.C.1 for details. In homogeneous systems, only the  $\mathbf{q} = 0$  mode can contribute and we obtain

$$\begin{aligned} \mathbf{j}(\omega) + \frac{ne^2}{m} \mathbf{A}(\omega) = & + \frac{ie^2 \mathbf{A}(\omega)}{2m^2 \pi V} \sum_{\mathbf{k}_1} \sum_{\mathbf{k}_2} \mathbf{k}_1 \cdot \mathbf{k}_2 \int dE \\ & \times \left[ G_{E+\omega}^R(\mathbf{k}_1, \mathbf{k}_2) G_E^K(\mathbf{k}_2, \mathbf{k}_1) + G_{E+\omega}^K(\mathbf{k}_1, \mathbf{k}_2) G_E^A(\mathbf{k}_2, \mathbf{k}_1) \right. \\ & \left. - G_{E+\omega}^R(\mathbf{k}_1, \mathbf{k}_2) G_E^R(\mathbf{k}_2, \mathbf{k}_1) + G_{E+\omega}^A(\mathbf{k}_1, \mathbf{k}_2) G_E^A(\mathbf{k}_2, \mathbf{k}_1) \right] , \end{aligned} \quad (3.16)$$

c.f. Eq.(C.3). In thermal equilibrium, the components of the electron Green's function are related by Eq.(2.17), and hence

$$\begin{aligned} \mathbf{j}(\omega) + \frac{ne^2}{m}\mathbf{A}(\omega) = & + \frac{ie^2\mathbf{A}(\omega)}{2m^2\pi V} \sum_{\mathbf{k}_1} \sum_{\mathbf{k}_2} \mathbf{k}_1 \cdot \mathbf{k}_2 \int dE \\ & \times \left[ G_{E+\omega}^R(\mathbf{k}_1, \mathbf{k}_2) G_E^A(\mathbf{k}_2, \mathbf{k}_1) \left( \tanh \frac{\beta E}{2} - \tanh \frac{\beta(E+\omega)}{2} \right) \right. \\ & + G_{E+\omega}^R(\mathbf{k}_1, \mathbf{k}_2) G_E^R(\mathbf{k}_2, \mathbf{k}_1) \left( \tanh \frac{\beta E}{2} - 1 \right) \\ & \left. + G_{E+\omega}^A(\mathbf{k}_1, \mathbf{k}_2) G_E^A(\mathbf{k}_2, \mathbf{k}_1) \left( 1 - \tanh \frac{\beta(E+\omega)}{2} \right) \right]. \end{aligned} \quad (3.17)$$

The Fermi distribution satisfies

$$f(\epsilon) = \frac{1}{e^{\beta\epsilon} + 1} = \frac{1}{2} (1 - \tanh(\beta\epsilon/2)) , \quad (3.18)$$

and thus Eq.(3.17) can be rewritten as follows:

$$\begin{aligned} \mathbf{j}(\omega) + \frac{ne^2}{m}\mathbf{A}(\omega) = & + \frac{ie^2\mathbf{A}(\omega)}{m^2\pi V} \sum_{\mathbf{k}_1} \sum_{\mathbf{k}_2} \mathbf{k}_1 \cdot \mathbf{k}_2 \int dE \\ & \times \left[ \left( f(E) - f(E+\omega) \right) G_{E+\omega}^R(\mathbf{k}_1, \mathbf{k}_2) G_E^A(\mathbf{k}_2, \mathbf{k}_1) \right. \\ & - f(E) G_{E+\omega}^R(\mathbf{k}_1, \mathbf{k}_2) G_E^R(\mathbf{k}_2, \mathbf{k}_1) \\ & \left. + f(E+\omega) G_{E+\omega}^A(\mathbf{k}_1, \mathbf{k}_2) G_E^A(\mathbf{k}_2, \mathbf{k}_1) \right]. \end{aligned} \quad (3.19)$$

By Eq.(3.1), we identify the conductivity  $\sigma(\omega)$  [9]:

$$\begin{aligned} \sigma(\omega) + \frac{ne^2}{im\omega} = & + \frac{e^2}{m^2\omega\pi dV} \sum_{\mathbf{k}_1} \sum_{\mathbf{k}_2} \mathbf{k}_1 \cdot \mathbf{k}_2 \int dE \\ & \times \left[ \left( f(E) - f(E+\omega) \right) G_{E+\omega}^R(\mathbf{k}_1, \mathbf{k}_2) G_E^A(\mathbf{k}_2, \mathbf{k}_1) \right. \\ & - f(E) G_{E+\omega}^R(\mathbf{k}_1, \mathbf{k}_2) G_E^R(\mathbf{k}_2, \mathbf{k}_1) \\ & \left. + f(E+\omega) G_{E+\omega}^A(\mathbf{k}_1, \mathbf{k}_2) G_E^A(\mathbf{k}_2, \mathbf{k}_1) \right], \end{aligned} \quad (3.20)$$

where  $d$  is the spatial dimension. In this section, we consider only small excitations at low temperature,  $\omega \ll E_F$  and  $T \ll E_F$ , for which the following replacement is valid:

$$\frac{f(E) - f(E+\omega)}{\omega} \approx -\frac{\partial f(E)}{\partial E} \approx -\delta(E - E_F). \quad (3.21)$$

Eq.(3.21) reflects the fact that at low temperatures and excitation energies only electrons at the Fermi energy are relevant for transport phenomena. We adopt this approximation and obtain from Eq.(3.20):

$$\begin{aligned} \sigma(\omega) + \frac{ne^2}{im\omega} = & + \frac{e^2}{m^2\pi dV} \sum_{\mathbf{k}_1} \sum_{\mathbf{k}_2} \mathbf{k}_1 \cdot \mathbf{k}_2 G_{E_F+\omega}^R(\mathbf{k}_1, \mathbf{k}_2) G_{E_F}^A(\mathbf{k}_2, \mathbf{k}_1) \\ & + \frac{e^2}{m^2\omega\pi dV} \sum_{\mathbf{k}_1} \sum_{\mathbf{k}_2} \mathbf{k}_1 \cdot \mathbf{k}_2 \int dE \\ & \times [f(E+\omega) G_{E+\omega}^A(\mathbf{k}_1, \mathbf{k}_2) G_E^A(\mathbf{k}_2, \mathbf{k}_1) - f(E) G_{E+\omega}^R(\mathbf{k}_1, \mathbf{k}_2) G_E^R(\mathbf{k}_2, \mathbf{k}_1)] . \end{aligned} \quad (3.22)$$

## 3.2 Disorder averaged conductivity

This section is devoted to a disorder average of Eq.(3.22). As in Ch.1, we denote disorder average by a bar on the quantity to be averaged, and we find from Eq.(3.22)

$$\begin{aligned} \sigma(\omega) + \frac{ne^2}{im\omega} = & + \frac{e^2}{m^2\pi dV} \sum_{\mathbf{k}_1} \sum_{\mathbf{k}_2} \mathbf{k}_1 \cdot \mathbf{k}_2 \overline{G_{E_F+\omega}^R(\mathbf{k}_1, \mathbf{k}_2) G_{E_F}^A(\mathbf{k}_2, \mathbf{k}_1)} \\ & + \frac{e^2}{m^2\omega\pi dV} \sum_{\mathbf{k}_1} \sum_{\mathbf{k}_2} \mathbf{k}_1 \cdot \mathbf{k}_2 \int dE \\ & \times \left[ f(E+\omega) \overline{G_{E+\omega}^A(\mathbf{k}_1, \mathbf{k}_2) G_E^A(\mathbf{k}_2, \mathbf{k}_1)} - f(E) \overline{G_{E+\omega}^R(\mathbf{k}_1, \mathbf{k}_2) G_E^R(\mathbf{k}_2, \mathbf{k}_1)} \right] . \end{aligned} \quad (3.23)$$

Note that the second term on the l.h.s. of Eq.(3.23), the so-called diamagnetic term, diverges in the limit  $\omega \rightarrow 0$ .  $\overline{G^{R/A} G^{R/A}} = \overline{G}^{R/A} \overline{G}^{R/A} + \mathcal{O}(1/k_F l_e)$  in the diffusive limit [5, Eq.4.194], i.e. correlations between propagators with equal retardation is negligible, and we will use that fact to show in Appendix C.2, that the  $\overline{G^{R/A} G^{R/A}}$ -contributions to Eq.(3.23) cancel the diamagnetic term. Hence, we are left with

$$\sigma(\omega) = \frac{e^2}{m^2\pi dV} \sum_{\mathbf{k}_1} \sum_{\mathbf{k}_2} \mathbf{k}_1 \cdot \mathbf{k}_2 \overline{G_{E_F+\omega}^R(\mathbf{k}_1, \mathbf{k}_2) G_{E_F}^A(\mathbf{k}_2, \mathbf{k}_1)} . \quad (3.24)$$

### 3.2.1 Drude limit

In this section, we will derive the Drude result for the conductivity, denoted  $\sigma_d(\omega)$ . The Drude result corresponds to the neglect of all correlation between the propagators, and hence corresponds to the Drude-Boltzmann approximation discussed in Sec.1.2.2. The Drude approximation can be represented by the diagram in Fig.3.1. This diagram equals to the following expression:

$$\sigma(\omega) = \frac{e^2}{m^2\pi dV} \sum_{\mathbf{k}} \mathbf{k}^2 \overline{G_{E_F+\omega}^R(\mathbf{k}) G_{E_F}^A(\mathbf{k})} . \quad (3.25)$$

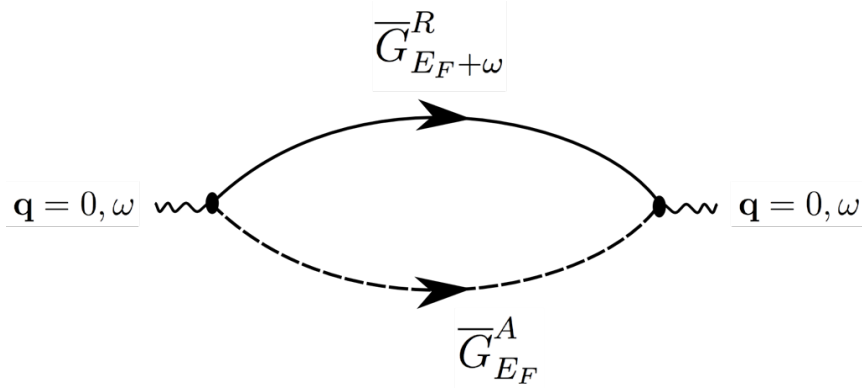


Figure 3.1: Classical conductivity diagram.

Since the relevant contribution to electronic transport comes from electrons in the vicinity of the Fermi surface, we substitute  $\mathbf{k}^2 = k_F^2$  in Eq.(3.25). Thus, we are left with:

$$\sigma(\omega) = \frac{k_F^2 e^2}{m^2 \pi d V} \sum_{\mathbf{k}} \overline{G}_{E_F + \omega}^R(\mathbf{k}) \overline{G}_{E_F}^A(\mathbf{k}). \quad (3.26)$$

Using Eq.(1.19) and Eq.(1.25), we find:

$$\sigma(\omega) = \frac{2\rho k_F^2 e^2}{m^2 d} \frac{\tau}{1 - i\omega\tau}, \quad (3.27)$$

and using Eqs.(A.12), we obtain the Drude expression for the conductivity:

$$\sigma_d(\omega) = \frac{\sigma_0}{1 - i\omega\tau}, \quad (3.28)$$

where we have introduced the static limit,

$$\sigma_0 \equiv \sigma_d(\omega = 0) = \frac{e^2 n \tau}{m}. \quad (3.29)$$

### 3.2.2 Weak localization

The Drude approximation neglects all correlations between the electron propagators in Eq.(3.22). In this subsection, we discuss the leading contributions associated with correlations. It is well known, that the diffusion ladder diagrams discussed in Sec.1.2.3 give no contribution to the conductivity in the case of isotropic collisions considered here [2]. In our case the leading correction to the classical Drude result comes from the set of maximally crossed diagrams [4, 12, 13], which are associated with the Cooperon, c.f. Sec. 1.2.4, and which corresponds to the leading contribution in a  $1/g$ -expansion, as pointed out in

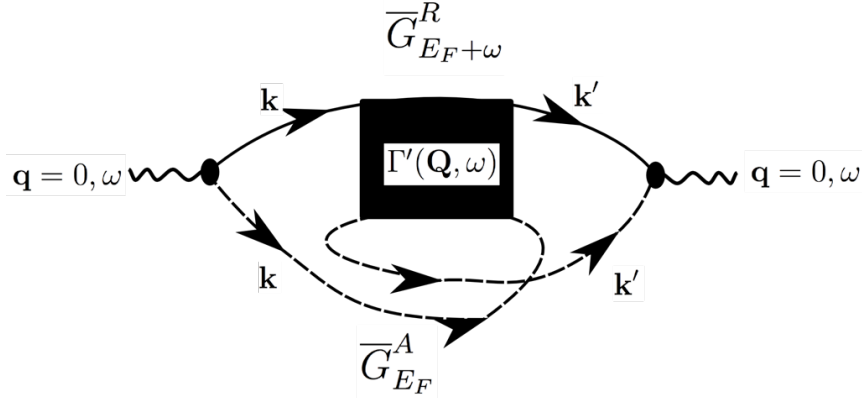


Figure 3.2: Weak localization correction to the AC-conductivity.  $\mathbf{Q} = \mathbf{k} + \mathbf{k}'$

Sec.1.1.5. This correction, depicted in Fig.3.2, is called weak localization correction. We make use of the results from Sec.1.2.4. The diagram corresponds to the following expression:

$$\delta\sigma(\omega) = \frac{e^2}{\pi d m^2} \sum_{\mathbf{k}, \mathbf{k}'} \mathbf{k} \cdot \mathbf{k}' \bar{G}_{E_F+\omega}^R(\mathbf{k}) \bar{G}_{E_F+\omega}^R(\mathbf{k}') \bar{G}_{E_F}^A(\mathbf{k}) \bar{G}_{E_F}^A(\mathbf{k}') \Gamma'_{\mathbf{Q}}(\omega), \quad (3.30)$$

We average  $\mathbf{k} \cdot \mathbf{k}' = -k_F^2$  in Eq.(3.30), due to the peaked structure of  $\Gamma'_{\mathbf{Q}}(\omega)$ , and since contribution to transport comes from electrons at  $E_F$ . Further, we set  $\mathbf{k}' = -\mathbf{k}$  in the Green's functions. By a calculation similar to Sec.1.2.4, we find the final result for the weak localization correction, expressed in units of the DC-Drude result  $\sigma_0$ , c.f. Eq.(3.29):

$$\frac{\delta\sigma(\omega)}{\sigma_0} = -\frac{1}{\pi\nu} \sum_{\mathbf{Q}} \frac{1}{D\mathbf{Q}^2 - i\omega}. \quad (3.31)$$

where  $\nu = \rho V$  is the level-density. Note that the weak localization correction is negative. If time-reversal symmetry is broken by a magnetic field, the correction vanishes and hence leads to a negative magneto-resistance, which has been observed experimentally [6].



# Chapter 4

## Bethe-Salpeter equation for interacting Cooperon

At low temperatures, when phonons are frozen out, and in the absence of magnetic fields, electron-electron interactions are the primary cause for dephasing in disordered conductors [3]. Interactions lead to dephasing of the Cooperon, and hence the weak localization correction to the AC-conductivity, which was calculated in Ch.3.2.2, is decreased. The characteristic time scale of interactions-induced dephasing is denoted  $\tau_\phi$ . In diagrammatic perturbation theory, the Cooperon in the presence of interactions is the solution of a Bethe-Salpeter equation, an intricate integral equation which has not been solved analytically. However, approximate results have been obtained by von Delft et al. [11]. Using Keldysh diagrammatic perturbation theory, the authors found expressions for the first-order-in-interaction correction to the Cooperon. To obtain these results, they transcribed the linearized (first-order-in-interaction) Bethe-Salpeter equation to the position-time representation and approximately solved it using an exponential ansatz. In this chapter, we will review how to linearize the Bethe-Salpeter equation. We will stay in the energy-momentum representation for clarity, and we will explain that the latter equation can be reduced to a Dyson equation, if vertex type diagrams are neglected [11]. We will discuss the consequences of neglecting the vertex diagrams, and we will define the dephasing time in terms of the self-energy which appears in the Dyson equation. Note that the thus obtained expression for  $\tau_\phi$  will contain the full dependence of a finite external AC-frequency  $\omega$ .

## 4.1 Bethe-Salpeter equation for the Cooperon

### 4.1.1 Bethe-Salpeter equation

In the presence of interactions, the Cooperon structure factor, which we denote by  $\Gamma^E$ , is given by the following Bethe-Salpeter equation [11, Eq.(7a)]:

$$\Gamma_{\mathbf{q}}^E(\Omega_{\text{out}}, \Omega_{\text{in}}) = \Gamma_{\mathbf{q}}^0(\Omega_{\text{out}}) \left[ 2\pi\delta(\Omega_{\text{out}} - \Omega_{\text{in}}) + \int d\Omega \Sigma_{\mathbf{q}}^E(\Omega_{\text{out}}, \Omega) \Gamma_{\mathbf{q}}^E(\Omega, \Omega_{\text{in}}) \right], \quad (4.1)$$

where the superscript  $E$  denotes the electronic energy and  $\Gamma_{\mathbf{q}}^0(\Omega_{\text{out}})$  denotes the structure factor in the absence of interactions, c.f. Eq.(1.43):

$$\Gamma_{\mathbf{q}}^0(\Omega_{\text{out}}) = \frac{1}{2\pi\rho\tau^2} \frac{1}{D\mathbf{q}^2 - i\Omega_{\text{out}}}. \quad (4.2)$$

In the presence of interactions, the Cooperon depends on the two energy differences  $\Omega_{\text{in}}$  and  $\Omega_{\text{out}}$ , i.e. the incoming and outgoing difference of upper/lower electron line. In the absence of interactions, Eq.(4.1) reduces to

$$\Gamma_{\mathbf{q}}^E(\Omega_{\text{out}}, \Omega_{\text{in}}) = \Gamma_{\mathbf{q}}^0(\Omega_{\text{out}}) 2\pi \delta(\Omega_{\text{out}} - \Omega_{\text{in}}) \quad (4.3)$$

The Bethe-Salpeter equation Eq.(4.1) corresponds to the diagrams in Fig.4.1.

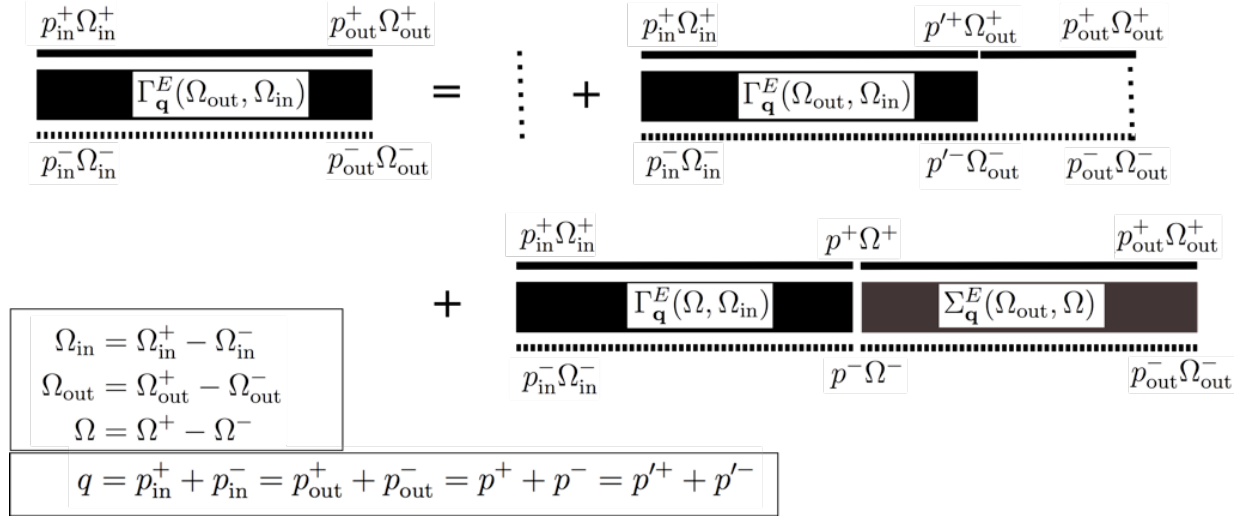


Figure 4.1: Bethe-Salpeter equation for the Cooperon.

We mentioned above, that the Cooperon depends on the electronic energy  $E$ . We define the in-going Cooperon energies  $(\Omega_{\text{in}}^+, \Omega_{\text{in}}^-)$  and thus our energy convention as follows:

$$\begin{aligned} \Omega_{\text{in}}^+ &= E + \omega, \\ \Omega_{\text{in}}^- &= E. \end{aligned} \quad (4.4)$$

with the AC-frequency  $\omega$ . Thus we match our notations with the conventions in Ch.1.

### 4.1.2 Interaction propagators

We use the unitary limit of the disorder-averaged<sup>1</sup> screened interaction propagator  $\underline{L}_{\bar{\mathbf{q}}}(\bar{\omega})$ , which is given as follows [11, Eq.(A3)]:

$$\underline{L}_{\bar{\mathbf{q}}}(\bar{\omega}) = \begin{pmatrix} L_{\bar{\mathbf{q}}}^R(\bar{\omega}) & L_{\bar{\mathbf{q}}}^K(\bar{\omega}) \\ 0 & L_{\bar{\mathbf{q}}}^A(\bar{\omega}) \end{pmatrix}, \quad (4.5)$$

with components

$$\begin{aligned} L_{\bar{\mathbf{q}}}^K(\bar{\omega}) &= 2i \coth \frac{\bar{\omega}}{2T} \Im L_{\bar{\mathbf{q}}}^R(\bar{\omega}) \\ L_{\bar{\mathbf{q}}}^R(\bar{\omega}) &= [L_{\bar{\mathbf{q}}}^A(\bar{\omega})]^* = -\frac{D\bar{\mathbf{q}}^2 - i\bar{\omega}}{2\nu D\bar{\mathbf{q}}^2}, \end{aligned} \quad (4.6)$$

to describe interactions involving momentum/energy transfer  $(\bar{\mathbf{q}}, \bar{\omega})$  between electrons. The given form of the interaction propagator corresponds to the impurity-averaged random phase approximation [7, 14, 15].

### 4.1.3 Cooperon self-energy

The cooperon self-energy  $\Sigma_{\bar{\mathbf{q}}}^E(\Omega_{\text{out}}, \Omega)$ , which appears in Eq.(4.1), accounts for all possible Coulomb interaction processes between Cooperon and Fermi sea and we write it as an integral over  $(\bar{\mathbf{q}}, \bar{\omega})$ :

$$\Sigma_{\bar{\mathbf{q}}}^E(\Omega_{\text{out}}, \Omega) = \frac{1}{V} \sum_{\bar{\mathbf{q}}} \int_{-\infty}^{\infty} \frac{d\bar{\omega}}{2\pi} \Sigma_{\bar{\mathbf{q}}, \bar{\mathbf{q}}}^E(\Omega_{\text{out}}, \Omega, \bar{\omega}), \quad (4.7)$$

s.t.  $\Sigma_{\bar{\mathbf{q}}, \bar{\mathbf{q}}}^E(\Omega_{\text{out}}, \Omega, \bar{\omega})$  includes all possible interactions at momentum and energy transfer  $(\bar{\mathbf{q}}, \bar{\omega})$ . In the next section, we will linearize the Bethe-Salpeter equation and present all diagrams which contribute to the self-energy of the Cooperon to first order in interaction.

## 4.2 Linearization of Bethe-Salpeter equation

### 4.2.1 Linearization

The Bethe-Salpeter equation can be linearized in the interaction by making the replacement Eq.(4.3) in all Cooperons which appear in the self-energy  $\Sigma_{\bar{\mathbf{q}}}^E(\Omega_{\text{out}}, \Omega)$ . This replacement leads to an expression for the so-called bare self-energy  $\Sigma_{\bar{\mathbf{q}}}^{1,E}(\Omega_{\text{out}}, \Omega)$ , where the superscript "1" indicates that it consists of diagrams which contribute in first order in interaction. The interaction must be of one of the following types: Either, the interaction line connects to

<sup>1</sup>In the discussion on interactions, we use disorder averaged propagators throughout. The "overbar" is omitted for brevity.

only one electron line of the Cooperon, or it connects to both. In the former case, we speak of self-energy type processes, and in the latter of vertex-type processes, inspired by the nomenclature in [11]. Using the energy convention Eq.(4.4), we display a typical first-order vertex type and a typical first-order self-energy type diagram in Fig.4.2<sup>2</sup>:

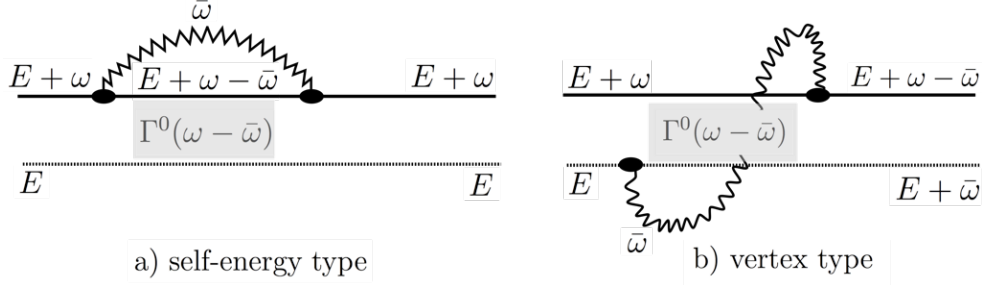


Figure 4.2: Self-energy vs. vertex type diagrams.

For self-energy type diagrams, the energy difference between in-coming upper and lower electron line equals the energy difference between out-going upper and lower line:  $\Omega_{\text{out}} - \Omega_{\text{in}} = 0$ . For vertex type, we have that  $\Omega_{\text{out}} - \Omega_{\text{in}} + 2\bar{\omega} = 0$ . The bare self-energy can be written in the following form:

$$\begin{aligned} \Sigma_{\mathbf{q}}^{1,E}(\Omega_{\text{out}}, \Omega_1) &= \frac{1}{V} \sum_{\mathbf{q}} \int_{-\infty}^{\infty} d\bar{\omega} \times \\ & \left[ \delta(\Omega_{\text{out}} - \Omega_1) \Sigma_{\mathbf{q},\bar{\mathbf{q}}}^{1,E,S}(\Omega_{\text{out}}, \bar{\omega}) \right. \\ & \left. + \delta(\Omega_{\text{out}} - \Omega_1 + 2\bar{\omega}) \Sigma_{\mathbf{q},\bar{\mathbf{q}}}^{1,E,V}(\Omega_{\text{out}}, \bar{\omega}) \right], \end{aligned} \quad (4.8)$$

where  $\Sigma^{1,E,S}$  collects all first-order self-energy type diagrams and  $\Sigma^{1,E,V}$  consists of all first-order vertex-type diagrams with energy-momentum transfer  $(\mathbf{q}, \bar{\omega})$ . In the following, we will show and discuss the diagrams which contribute to  $\Sigma^{1,E}$ , c.f. [11, Eq.(A5)].

## 4.2.2 First-order diagrams

The diagrams contributing to the Cooperon self-energy to first order in the interaction are depicted in Fig.4.3. For clarity, we give meaning to all symbols which appear in the diagrams in Fig.4.4 below. In the bare self-energy diagrams, we distinguish three groups.

- The self-energy type diagrams depicted in Fig.4.3a) are equivalent to the diagrams in Fig.2.6: The diagrams in Fig.4.3a) with Keldysh component of interaction propagators correspond to the two to the left in Fig.2.6, and the diagrams with retarded/advanced component of the interaction propagator correspond to the upper/lower diagram to the right, when keeping only the retarded/advanced part of the Keldysh component of the electronic propagator, c.f. Eq.(2.17).

<sup>2</sup>We suppress the momenta-dependence, as we only want to make an argument concerning energy labels.

- The two diagrams shown in Fig.4.3b) with retarded/advanced component of the interaction propagator derive from the upper/lower diagram to the right in Fig.2.6 by keeping only the advanced/retarded part of the Keldysh component of the electronic Green's function. Thus, instead of free Cooperon propagators, the diagrams in Fig.4.3b) contain a product of four alternating retarded and advanced electronic propagators, denoted as boxes with capital  $R/A$ , referring to the retardation  $R/A$  of the interaction. Those boxes are conveniently called Hikami boxes, and we sketch the calculation of those objects in Appendix H. It is important to note, that although the Hikami diagrams contain two additional diffusion propagators, denoted by the thick bars, they are of the same order in  $\omega\tau$  and  $ql_e$  as the other diagrams, c.f. Eq.(4.9) and Appendix H. Note further, that the Hikami box has to be dressed with additional impurity lines, c.f. Fig.H.1, because this dressing gives contributions of the same order.
- The vertex diagrams depicted in Fig.4.3c) correspond to Fig.2.7.

The diagrams translate into the following analytic expressions:

$$\begin{aligned}
& \frac{1}{2\pi\rho\tau^2} \Sigma_{\mathbf{q},\bar{\mathbf{q}}}^{1,E,S}(\omega, \bar{\omega}) = \\
& + \frac{i}{2} L_{\bar{\mathbf{q}}}^K(\bar{\omega}) [\Gamma_{\mathbf{q}-\bar{\mathbf{q}}}^0(\omega + \bar{\omega}) + \Gamma_{\mathbf{q}-\bar{\mathbf{q}}}^0(\omega - \bar{\omega})] \times 2\pi\rho\tau^2 \\
& + \frac{i}{2} L_{\bar{\mathbf{q}}}^R(\bar{\omega}) \tanh\left(\frac{E + \omega - \bar{\omega}}{2T}\right) \times 2\pi\rho\tau^2 \Gamma_{\mathbf{q}-\bar{\mathbf{q}}}^0(\omega - \bar{\omega}) \\
& - \frac{i}{2} L_{\bar{\mathbf{q}}}^A(\bar{\omega}) \tanh\left(\frac{E - \bar{\omega}}{2T}\right) \times 2\pi\rho\tau^2 \Gamma_{\mathbf{q}-\bar{\mathbf{q}}}^0(\omega + \bar{\omega}) \\
& + \frac{i}{2} L_{\bar{\mathbf{q}}}^R(\bar{\omega}) \tanh\left(\frac{E + \omega - \bar{\omega}}{2T}\right) [2\pi\rho\tau^2 \Gamma_{\bar{\mathbf{q}}}^0(\bar{\omega})]^2 [D(\mathbf{q} - \bar{\mathbf{q}})^2 - i(\omega + \bar{\omega})] \\
& - \frac{i}{2} L_{\bar{\mathbf{q}}}^A(\bar{\omega}) \tanh\left(\frac{E - \bar{\omega}}{2T}\right) [2\pi\rho\tau^2 \Gamma_{-\bar{\mathbf{q}}}^0(-\bar{\omega})]^2 [D(\mathbf{q} - \bar{\mathbf{q}})^2 - i(\omega - \bar{\omega})] \\
& \frac{1}{2\pi\rho\tau^2} \Sigma_{\mathbf{q},\bar{\mathbf{q}}}^{1,E,V}(\omega, \bar{\omega}) = \\
& - \frac{i}{2} \left[ L_{\bar{\mathbf{q}}}^K(\bar{\omega}) + L_{\bar{\mathbf{q}}}^R(\bar{\omega}) \tanh\left(\frac{E + \omega + \bar{\omega}}{2T}\right) - L_{\bar{\mathbf{q}}}^A(\bar{\omega}) \tanh\left(\frac{E}{2T}\right) \right] \times \\
& 2\pi\rho\tau^2 [\Gamma_{\mathbf{q}+\bar{\mathbf{q}}}^0(\omega - \bar{\omega}) + \Gamma_{\mathbf{q}-\bar{\mathbf{q}}}^0(\omega - \bar{\omega})] .
\end{aligned} \tag{4.9}$$

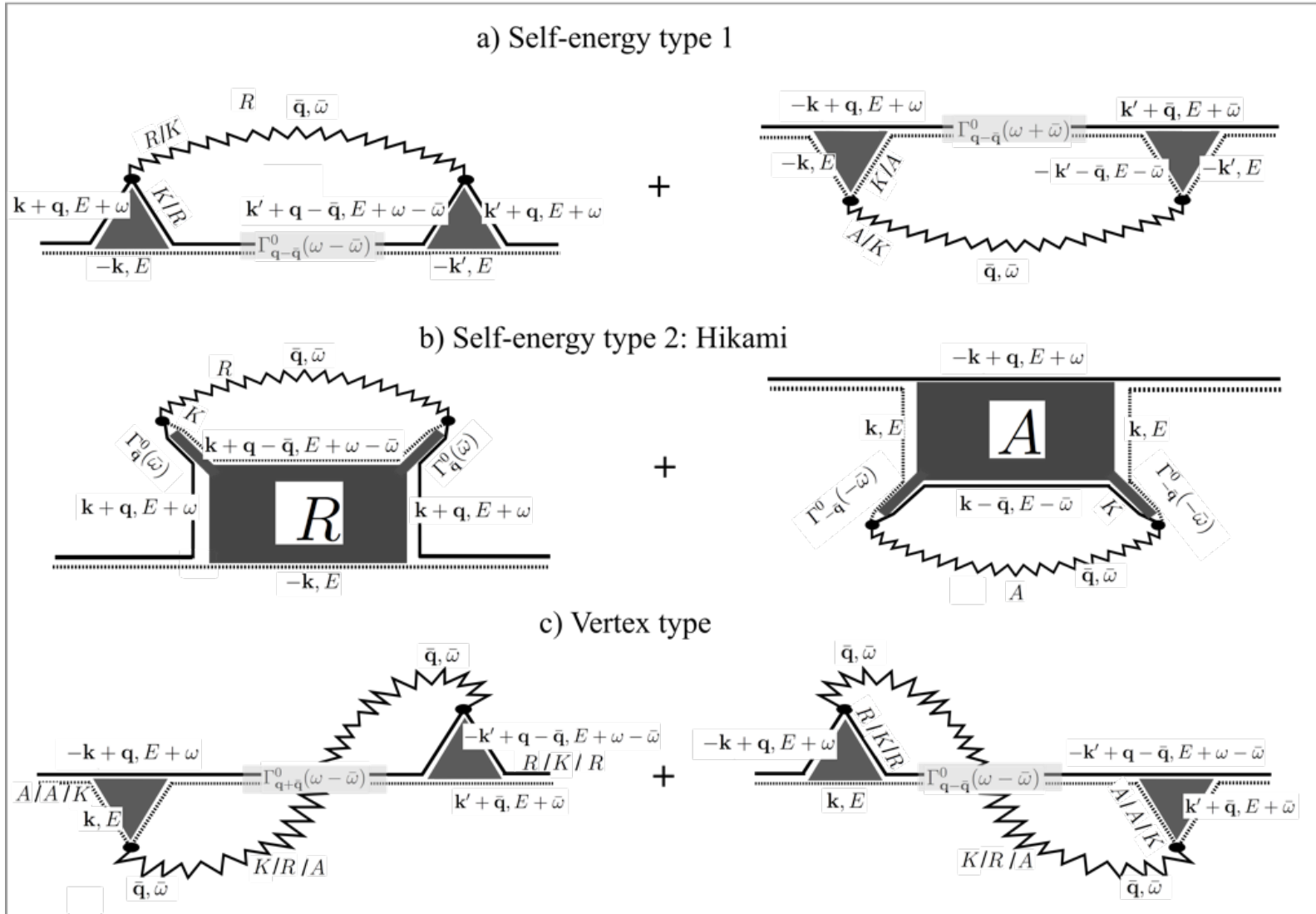


Figure 4.3: Diagrams contributing to the bare self-energy.

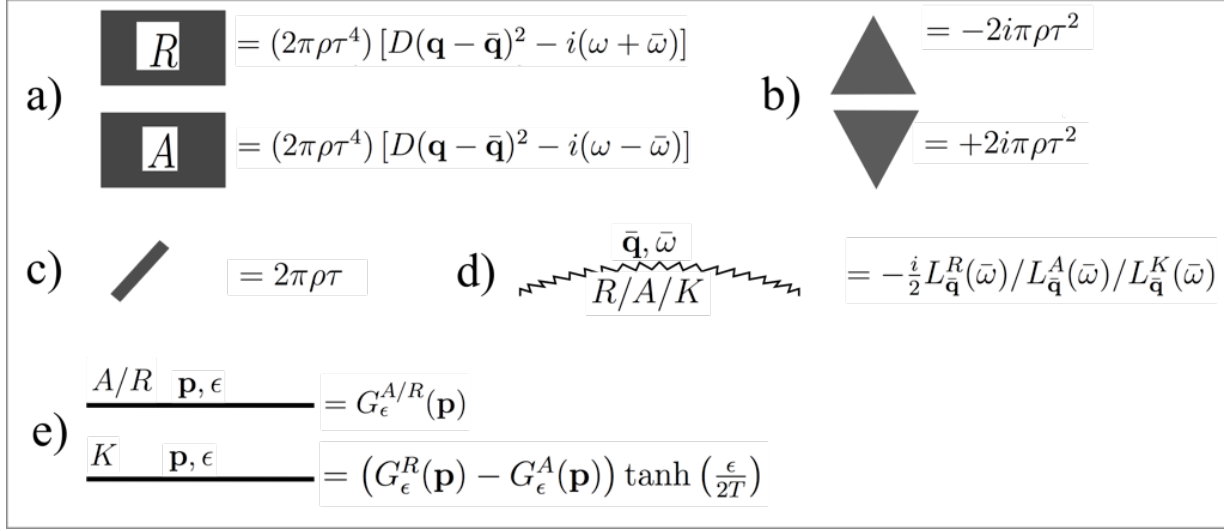


Figure 4.4: Ingredients of self-energy diagrams.

- Energy and momentum are conserved on each interaction vertex.
- The Hikami boxes in a) are derived in Appendix H.
- At the interaction vertices, sums over external momenta of products of three electronic propagators are performed. The retardation of the propagators in those products is either  $RRA$  or  $RAA$ , symbolically written in b) as a triangle pointing up or down, respectively. The sum over those products is performed by the residual calculus or by consulting [5, Table 3.2].
- The bars in c) denote diffusion propagators.
- The wavy lines in d) denote interaction propagators, c.f. Eq.(4.6). The interaction propagators come with a factor of "1/2". This factor accounts for the two vortices in Keldysh space, which bring a factor of  $1/\sqrt{2}$  each, c.f. Eq.(2.26). The additional factor of "i" comes from the usual Feynman rules [16].
- The straight lines in e) denote electronic Green's functions, whose retarded/advanced components are given via Eq.(1.20), and the Keldysh component is related to those via Eq.(2.17).

### 4.2.3 Linearized version of the Bethe-Salpeter equation

We substitute our result for the bare self-energy from Eq.(4.8) into the Bethe-Salpeter equation Eq.(4.1) and thus obtain an equation for a linearized Cooperon  $\Gamma_{\mathbf{q}}^{1,E}(\Omega_{\text{out}}, \omega)$  as follows:

$$\begin{aligned} \Gamma_{\mathbf{q}}^{1,E}(\Omega_{\text{out}}, \omega) &= \Gamma_{\mathbf{q}}^0(\Omega_{\text{out}}) \left[ 2\pi\delta(\Omega_{\text{out}} - \omega) + \int d\Omega \Sigma_{\mathbf{q}}^{1,E}(\Omega_{\text{out}}, \Omega) \Gamma_{\mathbf{q}}^{1,E}(\Omega, \omega) \right], \\ \Sigma_{\mathbf{q}}^{1,E}(\Omega_{\text{out}}, \Omega) &= \frac{1}{V} \sum_{\bar{\mathbf{q}}} \int_{-\infty}^{\infty} d\bar{\omega} \times \\ &\quad \left[ \delta(\Omega_{\text{out}} - \Omega) \Sigma_{\mathbf{q},\bar{\mathbf{q}}}^{1,E,S}(\Omega_{\text{out}}, \bar{\omega}) \right. \\ &\quad \left. + \delta(\Omega_{\text{out}} - \Omega + 2\bar{\omega}) \Sigma_{\mathbf{q},\bar{\mathbf{q}}}^{1,E,V}(\Omega_{\text{out}}, \bar{\omega}) \right], \end{aligned} \quad (4.10)$$

with the energy convention from Eq.(4.4) and  $\Sigma_{\mathbf{q},\bar{\mathbf{q}}}^{1,E,S(V)}(\Omega_{\text{out}}, \Omega, \bar{\omega})$  taken from Eq.(4.9). Eq.(4.10) can be rewritten as follows:

$$\begin{aligned} \Gamma_{\mathbf{q}}^{1,E}(\Omega_{\text{out}}, \omega) &= 2\pi\delta(\Omega_{\text{out}} - \omega) \Gamma_{\mathbf{q}}^0(\Omega_{\text{out}}) \\ &\quad + \Gamma_{\mathbf{q}}^0(\Omega_{\text{out}}) \Sigma_{\mathbf{q}}^{1,E,S}(\Omega_{\text{out}}) \Gamma_{\mathbf{q}}^{1,E}(\Omega_{\text{out}}, \omega) \\ &\quad + \Gamma_{\mathbf{q}}^0(\Omega_{\text{out}}) \frac{1}{V} \sum_{\bar{\mathbf{q}}} \int d\bar{\omega} \Sigma_{\mathbf{q}}^{1,E,V}(\Omega_{\text{out}}, \bar{\omega}) \Gamma_{\mathbf{q}}^{1,E}(\bar{\omega}, \omega), \\ \Sigma_{\mathbf{q}}^{1,E,S}(\Omega_{\text{out}}, \omega) &= \frac{1}{V} \sum_{\bar{\mathbf{q}}} \int_{-\infty}^{\infty} d\bar{\omega} \Sigma_{\mathbf{q},\bar{\mathbf{q}}}^{1,E,S}(\Omega_{\text{out}}, \bar{\omega}), \end{aligned} \quad (4.11)$$

with  $\tilde{\omega} \equiv (\bar{\omega} - \Omega_{\text{out}})/2$ . We remind that for the vertex type diagrams,  $\Omega_{\text{out}} = \omega - 2\bar{\omega}$ .

### 4.2.4 SEO-approximation and Dyson summation

Due to the entangled frequency-dependence of Eq.(4.11), an analytic solution has not been found. However, it is possible to reduce Eq.(4.11) to a Dyson equation, if the vertex part  $\Sigma_{\mathbf{q}}^{1,E,V}(\Omega_{\text{out}}, \tilde{\omega})$  is neglected [11]. We call the corresponding approximation self-energy-only approximation(SEO), to indicate that only self-energy type diagrams are included.

#### Dyson summation

We thus neglect the vertex type diagrams and keep only self-energy type diagrams in Eq.(4.11). We make the following ansatz for the Cooperon propagator  $\Gamma_{\mathbf{q}}^{1,E}(\Omega_{\text{out}}, \omega)$ :

$$\Gamma_{\mathbf{q}}^{1,E}(\Omega_{\text{out}}, \omega) = 2\pi\delta(\Omega_{\text{out}} - \omega) \Gamma_{\mathbf{q}}^{1,E}(\omega), \quad (4.12)$$

which leads to a Dyson equation:

$$\Gamma_{\mathbf{q}}^{1,E}(\omega) = \Gamma_{\mathbf{q}}^0(\omega) \left[ 1 + \Sigma_{\mathbf{q}}^{1,E,S}(\omega) \Gamma_{\mathbf{q}}^{1,E}(\omega) \right], \quad (4.13)$$

and the latter is formally solved by

$$\Gamma_{\mathbf{q}}^{1,E}(\omega) = \frac{1}{2\pi\rho\tau^2} \frac{1}{D\mathbf{q}^2 - i\omega - \frac{1}{2\pi\rho\tau^2}\Sigma_{\mathbf{q}}^{1,E,S}(\omega)}. \quad (4.14)$$

### Self-energy and dephasing time

At this point, we can make contact with the dephasing time  $\tau_\phi$ . Let us separate real and imaginary part in the self-energy  $\Sigma_{\mathbf{q}}^{1,E,S}(\omega)$ :

$$\Gamma_{\mathbf{q}}^{1,E}(\omega) = \frac{\frac{1}{2\pi\rho\tau^2}}{D\mathbf{q}^2 - i \left[ \omega + \Im\Sigma_{\mathbf{q}}^{1,E,S}(\omega) \right] - \frac{1}{2\pi\rho\tau^2}\Re\Sigma_{\mathbf{q}}^{1,E,S}(\omega)}. \quad (4.15)$$

The imaginary part leads to a shift of the AC-frequency, which corresponds to a retardation in the time domain, which we will not touch in this work. The real part of the self-energy corresponds to exponential decay in the time domain, and the dephasing time will be defined in terms of the real part below, c.f. Eq.(4.25).

### 4.2.5 Neglect of vertex terms and infrared divergence

We will see explicitly in due course, that the  $\Sigma_{\mathbf{q}}^{1,E,S}(\omega)$  is infrared divergent in the limit ( $\mathbf{q} = 0, \bar{\omega} = 0$ ) for  $d = 1, 2$ . It will turn out, c.f. Ch.4.3, that the infrared divergence comes from the  $L_{\mathbf{q}}^K(\bar{\omega})$ -terms which contain factors of  $\coth(\bar{\omega}/2T)$ . An infrared divergence is unphysical. The dephasing time  $\tau_\phi$  is associated with a finite life-time of the Cooperon, and since energy transfers  $\bar{\omega} \ll 1/\tau_\phi$  are simply too slow to affect the Cooperon during its life-time, they should not contribute to the self-energy integral. The full linearized self-energy, c.f. Eq.(4.9), is indeed divergence-free. By direct inspection of Eq.(4.9), one confirms that the  $L_{\mathbf{q}}^K(\bar{\omega})$ -terms cancel from the self-energy type and vertex type diagrams in the limit  $\bar{\omega} = 0$ . The neglect of vertex terms thus forces us to deal with an unphysical divergence, and we will cure this divergence by inserting an infrared cut-off by hand into the self-energy integral, which is intended to mimic the infrared behaviour of the full bare self-energy, see Ch.4.3.4 for details.

### 4.3 Cooperon self-energy in SEO-approximation

In the SEO-approximation, which amounts to neglect of vertex contributions to the Cooperon self-energy, the latter is given by  $\Sigma_{\mathbf{q}}^{1,E,S}(\omega)$ , c.f. Eq.(4.9). In this section, we will calculate a spatial average of this quantity with respect to the interaction, and thus we will take the limit  $\mathbf{q} = 0$  henceforth. Since the free Cooperon propagator, c.f.Eq.(1.43), is peaked around  $\mathbf{q} = 0$ , keeping finite  $\mathbf{q}$  would give only small corrections. In the limit  $\mathbf{q} = 0$ , we find the following expression:

$$\begin{aligned} \frac{1}{2\pi\rho\tau^2}\Sigma_{\mathbf{q}=0}^{1,E,S}(\omega) = & \frac{1}{2V} \sum_{\bar{\mathbf{q}}} \int_{-\infty}^{\infty} \frac{d\bar{\omega}}{2\pi} \times \left[ \right. \\ & iL_{\bar{\mathbf{q}}}^K(\bar{\omega}) [\Gamma_{\bar{\mathbf{q}}}^0(\omega + \bar{\omega}) + \Gamma_{\bar{\mathbf{q}}}^0(\omega - \bar{\omega})] \times 2\pi\rho\tau^2 \\ & + iL_{\bar{\mathbf{q}}}^R(\bar{\omega}) \tanh\left(\frac{E + \omega - \bar{\omega}}{2T}\right) \times 2\pi\rho\tau^2\Gamma_{\bar{\mathbf{q}}}^0(\omega - \bar{\omega}) \\ & - iL_{\bar{\mathbf{q}}}^A(\bar{\omega}) \tanh\left(\frac{E - \bar{\omega}}{2T}\right) \times 2\pi\rho\tau^2\Gamma_{\bar{\mathbf{q}}}^0(\omega + \bar{\omega}) \\ & + iL_{\bar{\mathbf{q}}}^R(\bar{\omega}) \tanh\left(\frac{E + \omega - \bar{\omega}}{2T}\right) [2\pi\rho\tau^2\Gamma_{\bar{\mathbf{q}}}^0(\bar{\omega})]^2 [D\bar{\mathbf{q}}^2 - i(\omega + \bar{\omega})] \\ & \left. - iL_{\bar{\mathbf{q}}}^A(\bar{\omega}) \tanh\left(\frac{E - \bar{\omega}}{2T}\right) [2\pi\rho\tau^2\Gamma_{\bar{\mathbf{q}}}^0(-\bar{\omega})]^2 [D\bar{\mathbf{q}}^2 - i(\omega - \bar{\omega})] \right]. \end{aligned} \quad (4.16)$$

Using Eq.(1.43) for the Cooperon structure factor, and rearranging the terms yields:

$$\begin{aligned} \frac{1}{2\pi\rho\tau^2}\Sigma_{\mathbf{q}=0}^{1,E,S}(\omega) = & \frac{1}{2V} \sum_{\bar{\mathbf{q}}} \int_{-\infty}^{\infty} \frac{d\bar{\omega}}{2\pi} \times \left[ \right. \\ & i \left[ L_{\bar{\mathbf{q}}}^K(\bar{\omega}) + L_{\bar{\mathbf{q}}}^R(\bar{\omega}) \tanh\left(\frac{E + \omega - \bar{\omega}}{2T}\right) \right] \frac{1}{D\bar{\mathbf{q}}^2 - i(\omega - \bar{\omega})} \\ & + i \left[ L_{\bar{\mathbf{q}}}^K(\bar{\omega}) - L_{\bar{\mathbf{q}}}^A(\bar{\omega}) \tanh\left(\frac{E - \bar{\omega}}{2T}\right) \right] \frac{1}{D\bar{\mathbf{q}}^2 - i(\omega + \bar{\omega})} \\ & + iL_{\bar{\mathbf{q}}}^R(\bar{\omega}) \tanh\left(\frac{E + \omega - \bar{\omega}}{2T}\right) \frac{D\bar{\mathbf{q}}^2 - i(\omega + \bar{\omega})}{(D\bar{\mathbf{q}}^2 - i\bar{\omega})^2} \\ & \left. - iL_{\bar{\mathbf{q}}}^A(\bar{\omega}) \tanh\left(\frac{E - \bar{\omega}}{2T}\right) \frac{D\bar{\mathbf{q}}^2 - i(\omega - \bar{\omega})}{(D\bar{\mathbf{q}}^2 + i\bar{\omega})^2} \right]. \end{aligned} \quad (4.17)$$

In the second and fifth line of the r.h.s. of Eq.(4.17), we shift  $\bar{\omega} \rightarrow -\bar{\omega}$ . This transformation leaves the integral over  $\bar{\omega}$  invariant and allows us to combine second with third as well as fourth with fifth line. Further we substitute the explicit form of the interaction propagator

components, c.f. Eq.(4.6). Hence,

$$\begin{aligned}
& \frac{1}{2\pi\rho\tau^2}\Sigma_{\mathbf{q}=0}^{1,E,S}(\omega) = \\
& \frac{1}{2\nu V} \sum_{\mathbf{q}} \int_{-\infty}^{\infty} \frac{d\bar{\omega}}{2\pi} \times \left[ \right. \\
& i \left[ \frac{2i\bar{\omega}}{D\bar{\mathbf{q}}^2} \coth\left(\frac{\bar{\omega}}{2T}\right) + \frac{D\bar{\mathbf{q}}^2 + i\bar{\omega}}{2D\bar{\mathbf{q}}^2} \left( \tanh\left(\frac{E + \omega + \bar{\omega}}{2T}\right) + \tanh\left(\frac{E - \bar{\omega}}{2T}\right) \right) \right] \frac{1}{D\bar{\mathbf{q}}^2 - i(\omega + \bar{\omega})} \\
& \left. - \frac{i}{2D\bar{\mathbf{q}}^2} \left[ \tanh\left(\frac{E + \omega - \bar{\omega}}{2T}\right) + \tanh\left(\frac{E + \bar{\omega}}{2T}\right) \right] \frac{D\bar{\mathbf{q}}^2 - i(\omega + \bar{\omega})}{D\bar{\mathbf{q}}^2 - i\bar{\omega}} \right].
\end{aligned} \tag{4.18}$$

Next, we shift  $\bar{\omega} \rightarrow \bar{\omega} - \omega$  in the second line of the r.h.s. of Eq.(4.18) to combine the second with the third line. We obtain:

$$\begin{aligned}
& \frac{1}{2\pi\rho\tau^2}\Sigma_{\mathbf{q}=0}^{1,E,S}(\omega) = \\
& -\frac{1}{2\pi\nu V} \sum_{\mathbf{q}} \int_{-\infty}^{\infty} \frac{d\bar{\omega}}{D\bar{\mathbf{q}}^2(D\bar{\mathbf{q}}^2 - i\bar{\omega})} \times \\
& \left[ (\bar{\omega} - \omega) \coth\left(\frac{\bar{\omega} - \omega}{2T}\right) + \frac{\bar{\omega}}{2} \left[ \tanh\left(\frac{E + \omega - \bar{\omega}}{2T}\right) + \tanh\left(\frac{E + \bar{\omega}}{2T}\right) \right] \right].
\end{aligned} \tag{4.19}$$

### 4.3.1 Electronic energy averaging

A finite external frequency  $\omega$  changes the energy statistics of the electrons, since the electrons may get excited by the external field. To take this effect into account, we average our final results for  $\Gamma_{\mathbf{q}=0}^{1,E}(\omega)$  over electronic energy  $E$ . This average is defined as follows, c.f. [11, Eq.(4)]:

$$\langle \dots \rangle_E = - \int_{-\infty}^{+\infty} dE \frac{f(E + \omega) - f(E)}{\omega} (\dots), \tag{4.20}$$

Instead of averaging  $\Gamma_{\mathbf{q}=0}^{1,E}(\omega)$  directly, we adopt an approximation and only replace  $\Sigma_{\mathbf{q}=0}^{1,E,S}(\omega)$  with its average  $\langle \Sigma_{\mathbf{q}=0}^{1,E,S}(\omega) \rangle_E$ , see the discussion after [10, Eq.24] for arguments for the validity of this approximation. To calculate  $\langle \Sigma_{\mathbf{q}=0}^{1,E,S}(\omega) \rangle_E$ , we need the averages of  $\tanh((E + \omega - \bar{\omega})/2T)$  and  $\tanh((E + \bar{\omega})/2T)$ , as apparent from Eq.(4.19). The explicit

calculation of these averages is found in Sec.D, and the results are given as follows:

$$\begin{aligned} \left\langle \tanh \left( \frac{E + \omega - \bar{\omega}}{2T} \right) \right\rangle_E &= \frac{\bar{\omega} - \omega}{\omega} \coth \left( \frac{\bar{\omega} - \omega}{2T} \right) - \frac{\bar{\omega}}{\omega} \coth \left( \frac{\bar{\omega}}{2T} \right) \\ \left\langle \tanh \left( \frac{E + \bar{\omega}}{2T} \right) \right\rangle_E &= -\frac{\bar{\omega}}{\omega} \coth \left( \frac{-\bar{\omega}}{2T} \right) - \frac{-\bar{\omega} + \omega}{\omega} \coth \left( \frac{-\bar{\omega} + \omega}{2T} \right). \end{aligned} \quad (4.21)$$

We insert Eq.(4.21) into Eq.(4.19) and after rearranging terms, we find:

$$\begin{aligned} \frac{1}{2\pi\rho\tau^2} \left\langle \Sigma_{\mathbf{q}=0}^{1,E,S}(\omega) \right\rangle_E &= \frac{1}{2\pi\nu V} \sum_{\bar{\mathbf{q}}} \int_{-\infty}^{\infty} \frac{d\bar{\omega}}{D\bar{\mathbf{q}}^2 - i\bar{\omega}} \frac{\bar{\omega}^2}{\omega D\bar{\mathbf{q}}^2} \left[ \coth \left( \frac{\bar{\omega}}{2T} \right) - \coth \left( \frac{\bar{\omega} - \omega}{2T} \right) \right] \\ &+ \frac{1}{2\pi\nu V} \sum_{\bar{\mathbf{q}}} \int_{-\infty}^{\infty} \frac{d\bar{\omega}}{D\bar{\mathbf{q}}^2 - i\bar{\omega}} \frac{\omega}{D\bar{\mathbf{q}}^2} \coth \left( \frac{\bar{\omega} - \omega}{2T} \right). \end{aligned} \quad (4.22)$$

In the r.h.s. of Eq.(4.22), we symmetrize the integrands and furthermore separate real and imaginary part. We obtain for the real part:

$$\frac{1}{2\pi\rho\tau^2} \left\langle \Sigma_{\mathbf{q}=0}^{1,E,S}(\omega) \right\rangle_E = \frac{1}{\pi\nu V} \sum_{\bar{\mathbf{q}}} \int_0^{\infty} \frac{d\bar{\omega}}{D^2\bar{\mathbf{q}}^4 + \bar{\omega}^2} \frac{\bar{\omega}^2 - \omega^2}{4\omega} \left[ \coth \left( \frac{\bar{\omega} + \omega}{2T} \right) - \coth \left( \frac{\bar{\omega} - \omega}{2T} \right) \right], \quad (4.23)$$

and the imaginary part is given by:

$$\begin{aligned} \frac{1}{2\pi\rho\tau^2} \left\langle \Im \Sigma_{\mathbf{q}=0}^{\text{SOA}}(\omega) \right\rangle_E &= \frac{1}{\pi\nu V} \sum_{\bar{\mathbf{q}}} \int_0^{\infty} \frac{d\bar{\omega}}{D^2\bar{\mathbf{q}}^4 + \bar{\omega}^2} \frac{\bar{\omega}^3}{4\omega D\bar{\mathbf{q}}^2} \left[ 2 \coth \left( \frac{\bar{\omega}}{2T} \right) - \coth \left( \frac{\bar{\omega} + \omega}{2T} \right) - \coth \left( \frac{\bar{\omega} - \omega}{2T} \right) \right] \\ &+ \frac{1}{\pi\nu V} \sum_{\bar{\mathbf{q}}} \int_0^{\infty} \frac{d\bar{\omega}}{D^2\bar{\mathbf{q}}^4 + \bar{\omega}^2} \frac{\omega\bar{\omega}}{4D\bar{\mathbf{q}}^2} \left[ \coth \left( \frac{\bar{\omega} + \omega}{2T} \right) + \coth \left( \frac{\bar{\omega} - \omega}{2T} \right) \right]. \end{aligned} \quad (4.24)$$

The imaginary part will not be considered further.

### 4.3.2 Energy-averaged dephasing rate

We define the energy-averaged dephasing rate of the Cooperon due to interactions,  $1/\tau_\phi$ , in terms of the real part of the self-energy Eq.(4.23) as follows:

$$\frac{1}{\tau_\phi}(\omega) = -\frac{1}{2\pi\rho\tau^2} \left\langle \Re \Sigma_{\mathbf{q}=0}^{1,E,S}(\omega) \right\rangle_E, \quad (4.25)$$

such that

$$\frac{1}{\tau_\phi}(\omega) = -\frac{1}{\pi\nu V} \sum_{\mathbf{q}} \int_{\Omega}^{\infty} \frac{d\bar{\omega}}{D^2\bar{\mathbf{q}}^4 + \bar{\omega}^2} \frac{\bar{\omega}^2 - \omega^2}{4\omega} \left[ \coth\left(\frac{\bar{\omega} + \omega}{2T}\right) - \coth\left(\frac{\bar{\omega} - \omega}{2T}\right) \right]. \quad (4.26)$$

In the integral in Eq.(4.26), we have introduced a finite infrared cut-off frequency  $\Omega$ , which is needed because the integral diverges in the infrared limit for  $d = 1, 2$ . In  $d = 3$ , the integral is finite. This divergence is an artefact of our neglect of vertex contributions, as noted before. We will specify our particular choice for  $\Omega$  in Ch. 4.3.4 below.

### 4.3.3 Energy-averaged spectrum

We write Eq.(4.26) as follows:

$$\frac{1}{\tau_\phi}(\omega) = +\frac{1}{\pi\nu V} \sum_{\mathbf{q}} \int_{\Omega}^{\infty} \frac{d\bar{\omega}}{D^2\bar{\mathbf{q}}^4 + \bar{\omega}^2} W(T, \omega, \bar{\omega}), \quad (4.27)$$

where the energy-averaged spectrum or weighting function  $W(T, \omega, \bar{\omega})$  is defined as follows:

$$W(T, \omega, \bar{\omega}) = -\frac{\bar{\omega}^2 - \omega^2}{4\omega} \left[ \coth\left(\frac{\bar{\omega} + \omega}{2T}\right) - \coth\left(\frac{\bar{\omega} - \omega}{2T}\right) \right]. \quad (4.28)$$

It is instructive to check the limiting cases of  $W(T, \omega, \bar{\omega})$ . An asymptotic analysis yields

$$\begin{aligned} W(\bar{\omega} \ll \omega \ll T) &\rightarrow T \\ W(\omega \ll \bar{\omega} \ll T) &\rightarrow T \\ W(\omega \ll T \ll \bar{\omega}) &\rightarrow T(\bar{\omega}/T)^2 e^{-\bar{\omega}/T} \\ W(\bar{\omega} \ll T \ll \omega) &\rightarrow T \\ W(T \ll \bar{\omega} \ll \omega) &\rightarrow \omega/2 \\ W(T \ll \omega \ll \bar{\omega}) &\rightarrow (\omega/2)(\bar{\omega}/\omega)^2 e^{(\omega-\bar{\omega})/T}. \end{aligned} \quad (4.29)$$

From this analysis we infer that our theory properly incorporates the Pauli principle. To see this, consider first the case  $\omega \ll T$ . In this case, transfer energies  $\bar{\omega} \gg T$  are exponentially suppressed, with the spectrum behaving as  $\sim \bar{\omega}^2 \exp -\bar{\omega}/T$  when  $\bar{\omega} \rightarrow \infty$ . In the case  $\omega \gg T$ , the AC-frequency plays the role of temperature, in the sense that now, transfer energies  $\bar{\omega} \gg \omega$  are suppressed. This reflects the fact, that a finite AC-frequency extends the phase space for electron-electron scattering. That the AC-driving plays the role of temperature in the regime  $\omega \gg T$  also becomes apparent by comparison of the first and fifth limit in Eq.(4.29). In the limit  $\omega = 0$ , we obtain from Eq.(4.28):

$$W(T, \omega, \bar{\omega}) = T \left[ \frac{\bar{\omega}/2T}{\sinh\left(\frac{\bar{\omega}}{T}\right)} \right]^2, \quad (4.30)$$

which is the result calculated by von Delft et al. [10, Eq.(70)]. The authors derived this result using a functional influence approach, hence it is nice to see the coincidence here. On the l.h.s. of Fig.4.5, we provide a plot of  $W(T, \omega, \bar{\omega})$  as a function of  $\bar{\omega}$  for different values of  $\omega$ , and on the r.h.s., we show a three-dimensional plot of  $2W(T, \omega, \bar{\omega})/T$  vs.  $\bar{\omega}/2T$  and  $\omega/2T$ . It is clearly apparent from Fig.4.5, that the phase space is extended as  $\omega$  grows.

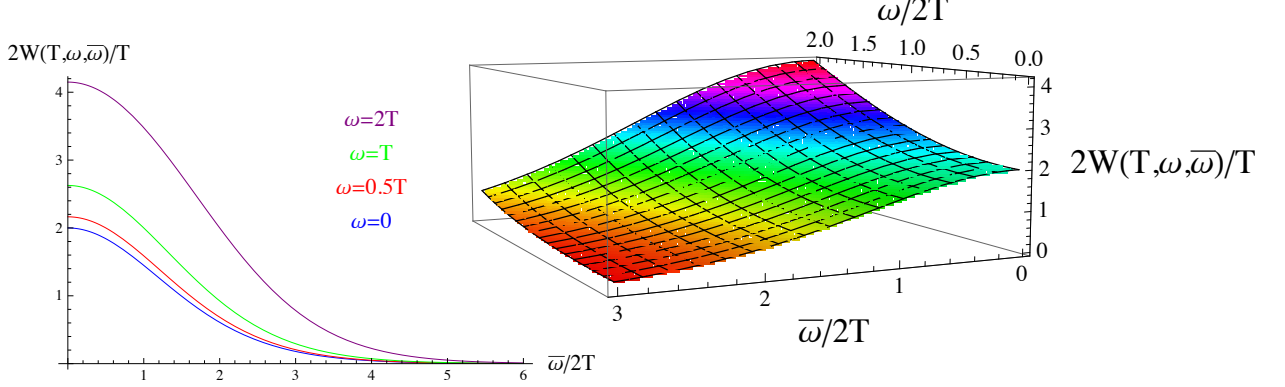


Figure 4.5: Spectrum  $W(T, \omega, \bar{\omega})$ .

After this short discussion on the spectrum of the interaction, we now turn to the specific choice for the infra-red cutoff  $\Omega$ .

#### 4.3.4 Self-consistent infrared cut-off treatment

The infrared cut-off  $\Omega$  is chosen in the following way:

$$\Omega = \sqrt{\omega^2 + \frac{1}{\tau_\phi^2}}, \quad (4.31)$$

For  $\omega \ll 1/\tau_\phi$ , this choice reproduces a self-consistent treatment of  $\tau_\phi$ , which is motivated as follows: Since modes  $\bar{\omega} \ll 1/\tau_\phi$  are simply too slow to affect the Cooperon during its life-time  $\tau_\phi$ , they do not contribute to dephasing. Hence, the cut-off should be provided by  $1/\tau_\phi$  itself. Consider  $\omega \gg 1/\tau_\phi$ . Here, as apparent from relation Eq.(4.15), the dephasing is dominated by the AC-frequency itself. A finite AC-frequency corresponds to oscillations of the Cooperon amplitude in the time-domain. On time scales  $t \gg 1/\omega$ , the Cooperon vanishes to zero, hence for  $\omega \gg 1/\tau_\phi$ , the Cooperon dephasing is mainly due to  $\omega$ . In the limit  $\omega \gg 1/\tau_\phi$ ,  $\Omega \sim \omega$ . From the discussion in Ch.4.3.3, we also have the ultra-violet cut-off  $\omega$ , such that the window for  $\bar{\omega}$  becomes very small. We will see below in Ch.5, that this leads to very weak dephasing. Again, this is consistent, since for  $1/\tau_\phi$ , dephasing should be due to AC-frequency merely than due to interactions. Our choice Eq.(4.31) for the cut-off takes care of the two limiting cases in a symmetric way and is hence considered a reasonable model, which, however, can only be confirmed after a calculation including the vertex contributions has been performed.

# Chapter 5

## Dephasing in large system-size limit

### 5.1 Large system-size limit and regimes

#### 5.1.1 Quasi-infinite limit

We consider disordered metals of very large but finite volume  $L^d$ . In a finite volume, the smallest possible value of the internal momentum  $\bar{q}$  is of order of  $1/L$ . As long as  $D/L^2 \equiv E_{\text{th}} \ll \Omega$ , a replacement of the sum over internal momenta in Eq.(4.27) with an integral is valid. From Eq.(4.31),  $\Omega > 1/\tau_\phi$ . We define the limit of large system-size as the limit in which the Thouless energy is smaller than the dephasing rate, i.e.  $E_{\text{th}} \ll 1/\tau_\phi$ . In this limit, the energy-averaged dephasing rate is given by the following expression, which is derived from Eq.(4.27) in Appendix F:

$$\frac{1}{\tau_\phi}(\omega) = \frac{c_d(E_{\text{th}})^{1-d/2}}{g_d} \int_{\Omega}^{\infty} \frac{d\bar{\omega}}{\bar{\omega}^{2-d/2}} W(T, \omega, \bar{\omega}). \quad (5.1)$$

$c_d$  is a small constant of order  $\mathcal{O}(10^{-d})$  and  $g_d$  is the dimensionless conductance. We will always assume good conductors, hence  $g_d \gg 1$ . The cut-off  $\Omega$  is given by Eq.(4.31) and the weighting function is defined by Eq.(4.28).

#### 5.1.2 Energy scales and regimes

We consider four energy scales. Temperature  $T$ , AC-frequency  $\omega$ , dephasing  $1/\tau_\phi$  and Thouless energy  $E_{\text{th}}$ . In general, we would thus have 24 possible orderings of them with respect to magnitude. However, this number is severely reduced by constraints, as we would like to discuss. In the regime of weak localization, the relation  $T\tau_\phi \gg 1$  holds [8]. Further, we have  $E_{\text{th}} \ll 1/\tau_\phi$ , from the discussion in Ch.5.1.1. Thus, we have the fixed ordering  $E_{\text{th}} \ll 1/\tau_\phi \ll T$ , and hence there are only four possible orderings left: It is the question where to put  $\omega$ . In our analysis, we will divide as follows: The external frequency can be a) larger or b) smaller than temperature. If smaller, i.e. in the high-temperature regime, both  $\omega \ll 1/\tau_\phi$  and  $1/\tau_\phi \ll \omega$  are possible. In the former case, we may have

$\omega \ll E_{\text{th}}$  or  $E_{\text{th}} \ll \omega$ , in the latter  $E_{\text{th}} \ll 1/\tau_\phi \ll \omega$ . If the AC-frequency exceeds the temperature scale, in the so-called AC-regime, then  $E_{\text{th}} \ll 1/\tau_\phi \ll T \ll \omega$ . We give a sketch of those four regimes in Fig.5.1, and the rest of this chapter is devoted to examine  $1/\tau_\phi$  in all four regions of this "phase diagram", for all effective dimensions  $d = 1, 2, 3$ .

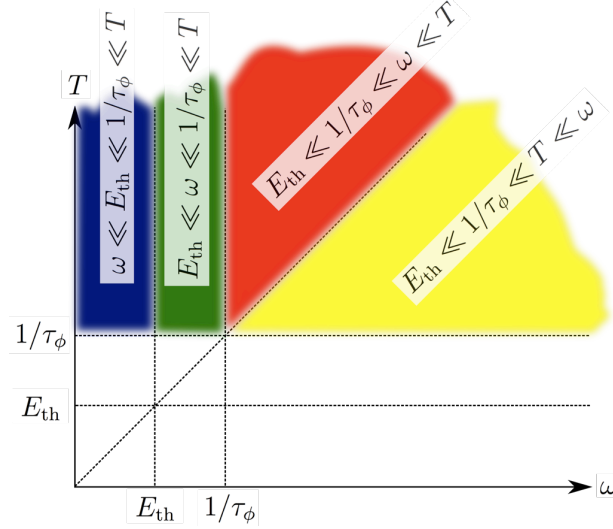


Figure 5.1: Phase diagram for the dephasing rate  $1/\tau_\phi$  as a function of  $(\omega, T)$ .

## 5.2 Calculation of the dephasing rate

### 5.2.1 Prerequisites

For calculational use, we make the integral in Eq.(5.1) dimension-less by the transformation  $\xi = \bar{\omega}/2T$  and obtain

$$\frac{1}{\tau_\phi}(\theta) = -\frac{c_d E_{\text{th}}}{g_d} \left(\frac{2T}{E_{\text{th}}}\right)^{d/2} \int_{\Delta}^{\infty} \frac{d\xi}{\xi^{2-d/2}} \frac{\xi^2 - \theta^2}{4\theta} [\coth(\xi + \theta) - \coth(\xi - \theta)], \quad (5.2)$$

where  $\Delta = \Omega/2T$  is given by Eq.(4.31), and  $\theta = \omega/2T$ . The regimes introduced in Sec.5.1.2 are characterized as follows in terms of the dimension-less parameters, as immediately verified by use of Eq.(4.31):

$$\begin{aligned} E_{\text{th}} \ll \omega \ll 1/\tau_\phi \ll T &\rightarrow \theta \ll \Delta \ll 1 \\ \omega \ll E_{\text{th}} \ll 1/\tau_\phi \ll T &\rightarrow \theta \ll \Delta \ll 1 \\ E_{\text{th}} \ll 1/\tau_\phi \ll \omega \ll T &\rightarrow \theta \approx \Delta \ll 1 \\ E_{\text{th}} \ll 1/\tau_\phi \ll T \ll \omega &\rightarrow 1 \ll \theta \approx \Delta. \end{aligned}$$

We will now examine Eq.(5.2) in all of those regimes for  $d = 1, 2, 3$ .

## 5.2.2 Dephasing in the high-temperature regime

### General considerations

We will start and consider external frequencies much smaller than temperature. As long as  $\omega/T \ll 1$ , we have also  $\theta \ll 1$  and  $\Delta \ll 1$ . This motivates an expansion of the integrand in Eq.(5.2) in powers of  $\theta$ . We find

$$\frac{\xi^2 - \theta^2}{4\theta} [\coth(\xi + \theta) - \coth(\xi - \theta)] = -\frac{\xi^2}{2 \sinh^2 \xi} \left[ 1 + \theta^2 \left( \coth^2 \xi - \frac{1}{\xi^2} - \frac{1}{3} \right) + \mathcal{O}(\theta^4) \right], \quad (5.3)$$

We substitute Eq.(5.3) into Eq.(5.2). The result is written in the form

$$\frac{1}{\tau_\phi}(\theta) = \frac{c_d E_{\text{th}}}{2g_d} \left( \frac{2T}{E_{\text{th}}} \right)^{d/2} \left[ \left( 1 + \frac{\theta^2}{3} \right) \int_{\Delta}^{\infty} \frac{\xi^{d/2} d\xi}{\sinh^2 \xi} + \theta^2 \int_{\Delta}^{\infty} \frac{\xi^{d/2} d\xi}{\sinh^2 \xi} \left( \coth^2 \xi - \frac{1}{\xi^2} - \frac{2}{3} \right) \right]. \quad (5.4)$$

There is no general analytic solutions to the integrals in Eq.(5.4), and hence we will perform an asymptotic analysis. This analysis is carried out in Appendix G. We obtain the following result, valid up to leading order in  $\Delta$  and  $\theta$ :

$$\frac{1}{\tau_\phi}(\theta) = \left\{ \begin{array}{l} \frac{c_1}{g_1} \sqrt{\frac{2TE_{\text{th}}}{\Delta}} \left( 1 - 0.915\sqrt{\Delta} + \frac{\theta^2}{3} \right), \quad d = 1 \\ \frac{c_2 T}{g_2} \left[ \ln \frac{1}{\Delta} \left( 1 + \frac{\theta^2}{3} \right) + 1 - \ln 2 + \frac{\Delta^2}{6} \right], \quad d = 2 \\ \frac{2.456c_3 T}{g_3} \sqrt{\frac{2T}{E_{\text{th}}}} [1 - 0.814\Delta^{1/2} + 0.174\theta^2], \quad d = 3 \end{array} \right\}, \quad (5.5)$$

### Dephasing in the regime $\omega \ll 1/\tau_\phi \ll T$

We consider  $\Delta$  in the limit  $\omega \ll 1/\tau_\phi \ll T$  and obtain from Eq.(4.31):

$$\Delta = \frac{\Omega}{2T} = \frac{1}{2T\tau_\phi} \left[ 1 + \frac{(\omega\tau_\phi)^2}{2} + \mathcal{O}[(\omega\tau_\phi)^4] \right]. \quad (5.6)$$

The latter result is used in Eq.(5.5) and leads to the following implicit equations for  $\tau_\phi(\omega)$ , to leading order in all the small parameters  $1/T\tau_\phi$ ,  $\omega\tau_\phi$  and  $\omega/T$ :

$$\frac{1}{\tau_\phi}(\omega) = \left\{ \begin{array}{l} \frac{2c_1T}{g_1} \sqrt{E_{\text{th}}\tau_\phi} \left[ 1 - \frac{(\omega\tau_\phi)^2}{4} - \frac{0.915}{\sqrt{2T\tau_\phi}} + \frac{1}{12} \left( \frac{\omega}{T} \right)^2 \right], \quad d = 1 \\ \frac{c_2T}{g_2} \ln(T\tau_\phi) \left[ 1 + \frac{1}{\ln(T\tau_\phi)} - \frac{1}{2\ln(T\tau_\phi)} (\omega\tau_\phi)^2 + \frac{\ln(2T\tau_\phi)}{12\ln(T\tau_\phi)} \left( \frac{\omega}{T} \right)^2 \right], \quad d = 2 \\ \frac{2.456c_3T}{g_3} \sqrt{\frac{2T}{E_{\text{th}}}} \left[ 1 - \frac{0.814}{\sqrt{2T\tau_\phi}} \left( 1 + \frac{(\omega\tau_\phi)^2}{4} \right) + 0.041 \left( \frac{\omega}{T} \right)^2 \right], \quad d = 3 \end{array} \right\}. \quad (5.7)$$

We are interested in the leading corrections from finite external frequency and temperature. Thus, in Eq.(5.7), we compare the corrections using the restriction  $\omega \ll 1/\tau_\phi \ll T$ . For  $d = 1$ , the first and second correction cannot be directly compared by this relation, and we will discuss their relative importance in Ch.6.1. Since  $(\omega/T)/(\omega\tau_\phi) = 1/T\tau_\phi \ll 1$ , and  $(\omega/T)^2/(1/\sqrt{T\tau_\phi}) = (\omega\tau_\phi)^2/(T\tau_\phi)^{3/2} \ll 1$ , we neglect the third correction. In  $d = 2, 3$ , the third correction is neglected for similar arguments. We thus obtain:

$$\frac{1}{\tau_\phi}(\omega) = \left\{ \begin{array}{l} \frac{2c_1T}{g_1} \sqrt{E_{\text{th}}\tau_\phi} \left[ 1 - \frac{(\omega\tau_\phi)^2}{4} - \frac{0.915}{\sqrt{2T\tau_\phi}} \right], \quad d = 1 \\ \frac{c_2T}{g_2} \ln(T\tau_\phi) \left[ 1 + \frac{1}{\ln(T\tau_\phi)} - \frac{1}{2\ln(T\tau_\phi)} (\omega\tau_\phi)^2 \right], \quad d = 2 \\ \frac{2.456c_3T}{g_3} \sqrt{\frac{2T}{E_{\text{th}}}} \left[ 1 - \frac{0.814}{\sqrt{2T\tau_\phi}} \left( 1 + \frac{(\omega\tau_\phi)^2}{4} \right) \right], \quad d = 3 \end{array} \right\}. \quad (5.8)$$

We emphasize that our leading results parametrically coincide with those obtained by von Delft et al. in the DC-limit within a influence functional approach [10, Eq.(74)]. Further, the leading temperature correction which they wrote in [10, Eq.(75)] parametrically match our leading temperature corrections. The achievement of the present calculation is the prediction of the leading correction which arises from finite AC-frequency. We will discuss on the latter below, in Ch.6.1. We want to obtain explicit expressions for  $\tau_\phi$  and hence iterate Eq.(5.8). To this end, we find:

$$\frac{1}{\tau_\phi}(\omega) = \left\{ \begin{array}{l} \left( \frac{2c_1T\sqrt{E_{\text{th}}}}{g_1} \right)^{2/3} \left[ 1 - \frac{1}{6} \left( \frac{g_1^2\omega^3}{4c_1^2T^2E_{\text{th}}} \right)^{2/3} - 0.610 \left( \frac{c_1^2E_{\text{th}}}{2g_1^2T} \right)^{1/6} \right], \quad d = 1 \\ \frac{c_2T}{g_2} \ln \left( \frac{g_2}{c_2} \right) \left[ 1 + \frac{1}{\ln(g_2/c_2)} \left[ 1 - \frac{1}{2} \left( \frac{g_2\omega}{c_2T \ln(g_2/c_2)} \right)^2 \right] \right], \quad d = 2 \\ \frac{2.456c_3T}{g_3} \sqrt{\frac{2T}{E_{\text{th}}}} \left[ 1 - 1.517 \left( \frac{c_3^2T}{g_3^2E_{\text{th}}} \right)^{1/4} \left[ 1 + 0.021 \left( \frac{g_3^2\omega^2E_{\text{th}}}{c_3^2T^3} \right) \right] \right], \quad d = 3 \end{array} \right\}. \quad (5.9)$$

To find an explicit result in  $d = 2$ , we used  $1 \ll \ln(T\tau_\phi) \ll g_2/c_2$ , which is straightforward to check. Note that in  $d = 2, 3$ , the frequency corrections are parametrically small with respect to the temperature corrections. In the quasi-one-dimensional case, we will see that the frequency correction can dominate the temperature correction, c.f. Ch.6.1.

### Dephasing in the regime $1/\tau_\phi \ll \omega \ll T$

In this regime, we expand  $\Delta$  as follows:

$$\Delta = \frac{\Omega}{2T} = \frac{\omega}{2T} \left[ 1 + \frac{1}{2(\omega\tau_\phi)^2} + \mathcal{O} \left[ \frac{1}{(\omega\tau_\phi)^4} \right] \right]. \quad (5.10)$$

We see from this expansion, that corrections in  $1/\omega\tau_\phi$  are always subleading in the present regime, since they always come with an additional factor  $\omega/T \ll 1$ . Inserting the expansion into Eq.(5.5), we find the following results, accurate to leading order in  $1/\omega\tau_\phi$  and  $\omega/T$ :

$$\frac{1}{\tau_\phi} = \left\{ \begin{array}{l} \frac{2c_1T}{g_1} \sqrt{\frac{E_{\text{th}}}{\omega}} \left[ 1 - 0.915 \sqrt{\frac{\omega}{2T}} - \frac{1}{4(\omega\tau_\phi)^2} \right], \quad d = 1 \\ \frac{c_2T}{g_2} \ln \left( \frac{T}{\omega} \right) \left[ 1 + \frac{1}{\ln \left( \frac{T}{\omega} \right)} \left[ 1 - \frac{1}{2(\omega\tau_\phi)^2} \right] \right], \quad d = 2 \\ \frac{2.456c_3T}{g_3} \sqrt{\frac{2T}{E_{\text{th}}}} \left[ 1 - 0.814 \sqrt{\frac{\omega}{2T}} \left( 1 + \frac{1}{4(\omega\tau_\phi)^2} \right) \right], \quad d = 3 \end{array} \right\}, \quad (5.11)$$

In the present regime,  $(\omega/T)/(1/\omega\tau_\phi) = (\omega\tau_\phi)^2/T\tau_\phi$ , which can not be estimated in general. Hence, we expect that in  $d = 1$ , the corrections can compete. We will discuss this competition in Ch.6.2. In  $d = 2, 3$ , the  $(1/\omega\tau_\phi)$ -correction is sub-subleading, as pointed out above. In  $d = 1$ , we find an explicit expression for  $\tau_\phi(\omega)$  by iteration, and in  $d = 2, 3$ , we neglect sub-subleading corrections:

$$\frac{1}{\tau_\phi} = \left\{ \begin{array}{l} \frac{2c_1T}{g_1} \sqrt{\frac{E_{\text{th}}}{\omega}} \left[ 1 - 0.915 \sqrt{\frac{\omega}{2T}} - \frac{c_1^2 T^2 E_{\text{th}}}{g_1^2 \omega^3} \right], \quad d = 1 \\ \frac{c_2T}{g_2} \ln \left( \frac{T}{\omega} \right) \left[ 1 + \frac{1}{\ln \left( \frac{T}{\omega} \right)} \right], \quad d = 2 \\ \frac{2.456c_3T}{g_3} \sqrt{\frac{2T}{E_{\text{th}}}} \left[ 1 - 0.814 \sqrt{\frac{\omega}{2T}} \right], \quad d = 3 \end{array} \right\}, \quad (5.12)$$

The discussion of the results obtain above is devoted to Ch.6.2. We emphasize that in the present regime, the dependence of  $\tau_\phi$  on AC-frequency is leading in  $d = 1, 2$ , and to our knowledge, this regime was not examined before.

### 5.2.3 Dephasing in the AC-regime $\omega \gg T$

If  $\theta \gg 1$ , the cut-off  $\Delta \gg 1$ . We perform the shift  $\xi \rightarrow \xi + \theta$  on the integral in Eq.(5.2) and obtain the expression

$$\frac{1}{\tau_\phi}(\theta) = -\frac{c_d E_{\text{th}}}{g_d} \left( \frac{2T}{E_{\text{th}}} \right)^{d/2} \int_{\delta}^{\infty} \frac{d\xi}{(\xi + \theta)^{2-d/2}} \frac{\xi(\xi + 2\theta)}{4\theta} [\coth(\xi + 2\theta) - \coth \xi], \quad (5.13)$$

where  $\delta \ll 1$ , c.f. Eq.(4.31). More precisely:

$$\delta = \frac{\Omega - \omega}{2T} = \frac{1}{4T\tau_\phi^2\omega} \left[ 1 + \mathcal{O} \left[ \frac{1}{(\omega\tau_\phi)^2} \right] \right]. \quad (5.14)$$

Next we will perform an expansion of the integrand in Eq.(5.2) in powers of  $\xi/\theta$ . Since the integrand goes as  $\xi^{d/2} \exp(-2\xi)$  when  $\xi \rightarrow \infty$ , only  $\xi$  up to  $\mathcal{O}(1)$  contribute substantially to the integral, and the error in keeping only leading powers of  $\xi/\theta$  is exponentially small. We rewrite Eq.(5.13) in terms of powers of  $\xi/\theta$ :

$$\frac{1}{\tau_\phi}(\theta) = -\frac{c_d E_{\text{th}}}{4g_d} \left( \frac{\omega}{E_{\text{th}}} \right)^{d/2} \frac{1}{\theta} \int_{\delta}^{\infty} d\xi \frac{2(\xi/\theta) + (\xi/\theta)^2}{(1 + \xi/\theta)^{2-d/2}} [\coth(\xi + 2\theta) - \coth \xi], \quad (5.15)$$

We set  $\coth(\xi + 2\theta) = 1$  in Eq.(5.15), which amounts to neglect of exponentially small corrections. Further, we expand the integrand in  $(\xi/\theta)$  and are thus left with

$$\frac{1}{\tau_\phi}(\theta) = \frac{c_d E_{\text{th}}}{2g_d} \left( \frac{\omega}{E_{\text{th}}} \right)^{d/2} \frac{1}{\theta^2} \int_{\delta}^{\infty} d\xi \left[ \xi + \frac{(3-d/2)}{\theta} \xi^2 + \mathcal{O} \left( \frac{1}{\theta^2} \right) \right] (\coth \xi - 1). \quad (5.16)$$

Using Eqs.(E.2),(E.3) and the following expansion:

$$\xi(\coth \xi - 1) = 1 - \xi + \frac{\xi^2}{3} + \mathcal{O}(\xi^4), \quad (5.17)$$

we obtain to next-to-leading order in  $1/\theta$  and  $\delta$ :

$$\frac{1}{\tau_\phi}(\theta) = \left\{ \begin{array}{l} \frac{\pi^2 c_1 \sqrt{\omega E_{\text{th}}}}{6g_1 \theta^2} \left[ 1 + \frac{15\zeta(3)}{\pi^2 \theta} - \frac{12\delta}{\pi^2} \right], \quad d = 1 \\ \frac{\pi^2 c_2 T}{12g_2 \theta} \left[ 1 + \frac{12\zeta(3)}{\pi^2 \theta} - \frac{12\delta}{\pi^2} \right], \quad d = 2 \\ \frac{\pi^2 c_3 T}{12g_3 \theta} \sqrt{\frac{\omega}{E_{\text{th}}}} \left[ 1 + \frac{9\zeta(3)}{\pi^2 \theta} - \frac{12\delta}{\pi^2} \right], \quad d = 3 \end{array} \right\}. \quad (5.18)$$

We restore the variables  $\omega, \tau_\phi$  and by use of Eq.(5.14) we get, neglecting sub-leading corrections:

$$\frac{1}{\tau_\phi}(\omega) = \left\{ \begin{array}{l} \frac{2\pi^2 c_1 \sqrt{\omega E_{\text{th}}}}{3g_1} \left(\frac{T}{\omega}\right)^2 \left[ 1 + \frac{30\zeta(3)}{\pi^2} \left(\frac{T}{\omega}\right) \right], \quad d = 1 \\ \frac{\pi^2 c_2 T}{6g_2} \left(\frac{T}{\omega}\right) \left[ 1 + \frac{24\zeta(3)}{\pi^2} \left(\frac{T}{\omega}\right) \right], \quad d = 2 \\ \frac{\pi^2 c_3 T}{6g_3} \sqrt{\frac{\omega}{E_{\text{th}}}} \left(\frac{T}{\omega}\right) \left[ 1 + \frac{18\zeta(3)}{\pi^2} \left(\frac{T}{\omega}\right) \right], \quad d = 3 \end{array} \right\}. \quad (5.19)$$

The results for the AC-regime will be discussed in Ch.6.3.



# Chapter 6

## Discussion of the results

In Ch.5, we have derived the leading  $\omega$ - and  $T$ -contributions to  $\tau_\phi$  in dimensions  $d = 1, 2, 3$ . The present chapter is devoted to a discussion of the results obtained there.

### 6.1 The high-temperature regime $\omega \ll 1/\tau_\phi \ll T$

We present the results from Eq.(5.9) in dimensionless form:

$$\frac{1}{\tau_\phi E_{\text{th}}} = \left\{ \begin{array}{l} \left( \frac{2c_1 T}{g_1 E_{\text{th}}} \right)^{2/3} \left[ 1 - \frac{1}{6} \left( \frac{g_1^2 \omega^3}{4c_1^2 T^2 E_{\text{th}}} \right)^{2/3} - 0.610 \left( \frac{c_1^2 E_{\text{th}}}{2g_1^2 T} \right)^{1/6} \right], \quad d = 1 \\ \frac{c_2 T}{g_2 E_{\text{th}}} \ln \left( \frac{g_2}{c_2} \right) \left[ 1 + \frac{1}{\ln(g_2/c_2)} \left[ 1 - \frac{1}{2} \left( \frac{g_2 \omega}{c_2 T \ln(g_2/c_2)} \right)^2 \right] \right], \quad d = 2 \\ \frac{3.473c_3}{g_3} \left( \frac{T}{E_{\text{th}}} \right)^{3/2} \left[ 1 - 1.517 \left( \frac{c_3^2 T}{g_3^2 E_{\text{th}}} \right)^{1/4} \left[ 1 + 0.021 \left( \frac{g_3^2 \omega^2 E_{\text{th}}}{c_3^2 T^3} \right) \right] \right], \quad d = 3 \end{array} \right. . \quad (6.1)$$

It is important to note, that these results have been derived using the assumptions  $\tau_\phi E_{\text{th}} \ll 1$  and  $\omega \ll 1/\tau_\phi \ll T$ . We note further that the leading results for  $\tau_\phi$  and the leading corrections from finite temperature have already been obtained before, as pointed out in Ch.5 [10, 11]. In this work, we have derived the AC-frequency corrections to  $\tau_\phi$ , and the discussion of the latter will be central to what follows. We will consider the cases  $d = 1, 2, 3$  one after another.

#### 6.1.1 Quasi-one-dimensional systems

We consider only the leading contribution to the result in  $d = 1$ , from Eq.(6.1), and we readily find that the validity of this result requires:

$$\begin{aligned} E_{\text{th}} \ll 1/\tau_\phi &\iff T/E_{\text{th}} \gg g_1/2c_1 \\ \omega \ll 1/\tau_\phi &\iff \omega/E_{\text{th}} \ll 2c_1 T/g_1 E_{\text{th}} . \end{aligned} \quad (6.2)$$

Combining both results yields that provided that  $T$  is large enough to satisfy Eq.(6.2),  $\omega$  can be smaller or larger than  $E_{\text{th}}$  for the result to be valid. We will examine the ratio between the first and the second sub-leading correction in the  $d = 1$  result. We denote this ratio by  $r(\omega, T)$ :

$$r(\omega, T) = \frac{1}{6} \left( \frac{g_1^2 \omega^3}{4c_1^2 T^2 E_{\text{th}}} \right)^{2/3} / 0.610 \left( \frac{c_1^2 E_{\text{th}}}{2g_1^2 T} \right)^{1/6}. \quad (6.3)$$

We obtain the cross-over frequency  $\omega(T)_{r=1}$ :

$$\omega(T)_{r=1}/E_{\text{th}} = (1.541c_1/g_1)^{1/2} (2c_1 T/g_1 E_{\text{th}})^{7/6}, \quad (6.4)$$

We plot  $\omega(T)_{r=1}$  in Fig.6.1, and in Fig.6.2 we show plots of  $\tau_\phi$  for several values of  $\omega$ . As a reference, we also plot  $\tau_\phi(\omega = 0)$ , i.e. the DC-result of von Delft et al [10,11]. By  $\vartheta(\omega/E_{\text{th}})$  we mean the lower bound on temperature at given frequency  $\omega$ .

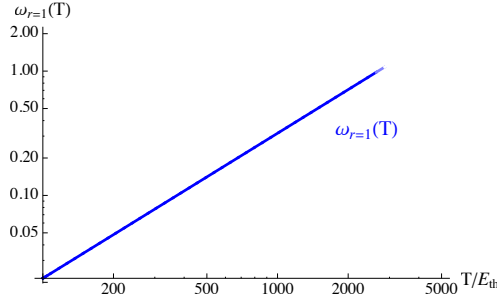


Figure 6.1:  $\omega(T)_{r=1}$ .  $g_1 = 50$ .

### 6.1.2 Quasi-two-dimensional systems

In  $d = 2$ , the  $\omega$ -corrections are parametrically smaller than the leading DC-corrections. As for  $d = 1$ , we check for validity of our result. We obtain

$$\begin{aligned} E_{\text{th}} \ll 1/\tau_\phi &\longleftrightarrow T/E_{\text{th}} \gg g_1/2c_1 \\ \omega \ll 1/\tau_\phi &\longleftrightarrow \omega/E_{\text{th}} \ll 2c_1 T/g_1 E_{\text{th}}. \end{aligned} \quad (6.5)$$

Hence, as in  $d = 1$ ,  $\omega$  can be larger or smaller than the Thouless energy, but this fact is of little importance here, compared to the one-dimensional case. We provide plots of  $\tau_\phi$  for different values of  $\omega$  in Fig.6.3.  $\vartheta(\omega/E_{\text{th}})$  is the lower bound on temperature at given frequency  $\omega$ .

### 6.1.3 Quasi-three-dimensional systems

The  $\omega$ -corrections are parametrically smaller than the DC-corrections, and the validity conditions read as follows:

$$\begin{aligned} E_{\text{th}} \ll 1/\tau_\phi &\longleftrightarrow T/E_{\text{th}} \gg (g_3/3.473c_3)^{2/3} \\ \omega \ll 1/\tau_\phi &\longleftrightarrow \omega/E_{\text{th}} \ll (3.473c_3/g_3)(T/E_{\text{th}})^{3/2}. \end{aligned} \quad (6.6)$$

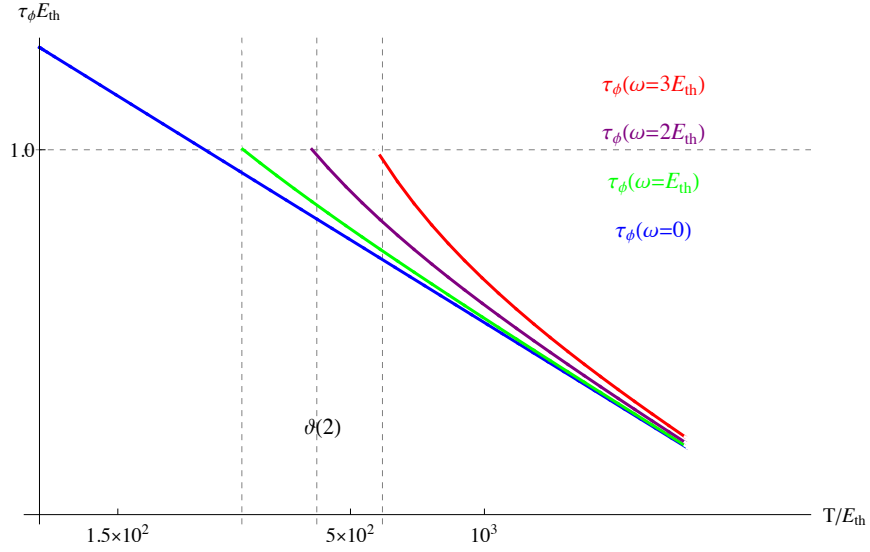


Figure 6.2:  $\tau_\phi$  in quasi-1d systems.  $\omega \ll 1/\tau_\phi \ll T$ .  $g_1 = 50$ .

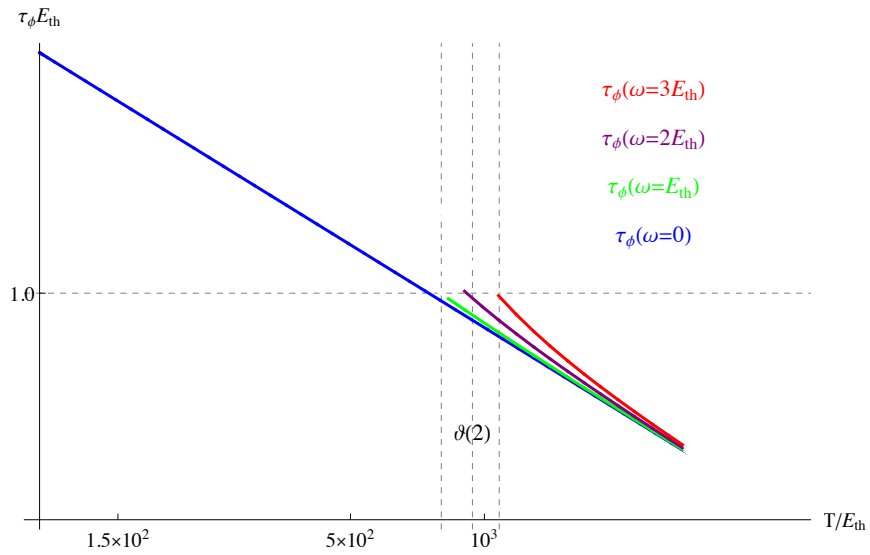


Figure 6.3:  $\tau_\phi$  in quasi-2d systems.  $\omega \ll 1/\tau_\phi \ll T$ .  $g_2 = 50$ .

We show plots for  $d = 3$  in Fig.6.4. Again,  $\vartheta(\omega/E_{\text{th}})$  refers to the lower bound on temperature at given frequency  $\omega$ .

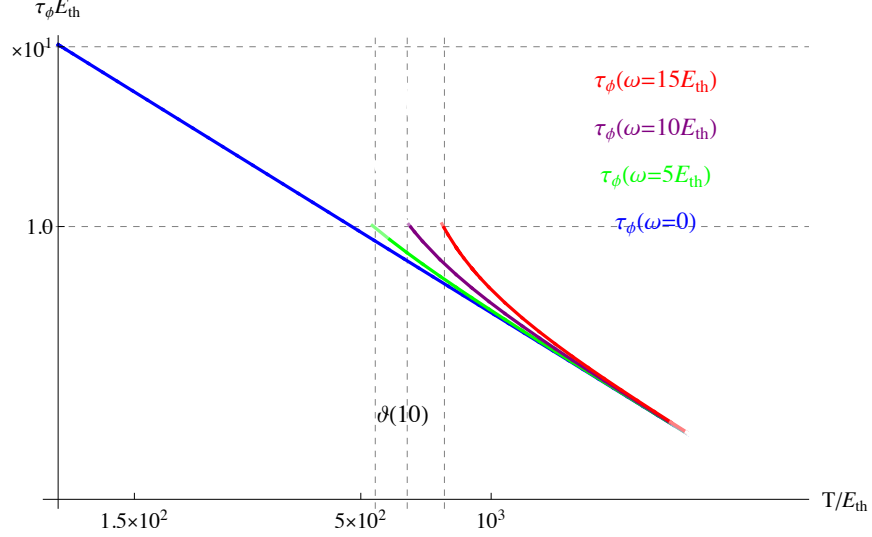


Figure 6.4:  $\tau_\phi$  in quasi-3d systems.  $\omega \ll 1/\tau_\phi \ll T$ .  $g_3 = 50$ .

### 6.1.4 Conclusion

We have found that as long as the AC-frequency is much smaller than both dephasing rate and temperature, the  $\omega$ -corrections to the DC results derived by von Delft et al. [10, 11] are sub-leading for all spatial dimensions. In  $d = 2, 3$ , they are parametrically small with respect to the next-to-leading finite-temperature correction. In  $d = 1$ , the finite-frequency contribution becomes dominant with respect to the leading DC-correction as soon as  $\omega \gg \omega_{r=1}(T)$ . The external frequency can be smaller or larger than the Thouless energy.

## 6.2 The high-temperature regime $1/\tau_\phi \ll \omega \ll T$

In dimensionless form, the results in this regime are given from Eq.(5.12) as follows:

$$\frac{1}{\tau_\phi E_{\text{th}}} = \begin{cases} \frac{2c_1 T}{g_1 E_{\text{th}}} \sqrt{\frac{E_{\text{th}}}{\omega}} \left[ 1 - 0.915 \sqrt{\frac{\omega}{2T}} - \frac{c_1^2 T^2 E_{\text{th}}}{g_1^2 \omega^3} \right], & d = 1 \\ \frac{c_2 T}{g_2 E_{\text{th}}} \ln\left(\frac{T}{\omega}\right) \left[ 1 + \frac{1}{\ln\left(\frac{T}{\omega}\right)} \right], & d = 2 \\ \frac{3.473 c_3}{g_3} \left(\frac{T}{E_{\text{th}}}\right)^{3/2} \left[ 1 - 0.814 \sqrt{\frac{\omega}{2T}} \right], & d = 3 \end{cases}, \quad (6.7)$$

As noted above, the contributions to the dephasing time from finite AC-frequency are leading in  $d = 1, 2$ . In  $d = 3$ , the  $\omega$ -contribution is sub-leading. This regime is substantially different from the last one considered, and we regard the prediction of this regime as one of the main results of this thesis. In what follows, we will discuss and plot the results for all  $d = 1, 2, 3$ .

### 6.2.1 Quasi-one-dimensional systems

Taking only the leading contribution to the result in  $d = 1$  into account, we find from Eq.(6.7) the following conditions:

$$\begin{aligned} E_{\text{th}} \ll 1/\tau_\phi &\iff T/\omega \gg g_1/2c_1\sqrt{E_{\text{th}}/\omega} \\ \omega \gg 1/\tau_\phi &\iff T/\omega \ll g_1/2c_1\sqrt{\omega/E_{\text{th}}}. \end{aligned} \quad (6.8)$$

We only obtain the requirement  $\omega > E_{\text{th}}$ , which directly follows from  $E_{\text{th}} \ll 1/\tau_\phi$  and  $\omega \gg 1/\tau_\phi$ . If this inequality is fulfilled, a temperature window opens which grows with increasing frequency:

$$g_1/2c_1\sqrt{E_{\text{th}}/\omega} \ll T/\omega \ll g_1/2c_1\sqrt{\omega/E_{\text{th}}}. \quad (6.9)$$

At a given frequency, the derived result for  $\tau_\phi$  is valid within a definite temperature range. We elaborate on the ratio between the first and the second sub-leading correction. Again, we denote this ratio by  $r(\omega, T)$ :

$$r(\omega, T) = 0.915\sqrt{\frac{\omega}{2T}} / \frac{c_1^2 T^2 E_{\text{th}}}{g_1^2 \omega^3}. \quad (6.10)$$

We obtain the cross-over frequency  $\omega(T)_{r=1}$ :

$$\omega(T)_{r=1}/E_{\text{th}} = (0.273(g_1/c_1)^{1/2}(2c_1 T/g_1 E_{\text{th}})^{5/2}). \quad (6.11)$$

and plots of dephasing time and cross-over frequency are provided in Fig.6.5 and Fig.6.6.

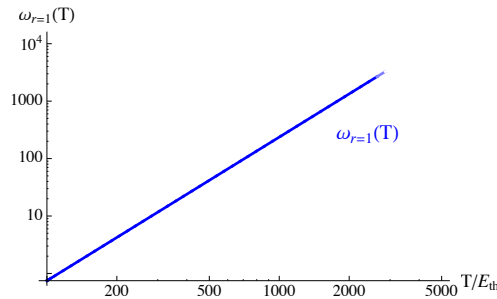


Figure 6.5:  $\omega_{r=1}(T)$ .  $g_1 = 50$ .

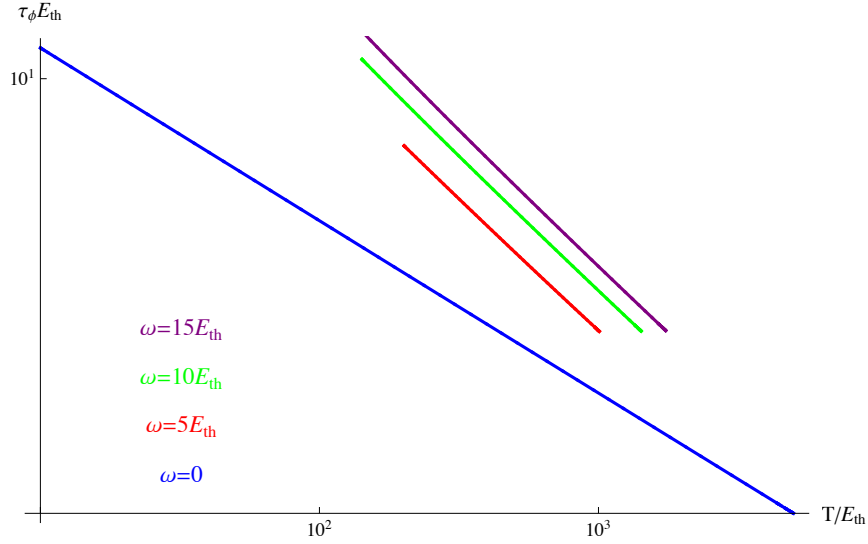


Figure 6.6:  $\tau_\phi$  in quasi-1d systems.  $1/\tau_\phi \ll \omega \ll T$ .  $g_1 = 100$ .

### 6.2.2 Quasi-two-dimensional case

In  $d = 2$ , the constraints  $1/\tau_\phi \gg E_{\text{th}}$  and  $\omega \gg 1/\tau_\phi$  yield the following temperature window:

$$\frac{g_2}{c_2 \ln(T/\omega)} \left( \frac{E_{\text{th}}}{\omega} \right) \ll \frac{T}{\omega} \ll \frac{g_2}{c_2 \ln(T/\omega)}, \quad (6.12)$$

which can be solved numerically for the bounds on  $T/\omega$ , after  $g_2$  has been specified. We plot the result for  $\tau_\phi$  in Fig.6.7.

### 6.2.3 Quasi-three-dimensional case

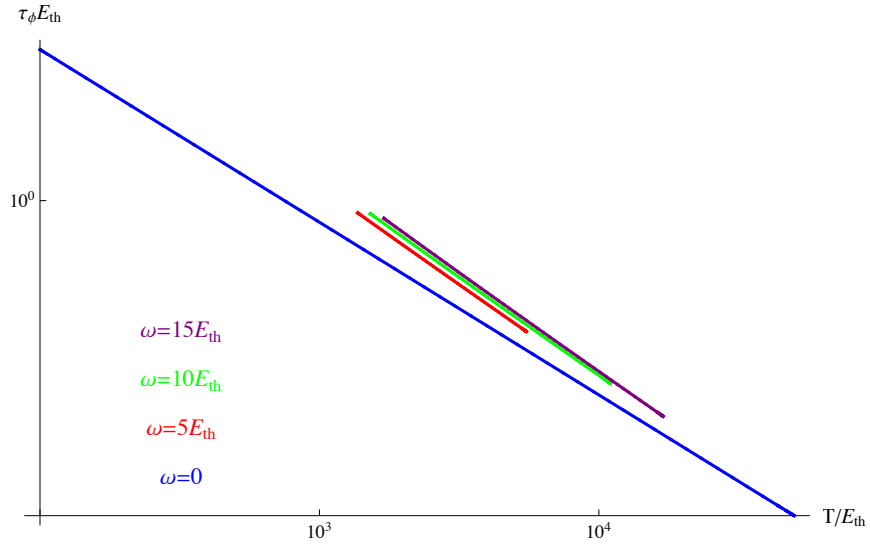
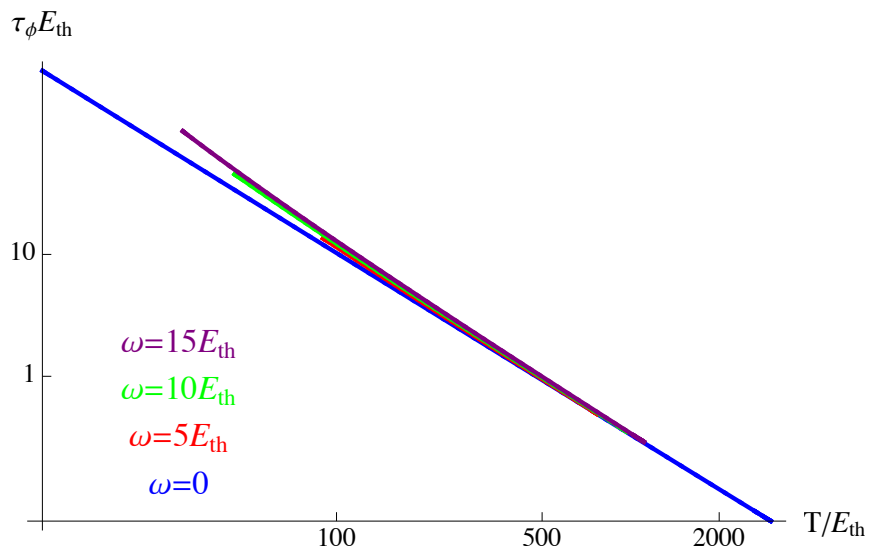
For the case of  $d = 3$ , the leading result is identical to the regime  $\omega \ll 1/\tau_\phi$ , but the finite-frequency contribution is much more pronounced in the present case. The regime constraints give the temperature window:

$$\left( \frac{g_3}{3.473c_3} \right)^{2/3} \left( \frac{E_{\text{th}}}{\omega} \right) \ll \frac{T}{\omega} \ll \left( \frac{g_3}{3.473c_3} \right)^{2/3} \left( \frac{E_{\text{th}}}{\omega} \right)^{1/3}. \quad (6.13)$$

We show plots of the results in  $d = 3$  in Fig.6.8.

### 6.2.4 Conclusion

The prediction of this regime is one of the main achievements of this work. We have found that the regime is accessible for  $\omega > E_{\text{th}}$ , in which case a temperature window opens, which grows with frequency. The upper bound on temperature arises due to the constraint

Figure 6.7:  $\tau_\phi$  in quasi-2d systems.  $1/\tau_\phi \ll \omega \ll T$ .  $g_2 = 100$ .Figure 6.8:  $\tau_\phi$  in quasi-3d systems.  $1/\tau_\phi \ll \omega \ll T$ .  $g_3 = 100$ .

$1/\tau_\phi \ll \omega$ . In  $d = 1, 2$ , the  $\omega$ -dependence is leading. In  $d = 2, 3$ , the frequency corrections are subleading with respect to the temperature corrections, while in  $d = 1$ , we found that both corrections can dominate, depending on system size and frequency.

### 6.3 The AC regime $1/\tau_\phi \ll T \ll \omega$

In the regime of large external frequencies,  $\omega \gg T$ , the results from Eq.(5.19) can be written in the following dimensionless form:

$$\frac{1}{\tau_\phi E_{\text{th}}} = \left\{ \begin{array}{l} \frac{2\pi^2 c_1}{3g_1} \sqrt{\frac{\omega}{E_{\text{th}}}} \left(\frac{T}{\omega}\right)^2 \left[ 1 + \frac{30\zeta(3)}{\pi^2} \left(\frac{T}{\omega}\right) \right], \quad d = 1 \\ \frac{\pi^2 c_2 T}{6g_2 E_{\text{th}}} \left(\frac{T}{\omega}\right) \left[ 1 + \frac{24\zeta(3)}{\pi^2} \left(\frac{T}{\omega}\right) \right], \quad d = 2 \\ \frac{\pi^2 c_3 T}{6g_3 E_{\text{th}}} \sqrt{\frac{\omega}{E_{\text{th}}}} \left(\frac{T}{\omega}\right) \left[ 1 + \frac{18\zeta(3)}{\pi^2} \left(\frac{T}{\omega}\right) \right], \quad d = 3 \end{array} \right\}. \quad (6.14)$$

We infer from the leading results, that dephasing is weak in the AC-regime, as the dephasing rate is proportional to at least one factor of  $(T/\omega) \ll 1$ . We have seen in the discussion on the spectrum  $W(T, \omega, \bar{\omega})$  in Ch.4.3.3, that  $\omega$  begins to play the role of temperature as soon as  $\omega > T$ . Further, in this regime,  $\omega$  provides the ultra-violet cut-off, and also the infra-red cut-off, due to our choice for  $\Omega$ . Hence, the window for dephasing is small in this case and weak interactions-induced dephasing in this regime should be no surprise.

#### 6.3.1 Quasi-one-dimensional systems

The regime constraints lead to the following temperature window:

$$\left(\frac{3g_1}{2\pi^2 c_1}\right)^{1/2} \left(\frac{E_{\text{th}}}{\omega}\right)^{1/4} \ll \frac{T}{\omega} \ll \left(\frac{3g_1}{2\pi^2 c_1}\right)^{1/2} \left(\frac{\omega}{E_{\text{th}}}\right)^{1/4}. \quad (6.15)$$

Since we need  $T/\omega \ll 1$ , we have to restrict Eq.(6.15):

$$\begin{aligned} \frac{T}{\omega} &\ll 1, \\ \frac{\omega}{E_{\text{th}}} &\gg \left(\frac{3g_1}{2\pi^2 c_1}\right)^2. \end{aligned} \quad (6.16)$$

In Fig.6.9, we plot the  $1d$ -result for several values of  $\omega/E_{\text{th}}$ .

#### 6.3.2 Quasi-two-dimensional systems

By the regime constraints, we have the following temperature window:

$$\left(\frac{6g_2 E_{\text{th}}}{\pi^2 c_2 \omega}\right)^{1/2} \ll \frac{T}{\omega} \ll \left(\frac{6g_2}{\pi^2 c_2}\right)^{1/2}, \quad (6.17)$$

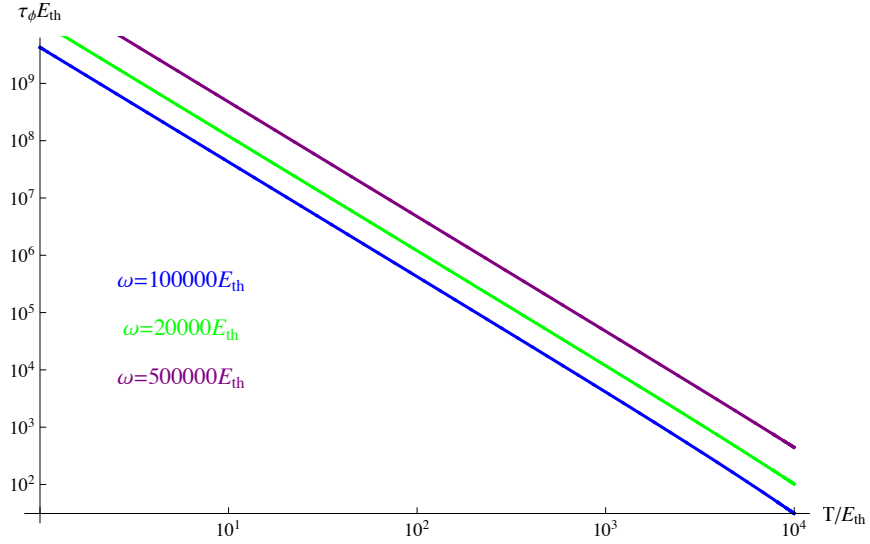


Figure 6.9:  $\tau_\phi$  in quasi-1d systems.  $1/\tau_\phi \ll T \ll \omega$ .  $g_3 = 100$ .

and using  $T/\omega \ll 1$ , we derive

$$\begin{aligned} \frac{T}{\omega} &\ll 1, \\ \frac{\omega}{E_{th}} &\gg \frac{6g_2}{\pi^2 c_2}. \end{aligned} \quad (6.18)$$

We plot the two-dimensional result in Fig.6.10.

### 6.3.3 Quasi-three-dimensional systems

Our result in  $d = 3$  is valid for the following range of temperature,

$$\begin{aligned} \frac{T}{\omega} &\ll 1, \\ \frac{\omega}{E_{th}} &\gg \left( \frac{6g_3}{\pi^2 c_3} \right)^{2/3}. \end{aligned} \quad (6.19)$$

We plot the result for  $d = 3$  in Fig.6.11.

### 6.3.4 Conclusion

In the AC-regime, dephasing is weak. For  $\omega \gg T$ , the AC-frequency provides both the infrared and the ultra-violet cut of the self-energy integral, hence the window for dephasing processes is very small.

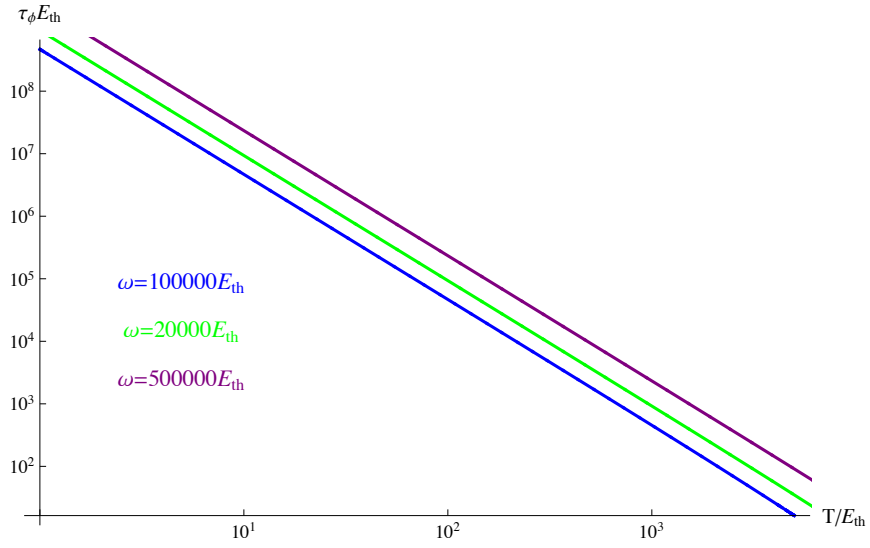


Figure 6.10:  $\tau_\phi$  in quasi-2d systems.  $1/\tau_\phi \ll T \ll \omega$ .  $g_3 = 100$ .

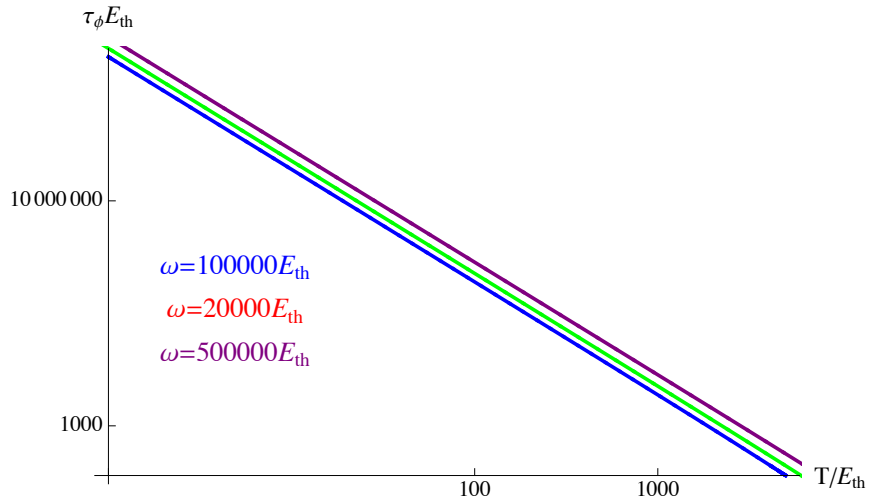


Figure 6.11:  $\tau_\phi$  in quasi-3d systems.  $1/\tau_\phi \ll T \ll \omega$ .  $g_3 = 100$ .

# Conclusion and outlook

## Conclusion

In this thesis, we have studied the interplay between interactions-induced dephasing and a finite AC-frequency in weakly disordered normal metals in the diffusive regime: We calculated the frequency-dependence of the Cooperon self-energy which defines the dephasing time due to interactions,  $\tau_\phi(\omega)$ . In this work, we considered the large system-size limit, defined by the condition  $E_{\text{th}} \ll 1/\tau_\phi$ , where  $E_{\text{th}}$  is the Thouless energy. In the diffusive regime, which we considered throughout, the temperature is always larger than the dephasing rate,  $T \gg 1/\tau_\phi$  [8]. Hence, the AC-frequency  $\omega$  can be a) smaller than both temperature and dephasing, can b) lie in between or can c) be larger than both. We found that these three possibilities correspond to three physically distinct regimes, which are distinguished by the different scaling of  $\tau_\phi$  in  $T$  and  $\omega$ .

- In the high-temperature regime  $\omega \ll 1/\tau_\phi \ll T$ , the frequency gives only subleading corrections to  $\tau_\phi$ . While in  $d = 2, 3$ , those are always parametrically smaller than the corrections from temperature, which were obtained before by von Delft et al. [10, 11], the situation is different in  $d = 1$ . In this case, we found that the frequency correction becomes comparable to the temperature correction as soon as  $\omega$  is of the order of the Thouless energy  $E_{\text{th}}$ , and even dominates, if  $\omega$  is increased further. This can be considered one of the main results of this work. The leading correction from finite  $\omega$ , denoted  $\Delta_\omega$  is given as follows for  $d = 1, 2, 3$ :

$$\begin{aligned}\Delta_{\omega,d=1} &= -\frac{1}{6} \left( \frac{g_1^2 \omega^3}{4c_1^2 T^2 E_{\text{th}}} \right)^{2/3} \\ \Delta_{\omega,d=2} &= -\frac{1}{2 \ln(g_2/c_2)} \left( \frac{g_2 \omega}{c_2 T \ln(g_2/c_2)} \right)^2 \\ \Delta_{\omega,d=3} &= -1.517 \left( \frac{c_3^2 T}{g_3^2 E_{\text{th}}} \right)^{1/4} \times 0.021 \left( \frac{g_3^2 \omega^2 E_{\text{th}}}{c_3^2 T^3} \right).\end{aligned}$$

- In the regime  $1/\tau_\phi \ll \omega \ll T$ , we found the frequency contributions to be leading, and the scaling of  $\tau_\phi$  is substantially different from the former regime. We obtained temperature windows within which the regime exists, and these windows grow with

increasing frequency. We give the leading results for the dephasing time:

$$\begin{aligned}\frac{1}{\tau_{\phi,d=1}E_{\text{th}}} &= \frac{2c_1T}{g_1E_{\text{th}}}\sqrt{\frac{E_{\text{th}}}{\omega}} \\ \frac{1}{\tau_{\phi,d=2}E_{\text{th}}} &= \frac{c_2T}{g_2E_{\text{th}}}\ln\left(\frac{T}{\omega}\right) \\ \frac{1}{\tau_{\phi,d=3}E_{\text{th}}} &= \frac{3.473c_3}{g_3}\left(\frac{T}{E_{\text{th}}}\right)^{3/2}.\end{aligned}$$

The temperature window is given as follows, for  $d = 1, 2, 3$ :

$$\begin{aligned}g_1/2c_1\sqrt{E_{\text{th}}/\omega} &\ll T/\omega \ll g_1/2c_1\sqrt{\omega/E_{\text{th}}} \\ \frac{g_2}{c_2\ln(T/\omega)}\left(\frac{E_{\text{th}}}{\omega}\right) &\ll \frac{T}{\omega} \ll \frac{g_2}{c_2\ln(T/\omega)} \\ \left(\frac{g_3}{3.473c_3}\right)^{2/3}\left(\frac{E_{\text{th}}}{\omega}\right) &\ll \frac{T}{\omega} \ll \left(\frac{g_3}{3.473c_3}\right)^{2/3}\left(\frac{E_{\text{th}}}{\omega}\right)^{1/3}.\end{aligned}$$

- The situation is again substantially changed as the frequency is further increased towards  $\omega \gg T$ . We found that in this last regime, the external frequency plays the role of temperature. This statement refers to the fact that the spectrum for electron-electron-collisions,  $W(T, \omega\bar{\omega})$ , behaves as  $\sim (\omega/2)$  for small  $\bar{\omega}$ , instead of the DC-behaviour  $\sim T$ , c.f. Eq.(4.28). Further, also the width is  $\sim \omega$  such that energies larger than  $T$  can contribute to dephasing. We found that the dephasing is weak in this regime. The leading expressions for the dephasing rate are given as follows:

$$\begin{aligned}\frac{1}{\tau_{\phi,d=1}E_{\text{th}}} &= \frac{2\pi^2c_1}{3g_1}\sqrt{\frac{\omega}{E_{\text{th}}}}\left(\frac{T}{\omega}\right)^2 \\ \frac{1}{\tau_{\phi,d=2}E_{\text{th}}} &= \frac{\pi^2c_2T}{6g_2E_{\text{th}}}\left(\frac{T}{\omega}\right) \\ \frac{1}{\tau_{\phi,d=3}E_{\text{th}}} &= \frac{\pi^2c_3T}{6g_3E_{\text{th}}}\sqrt{\frac{\omega}{E_{\text{th}}}}\left(\frac{T}{\omega}\right).\end{aligned}$$

## Outlook

The derived results rely heavily on our particular choice of the infrared cut-off, Eq.(4.31). We remind that our results are obtained after neglect of all vertex diagrams, which allowed us to reduce the Bethe-Salpeter equation to a Dyson equation and solve the self-energy integral self-consistently. It would be interesting to see, whether calculations which include the vertex contribution confirm the validity of our particular choice for the cut-off. Furthermore, it would also be very interesting to consider a finite system-size, such that the Thouless energy can exceed all other scales, and look for new regimes there. This motivates further study.

# Appendix A

## Diagrammatic disorder average

In this chapter, we will review the calculation of the disorder-averaged electronic Green's functions  $\bar{G}_\epsilon^{R/A}(\mathbf{k})$ , which leads to Eq.(1.20) of the main text [5]. We work in real space first and define the full electron Green's function  $G(\mathbf{r}, \mathbf{r}', t)$  and the free electron Green's function  $G^0(\mathbf{r}, \mathbf{r}', t)$  via the following equations:

$$\begin{aligned} \left( \epsilon + \frac{1}{2m} \Delta_{\mathbf{r}} \right) G_\epsilon^0(\mathbf{r}, \mathbf{r}') &= \delta(\mathbf{r}' - \mathbf{r}) \\ \left( \epsilon + \frac{1}{2m} \Delta_{\mathbf{r}} - V(\mathbf{r}) \right) G_\epsilon(\mathbf{r}, \mathbf{r}') &= \delta(\mathbf{r}' - \mathbf{r}), \end{aligned} \tag{A.1}$$

c.f. Eq.(1.15) of the main text. It is well-known [18], that an expansion for  $G_\epsilon(\mathbf{r}, \mathbf{r}')$  in powers of  $V(\mathbf{r})$  can be written as follows:

$$\begin{aligned} G_\epsilon(\mathbf{r}, \mathbf{r}') &= G_\epsilon^0(\mathbf{r}, \mathbf{r}') + \int d\mathbf{r}_1 G_\epsilon^0(\mathbf{r}, \mathbf{r}_1) V(\mathbf{r}_1) G_\epsilon^0(\mathbf{r}_1, \mathbf{r}') \\ &+ \iint d\mathbf{r}_1 d\mathbf{r}_2 G_\epsilon^0(\mathbf{r}, \mathbf{r}_1) V(\mathbf{r}_1) G_\epsilon^0(\mathbf{r}_1, \mathbf{r}_2) V(\mathbf{r}_2) G_\epsilon^0(\mathbf{r}_2, \mathbf{r}') \\ &+ \dots \end{aligned} \tag{A.2}$$

This expansion is depicted in Fig.A.1. Note that we draw interaction propagators as dotted lines and electron propagators as solid lines, while impurities are denoted by crosses. The disorder average is performed using Eq.(1.18), and the averaged Green's function is displayed in Fig.A.2. All odd moments vanish, hence the first non-zero contribution is quadratic in the potential:

$$\bar{G}_\epsilon(\mathbf{r}, \mathbf{r}') = G_\epsilon^0(\mathbf{r}, \mathbf{r}') + \gamma \iint d\mathbf{r}_1 d\mathbf{r}_2 G_\epsilon^0(\mathbf{r}, \mathbf{r}_1) \delta(\mathbf{r}_1 - \mathbf{r}_2) G_\epsilon^0(\mathbf{r}_1, \mathbf{r}_2) G_\epsilon^0(\mathbf{r}_2, \mathbf{r}') + \dots \tag{A.3}$$

It is important to note, that the disorder average restores translational invariance. This can be seen as follows:  $G^0$  is translationally invariant by definition, and the higher-order terms in the expansion in Eq.(A.3) are invariant by the definition of  $V(\mathbf{r})$ , c.f. Eq.(1.18). The

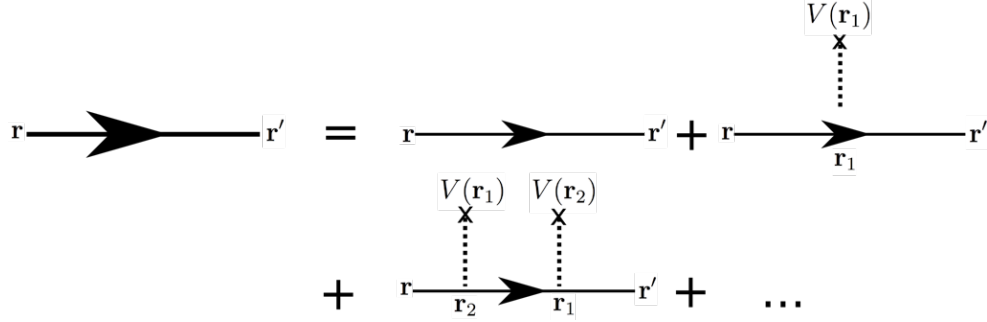


Figure A.1: Green's function before disorder-averaging.

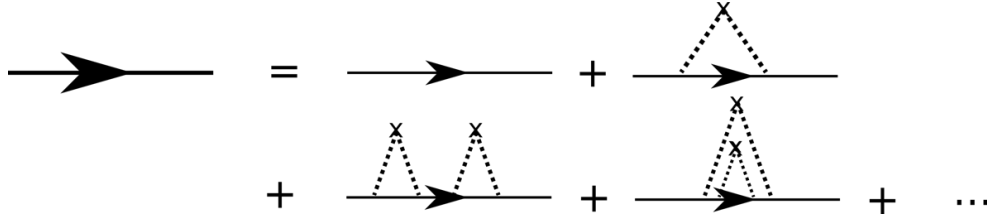


Figure A.2: Green's function after disorder-averaging.

diagrams which contribute to the disorder-averaged Green's function are built by pairing the interaction lines with impurities in all possible ways, c.f. Fig.A.2.

Due to the translational symmetry of Eq.(A.3), it is convenient to work in momentum space, and we obtain from Eq.(A.3):

$$\bar{G}_\epsilon(\mathbf{k}) = G_\epsilon^0(\mathbf{k}) + \frac{\gamma}{V} \sum_{\mathbf{q}} G_\epsilon^0(\mathbf{k}) G_\epsilon^0(\mathbf{k} - \mathbf{q}) G_\epsilon^0(\mathbf{k}) + \dots \quad (\text{A.4})$$

## A.1 Self-energy

In Fig.A.2, we encounter diagrams, which can be separated into two parts without cutting an impurity line, and diagrams which can not. For example, consider the third diagram on the r.h.s. of Fig.A.2, which can be separated. Its contribution can be written as follows:

$$\begin{aligned} & \frac{\gamma^2}{V^2} \sum_{\mathbf{q}} \sum_{\mathbf{q}'} G_\epsilon^0(\mathbf{k}) G_\epsilon^0(\mathbf{k} - \mathbf{q}) G_\epsilon^0(\mathbf{k}) G_\epsilon^0(\mathbf{k} - \mathbf{q}') G_\epsilon^0(\mathbf{k}) \\ & = G_\epsilon^0(\mathbf{k}) \left[ \sum_{\mathbf{q}} \frac{\gamma}{V} G_\epsilon^0(\mathbf{k} - \mathbf{q}) G_\epsilon^0(\mathbf{k}) \right]^2, \end{aligned} \quad (\text{A.5})$$

and can thus be expressed in terms of the second diagram on the r.h.s. of Fig.A.2, which is not separable. We call separable diagrams reducible, and non-separable diagrams irre-

ducible. In general, all reducible diagrams can be reduced and written in terms of irreducible diagrams, since the internal momenta are independent. It follows that the infinite sum of all diagrams can be written as a geometric series:

$$\bar{G}_\epsilon(\mathbf{k}) = G_\epsilon^0(\mathbf{k}) + G_\epsilon^0(\mathbf{k}) \sum_{n=1}^{\infty} [\Sigma_\epsilon(\mathbf{k}) G_\epsilon^0(\mathbf{k})]^n, \quad (\text{A.6})$$

where  $\Sigma_\epsilon(\mathbf{k})$  is called self-energy and equals by construction the sum over all irreducible diagrams. The self-energy is depicted in Fig.A.3.

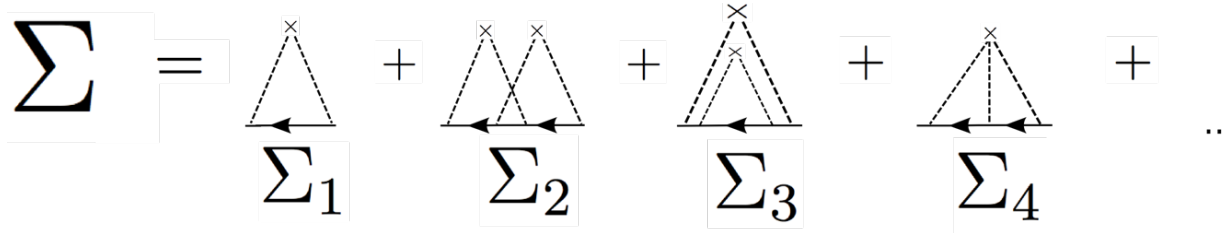


Figure A.3: Self-energy diagrams.

Eq.(A.6) can be rewritten in the form of a so-called Dyson equation [16]:

$$\bar{G}_\epsilon(\mathbf{k}) = G_\epsilon^0(\mathbf{k}) + G_\epsilon^0(\mathbf{k}) \Sigma_\epsilon(\mathbf{k}) \bar{G}_\epsilon(\mathbf{k}). \quad (\text{A.7})$$

In the main text, we will need the disorder-averaged version of the retarded and advanced electron propagators, which are defined via Eq.(1.17), in momentum representation. From Eq.(A.7), we obtain [5, Eq.3.68]:

$$\bar{G}_\epsilon^{R/A}(\mathbf{k}) = \frac{1}{\epsilon - \epsilon(\mathbf{k}) - \Sigma_\epsilon^{R/A}(\mathbf{k})}. \quad (\text{A.8})$$

The imaginary part of the self-energy defines a characteristic decay time  $\tau$  [5], conveniently called the transport time, which describes the decay of eigenstates of the momentum operator, due to scattering with impurities. Without loss of generality, we consider only the retarded self-energy. In Fig.A.3, the diagram denoted  $\Sigma_1$  gives the leading contribution to the self-energy, since the other diagrams are smaller by at least one factor of  $1/k_F l_e$  (phase space constraints), or  $c_i$  (impurity concentration), which are both small in the limit of weak disorder. According to Fig.A.3, the imaginary part of  $\Sigma_1$  is given by the expression

$$\Im \Sigma_1^R(\mathbf{k}, \epsilon) = \frac{\gamma}{V} \sum_{\mathbf{k}'} \Im G^R(\mathbf{k}', \epsilon). \quad (\text{A.9})$$

## A.2 Density of states and convenient definitions

It is convenient to define the imaginary part of  $\Im G^R$  as follows [5, Eq.3.21]:

$$\Im G_\epsilon^R = \frac{G_\epsilon^R - G_\epsilon^A}{2i}. \quad (\text{A.10})$$

We define the transport time as  $1/2\tau = \Im\Sigma_1^R$ , and we make use of the following relation for the density of states per unit volume  $\rho(\epsilon)$  [5, Eq.3.32]:

$$\rho(\epsilon) = -\frac{1}{\pi V} \sum_{\mathbf{k}} \Im G_{\epsilon}^R(\mathbf{k}). \quad (\text{A.11})$$

, Note that  $\rho$  is related to the level density  $\nu$ ,  $\nu = \rho V$ . Further, a useful relation valid for free electrons in  $d$  dimensions reads:

$$\rho(\epsilon) = \frac{n(\epsilon)d}{2s\epsilon}, \quad (\text{A.12})$$

where  $n\epsilon$  is the electronic density and  $s = 2$  for unpolarized electrons. In this thesis throughout,  $\epsilon = E_F$ , and we will put  $\rho \equiv \rho(E_F)$  as well as  $n \equiv n(E_F)$ .

### A.3 Transport time

Using the definitions above, we find from Eq.(A.9):

$$\frac{1}{2\tau} = \pi\rho\gamma, \quad (\text{A.13})$$

and the disorder-averaged retarded and advanced propagators can be finally written as

$$\bar{G}_{\epsilon}^{R/A}(\mathbf{k}) = \frac{1}{\epsilon - \epsilon(\mathbf{k}) \pm \frac{i}{2\tau}}, \quad (\text{A.14})$$

which is Eq.(1.20) of the main text.

# Appendix B

## Time evolution in Quantum mechanics

We review the characteristics of the three well-known and equivalent representations of quantum-mechanical time evolution [1].

### B.1 General remarks

Consider a given quantum system described by the Hamilton operator  $\hat{H}$ . According to the Schrödinger equation, the time evolution of a given quantum state  $|\Psi\rangle$  is given as follows:

$$i\frac{\partial}{\partial t}|\Psi\rangle = \hat{H}(t)|\Psi\rangle . \quad (\text{B.1})$$

Every measurable physical quantity  $A(t)$  is represented by an operator  $\hat{A}(t)$ , whose eigenvalues  $\{a_j\}$  equal to the possible outcomes of a measurement of  $A(t)$ . The expectation value of a measurement of  $A(t)$ ,  $\langle\hat{A}(t)\rangle$ , is defined as follows:

$$\langle\hat{A}(t)\rangle = \langle\Psi|\hat{A}(t)|\Psi\rangle , \quad (\text{B.2})$$

and is in general time-dependent.

### B.2 Schrödinger representation

We will first introduce time evolution within the Schrödinger picture. Within the Schrödinger representation, the dynamics due to Eq.(B.1) affect only the state vectors, not the observables. Eq.(B.1) allows us to write

$$|\Psi(t)\rangle = \hat{U}(t, t')|\Psi(t')\rangle , \quad (\text{B.3})$$

where the time evolution operator  $\hat{U}(t, t')$  obeys

$$\hat{U}(t, t) = \mathbb{1} \quad (\text{B.4})$$

$$\hat{U}^\dagger(t, t') = \hat{U}(t, t')^{-1} = \hat{U}(t', t) \quad (\text{B.5})$$

$$\hat{U}(t, t') = \hat{U}(t, t'')\hat{U}(t'', t'). \quad (\text{B.6})$$

We insert Eq.(B.3) into Eq.(B.1) and write the result in the equivalent form

$$\hat{U}(t, t') = \mathbb{1} - i \int_{t'}^t d\tau \hat{H}(\tau). \quad (\text{B.7})$$

From an iteration we obtain the formal solution

$$U(t, t') = \hat{\mathbf{T}}e^{-i \int_{t'}^t d\tau \hat{H}(\tau)}. \quad (\text{B.8})$$

In the special case of time-independent Hamilton operators, Eq.(B.8) simplifies to

$$U(t, t') = e^{-i\hat{H}t}. \quad (\text{B.9})$$

We may take a look on the scalar product  $\langle \Psi(t') | \Psi(t) \rangle$ , which is equivalent to a transition amplitude, and assume that we know the state at a given instant,  $|\Psi(t=0)\rangle = |\Psi_0\rangle$ , say. Then the scalar product may be rewritten in the form

$$\langle \Psi(t') | \Psi(t) \rangle = \langle \Psi_0 | \hat{S}(t, t') | \Psi_0 \rangle, \quad (\text{B.10})$$

where we employed the convenient definition of the scattering matrix  $\hat{S}(t, t')$ ,

$$\hat{S}(t, t') \equiv \hat{U}(t)\hat{U}^\dagger(t'). \quad (\text{B.11})$$

### B.3 Heisenberg representation

For the expectation values in Eq.(B.2) we may now explicitly write

$$\langle \hat{A}(t) \rangle = \langle \Psi(t') | \hat{U}^\dagger(t, t') \hat{A}(t) \hat{U}(t, t') | \Psi(t') \rangle. \quad (\text{B.12})$$

We may choose our time axis such that  $t' = 0$  and set  $|\Psi(t' = 0)\rangle = |\Psi_0\rangle$ . Using this choice in Eq.(B.12), we derive the Heisenberg representation<sup>1</sup> by identifying

$$\hat{A}_H(t) = \hat{U}^\dagger(t) \hat{A}(t) \hat{U}(t), \quad (\text{B.13})$$

i.e. we take the state vectors to be constant in time,  $|\Psi(t)\rangle \equiv |\Psi_0\rangle$ , and shift the dynamics upon the observables. Note the equivalence between the Schrödinger and Heisenberg pictures, which becomes apparent in Eq.(B.12). We immediately deduce an equation of motion for the Heisenberg operators, the so-called Heisenberg equation:

$$i \frac{d}{dt} \hat{A}_H(t) = \left[ \hat{A}_H(t), \hat{H}_H(t) \right] + i \frac{\partial}{\partial t} \hat{A}_H(t). \quad (\text{B.14})$$

<sup>1</sup>Quantities written in Heisenberg(Interaction) representation carry a subscript  $H(I)$ .

## B.4 Interaction representation

We consider Hamilton operators of the form  $\hat{H}(t) = \hat{H}_0 + \hat{W}(t)$ , where  $\hat{H}_0$  is time-independent. If  $\hat{W}(t)$  can be considered a perturbation small with respect to  $\hat{H}_0$ , the interaction representation suits best for the elaboration of such problems. The interaction representation of operators derives from the Schrödinger picture via

$$\hat{A}_H(t) = e^{i\hat{H}_0 t} \hat{A}(t) e^{-i\hat{H}_0 t}, \quad (\text{B.15})$$

and the transformation from the Heisenberg representation amounts to the replacement

$$\hat{A}_H(t) = \hat{U}^\dagger(t) e^{-i\hat{H}_0 t} \hat{A}_I(t) e^{i\hat{H}_0 t} \hat{U}(t). \quad (\text{B.16})$$

The quantum states in Interaction and Heisenberg picture relate via

$$|\Psi_I(t)\rangle = e^{+iH_0 t} U(t) |\Psi_0\rangle, \quad (\text{B.17})$$

and the relation between Schrödinger and Interaction picture is given by

$$|\Psi_I(t)\rangle = e^{iH_0 t} |\Psi(t)\rangle. \quad (\text{B.18})$$

The quantum states obey the following differential equation,

$$i \frac{\partial}{\partial t} |\Psi_I(t)\rangle = \hat{W}_I(t) |\Psi_I(t)\rangle. \quad (\text{B.19})$$

In interaction representation, the scattering matrix  $\hat{S}_I(t, t')$  is given as follows:

$$\hat{S}_I(t, t') = \hat{\mathbf{T}} e^{-i \int_{t'}^t d\tau \hat{W}_I(\tau)}, \quad (\text{B.20})$$

for  $t > t'$ . For convenience, we also give

$$\hat{S}_I^\dagger(t, t') = \tilde{\mathbf{T}} e^{-i \int_{t'}^t d\tau \hat{W}_I(\tau)}, \quad (\text{B.21})$$

where the time(anti-time) ordering  $\mathbf{T}(\tilde{\mathbf{T}})$  arranges operators acting at earlier times to the right(left) of operators acting on later times.



# Appendix C

## Derivation of the conductivity

### C.1 Fourier transform of the electric current

The goal of this appendix is to find the Fourier transform of Eq.(3.15) of the main text. We infer from this equation, that the expression for the current is a sum of terms of the following structure,

$$\Gamma(1) = - \int d\mathbf{x}_2 \int dt_2 [(\nabla_1 - \nabla_{1'}) (\nabla_2 - \nabla_{2'}) \mathbf{A}(t_2) G(1, 2') H(2, 1')]_{1'=1, 2'=2}, \quad (\text{C.1})$$

where  $G, H$  represent electron propagators. Note that the propagators are invariant under translations in time and thus satisfy

$$G(1, 2) = G(\mathbf{x}_1, \mathbf{x}_2, t_1 - t_2). \quad (\text{C.2})$$

We use Eq.(C.2) and rewrite Eq.(C.1) in terms of Fourier integrals,

$$\begin{aligned} \Gamma(\mathbf{x}_1, t_1) &= \frac{1}{(2\pi)^3 V^4} \int d\mathbf{x}_2 \int dt_2 \sum_{\mathbf{k}_1} \sum_{\mathbf{k}_{1'}} \sum_{\mathbf{k}_2} \sum_{\mathbf{k}_{2'}} \int d\alpha \int dE \int d\gamma \\ &\quad \times e^{-i\gamma t_2} e^{-i\alpha(t_1 - t_2)} e^{-iE(t_2 - t_1)} e^{i(\mathbf{k}_1 + \mathbf{k}_{1'}) \cdot \mathbf{x}_1} e^{i(\mathbf{k}_2 + \mathbf{k}_{2'}) \cdot \mathbf{x}_2} \\ &\quad \times \mathbf{A}(\gamma) G(\mathbf{k}_1, \mathbf{k}_{2'}, \alpha) H(\mathbf{k}_2, \mathbf{k}_{1'}, E) (\mathbf{k}_1 - \mathbf{k}_{1'}) \cdot (\mathbf{k}_2 - \mathbf{k}_{2'}) \\ &= \frac{1}{(2\pi)^3 V^4} \int d\mathbf{x}_2 \int dt_2 \sum_{\mathbf{k}_1} \sum_{\mathbf{k}_{1'}} \sum_{\mathbf{k}_2} \sum_{\mathbf{k}_{2'}} \int d\alpha \int dE \int d\gamma \\ &\quad \times e^{-i(\gamma - \alpha + E)t_2} e^{-i(\alpha - E)t_1} e^{i(\mathbf{k}_1 + \mathbf{k}_{1'}) \cdot \mathbf{x}_1} e^{i(\mathbf{k}_2 + \mathbf{k}_{2'}) \cdot \mathbf{x}_2} \\ &\quad \times \mathbf{A}(\gamma) G(\mathbf{k}_1, \mathbf{k}_{2'}, \alpha) H(\mathbf{k}_2, \mathbf{k}_{1'}, E) (\mathbf{k}_1 - \mathbf{k}_{1'}) \cdot (\mathbf{k}_2 - \mathbf{k}_{2'}). \end{aligned}$$

We evaluate the integrals over  $(\mathbf{x}_2, t_2)$ ,

$$\begin{aligned} \Gamma(\mathbf{x}_1, t_1) &= \frac{1}{(2\pi)^2 V^3} \sum_{\mathbf{k}_1} \sum_{\mathbf{k}_{1'}} \sum_{\mathbf{k}_2} \sum_{\mathbf{k}_{2'}} \int d\alpha \int dE \int d\gamma \\ &\quad \times e^{-i(\alpha - E)t_1} e^{i(\mathbf{k}_1 + \mathbf{k}_{1'}) \cdot \mathbf{x}_1} \delta(E + \gamma - \alpha) \delta_{\mathbf{k}_2 + \mathbf{k}_{2'}, 0} \\ &\quad \times \mathbf{A}(\gamma) G(\mathbf{k}_1, \mathbf{k}_{2'}, \alpha) H(\mathbf{k}_2, \mathbf{k}_{1'}, E) (\mathbf{k}_1 - \mathbf{k}_{1'}) \cdot (\mathbf{k}_2 - \mathbf{k}_{2'}), \end{aligned}$$

and in the next step the now trivial integrations over  $(\alpha, \mathbf{k}_{2'})$ :

$$\begin{aligned} \Gamma(\mathbf{x}_1, t_1) &= \frac{1}{(2\pi)^2 V^3} \sum_{\mathbf{k}_1} \sum_{\mathbf{k}_{1'}} \sum_{\mathbf{k}_2} \int dE \int d\gamma e^{-i\gamma t_1} e^{i(\mathbf{k}_1 + \mathbf{k}_{1'}) \cdot \mathbf{x}_1} \\ &\quad \times \mathbf{A}(\gamma) G(\mathbf{k}_1, -\mathbf{k}_2, E + \gamma) H(\mathbf{k}_2, \mathbf{k}_{1'}, E) 2\mathbf{k}_2 \cdot (\mathbf{k}_1 - \mathbf{k}_{1'}) . \end{aligned}$$

The Fourier transform of  $\Gamma(\mathbf{x}_1, t_1)$  equals to the following expression:

$$\begin{aligned} \Gamma(\mathbf{q}, \omega) &= \frac{1}{(2\pi)^2 V^2} \sum_{\mathbf{k}_1} \sum_{\mathbf{k}_{1'}} \sum_{\mathbf{k}_2} \int d\mathbf{x}_1 \int dt_1 \int dE \int d\gamma \\ &\quad \times e^{-i(\gamma - \omega)t_1} e^{i(\mathbf{k}_1 + \mathbf{k}_{1'} - \mathbf{q}) \cdot \mathbf{x}_1} \\ &\quad \times \mathbf{A}(\gamma) G(\mathbf{k}_1, -\mathbf{k}_2, E + \gamma) H(\mathbf{k}_2, \mathbf{k}_{1'}, E) 2\mathbf{k}_2 \cdot (\mathbf{k}_1 - \mathbf{k}_{1'}) \\ &= \frac{1}{2\pi V} \sum_{\mathbf{k}_1} \sum_{\mathbf{k}_{1'}} \sum_{\mathbf{k}_2} \int dE \int d\gamma \delta(\gamma - \omega) \delta_{\mathbf{k}_1 + \mathbf{k}_{1'} - \mathbf{q}, 0} \\ &\quad \times \mathbf{A}(\gamma) G(\mathbf{k}_1, -\mathbf{k}_2, E + \gamma) H(\mathbf{k}_2, \mathbf{k}_{1'}, E) 2\mathbf{k}_2 \cdot (\mathbf{k}_1 - \mathbf{k}_{1'}) \\ &= \frac{1}{\pi V} \int dE \sum_{\mathbf{k}_1} \sum_{\mathbf{k}_2} \mathbf{k}_2 \cdot (2\mathbf{k}_1 - \mathbf{q}) G(\mathbf{k}_1, -\mathbf{k}_2, E + \omega) \mathbf{A}(\omega) H(\mathbf{k}_2, \mathbf{q} - \mathbf{k}_1, E) . \end{aligned}$$

Finally, we obtain for the  $\mathbf{q} = 0$  mode:

$$\Gamma(\omega) = \frac{2}{\pi V} \int dE \sum_{\mathbf{k}_1} \sum_{\mathbf{k}_2} \mathbf{k}_1 \cdot \mathbf{k}_2 G_{E+\omega}(\mathbf{k}_1, \mathbf{k}_2) \mathbf{A}(\omega) H_E(\mathbf{k}_2, \mathbf{k}_1) . \quad (\text{C.3})$$

## C.2 Cancellation of the diamagnetic term

This section is devoted to show that the following equation holds true for small excitations,  $\omega \ll E_F$ :

$$\begin{aligned} \frac{ne^2}{im\omega} &= \frac{e^2}{m^2\omega\pi dV} \sum_{\mathbf{k}} \mathbf{k}^2 \int dE \\ &\quad \times \left[ f(E + \omega) \overline{G}_{E+\omega}^A(\mathbf{k}) \overline{G}_E^A(\mathbf{k}) - f(E) \overline{G}_{E+\omega}^R(\mathbf{k}) \overline{G}_E^R(\mathbf{k}) \right] . \end{aligned} \quad (\text{C.4})$$

In the square brackets of the integral, we shift  $E \rightarrow (E - \omega)$  in the first term and since we consider  $\omega \ll E$ , we further neglect the  $\omega$ -dependence in the Green's functions. Thus, we arrive at

$$\frac{ne^2}{im\omega} = \frac{e^2}{m^2\omega\pi dV} \sum_{\mathbf{k}} \mathbf{k}^2 \int dE f(E) \left[ \overline{G}_E^A(\mathbf{k}) \overline{G}_E^A(\mathbf{k}) - \overline{G}_E^R(\mathbf{k}) \overline{G}_E^R(\mathbf{k}) \right] . \quad (\text{C.5})$$

The following relation for the disordered Green's function is immediately proven by differentiation:

$$\frac{\partial \bar{G}_E^{R/A}}{\partial E} = -\bar{G}_E^{R/A} \bar{G}_E^{R/A}, \quad (\text{C.6})$$

and using this relation we obtain:

$$\frac{ne^2}{im\omega} = \frac{e^2}{m^2\omega\pi dV} \sum_{\mathbf{k}} \mathbf{k}^2 \int dE f(E) \frac{\partial}{\partial E} \left[ \bar{G}_E^R(\mathbf{k}) - \bar{G}_E^A(\mathbf{k}) \right]. \quad (\text{C.7})$$

At low temperatures,  $f(E) \approx \Theta(E_F - E)$ . Using this approximation and integrating by parts once, we find:

$$\frac{ne^2}{im\omega} = -\frac{e^2}{m^2\omega\pi dV} \sum_{\mathbf{k}} \mathbf{k}^2 \int dE \delta(E - E_F) \left[ \bar{G}_E^R(\mathbf{k}) - \bar{G}_E^A(\mathbf{k}) \right]. \quad (\text{C.8})$$

We use Eq.(A.10) for the definition of the imaginary part of  $G^R$  and obtain

$$\frac{ne^2}{im\omega} = -\frac{2ie^2}{m^2\omega\pi dV} \int dE \delta(E - E_F) \sum_{\mathbf{k}} \mathbf{k}^2 \Im \bar{G}_E^R(\mathbf{k}). \quad (\text{C.9})$$

Now the pinning of the energy to  $E = E_F$  allows for the approximation  $\mathbf{k}^2 \approx k_F^2$ , and to this accuracy, we find

$$\frac{ne^2}{im\omega} = -\frac{2ie^2 k_F^2}{m^2\omega\pi dV} \sum_{\mathbf{k}} \Im \bar{G}_{E_F}^R(\mathbf{k}). \quad (\text{C.10})$$

We write this last expression in a slightly different form,

$$\frac{ne^2}{m\omega} = \frac{2e^2 k_F^2}{m^2\omega d} \left[ -\frac{1}{\pi V} \sum_{\mathbf{k}} \Im \bar{G}_{E_F}^R(\mathbf{k}) \right], \quad (\text{C.11})$$

and use Eq.(A.12) to identify

$$\frac{n(E_F)e^2}{m\omega} = \frac{2e^2 k_F^2}{m^2\omega d} \rho(E_F). \quad (\text{C.12})$$

Setting  $E_F = k_F^2/2m$ , we obtain

$$\frac{ne^2}{m\omega} = \frac{2e^2 \times 2mE_F n d}{4E_F m^2 \omega d} = \frac{ne^2}{m\omega}, \quad (\text{C.13})$$

which proves the claim. The diamagnetic term is absent in normal metals.



# Appendix D

## Electron energy averaging

In this section we perform the average defined in Eq.(4.20) over  $\tanh [(E + \omega - \bar{\omega}) / 2T]$  and  $\tanh [(E + \bar{\omega}) / 2T]$ . The calculation goes along the following lines. For arbitrary  $\Theta$ ,

$$\begin{aligned} & \left\langle \tanh \left( \frac{E - \Theta}{2T} \right) \right\rangle_E \\ &= - \int_{-\infty}^{+\infty} dE \frac{f(E + \omega) - f(E)}{\omega} \tanh \left( \frac{E - \Theta}{2T} \right) \\ &= \frac{1}{2\omega} \int_{-\infty}^{+\infty} dE \left[ \tanh \left( \frac{E + \omega}{2T} \right) - \tanh \left( \frac{E}{2T} \right) \right] \tanh \left( \frac{E - \Theta}{2T} \right), \end{aligned} \quad (\text{D.1})$$

where we used that  $f(E) = 1/2(\tanh(E/2T) + 1)$ . Substitution,  $E/2T = x$ ,  $dE = 2Tdx$  and  $\Theta/2T = y$ , as well as  $\omega/2T = \Omega$ , leads to the following expression:

$$\langle \tanh(x - y) \rangle_x = \frac{1}{2\Omega} \int_{-\infty}^{+\infty} dx [\tanh(x + \Omega) - \tanh x] \tanh(x - y). \quad (\text{D.2})$$

Consider the indefinite version of the integral of Eq.(D.2), let us call it  $I$ . This indefinite integral is given by the following expression

$$\begin{aligned} I &= - \coth(\Omega + y) [\ln \cosh(x + \Omega) - \ln \cosh(x - y)] \\ &\quad + \coth(y) [\ln \cosh(x) - \ln \cosh(x - y)]. \end{aligned} \quad (\text{D.3})$$

which is readily confirmed by explicit differentiation. We use the further identity

$$\left[ \lim_{x \rightarrow \infty} \ln \cosh(x \pm a) - \lim_{x \rightarrow -\infty} \ln \cosh(x \pm a) \right] = \pm 2a, \quad (\text{D.4})$$

to proceed from Eq.(D.2) via Eq.(D.3) to the result,

$$\langle \tanh(x - y) \rangle_x = \frac{y}{\Omega} \coth y - \frac{\Omega + y}{\Omega} \coth(\Omega + y). \quad (\text{D.5})$$

Finally, we obtain the desired results:

$$\begin{aligned} \left\langle \tanh \left( \frac{E + \omega - \bar{\omega}}{2T} \right) \right\rangle_E &= \frac{\bar{\omega} - \omega}{\omega} \coth \left( \frac{\bar{\omega} - \omega}{2T} \right) - \frac{\bar{\omega}}{\omega} \coth \left( \frac{\bar{\omega}}{2T} \right) \\ \left\langle \tanh \left( \frac{E + \bar{\omega}}{2T} \right) \right\rangle_E &= -\frac{\bar{\omega}}{\omega} \coth \left( \frac{-\bar{\omega}}{2T} \right) - \frac{-\bar{\omega} + \omega}{\omega} \coth \left( \frac{-\bar{\omega} + \omega}{2T} \right). \end{aligned} \quad (\text{D.6})$$

# Appendix E

## Useful integrals

$$\int \frac{\xi d\xi}{\sinh^2 \xi} = -\xi \coth \xi + \ln \sinh \xi. \quad (\text{E.1})$$

$$\int_0^{\infty} d\xi \xi (\coth \xi - 1) = \frac{\pi^2}{12}. \quad (\text{E.2})$$

$$\int_0^{\infty} d\xi \xi^2 (\coth \xi - 1) = \frac{\zeta(3)}{2}. \quad (\text{E.3})$$



# Appendix F

## Integration over internal momenta in infinite system size approximation

In the approximation of infinite system size, we replace the momentum sum in Eq.(4.27) of the main text with an integral,

$$\frac{1}{\tau_\phi}(\omega) = \frac{2}{\nu(2\pi)^{d+1}} \int_{\mathbb{R}^d} d^d \bar{\mathbf{q}} \int_{\Omega} \frac{d\bar{\omega}}{D^2 \bar{\mathbf{q}}^4 + \bar{\omega}^2} W(T, \omega, \bar{\omega}), \quad (\text{F.1})$$

where  $d$  is the spatial dimension of the system. We see that the problem reduces to finding the integral of  $1/(D^2 \bar{\mathbf{q}}^4 + \bar{\omega}^2)$ . We adopt spherical coordinates and with  $S_d$  denoting the surface of a  $d$ -dimensional unit sphere, we obtain

$$\int_{\mathbb{R}^d} \frac{d^d \bar{\mathbf{q}}}{D^2 \bar{\mathbf{q}}^4 + \bar{\omega}^2} = \frac{S_d}{\bar{\omega}^2} \int_0^\infty \frac{\bar{q}^{d-1} d\bar{q}}{(D^2/\bar{\omega}^2) \bar{q}^4 + 1}. \quad (\text{F.2})$$

Scaling,  $\xi = \bar{q} \sqrt{D/\bar{\omega}}$ , gives

$$\int_{\mathbb{R}^d} \frac{d^d \bar{\mathbf{q}}}{D^2 \bar{\mathbf{q}}^4 + \bar{\omega}^2} = \frac{S_d}{D^{d/2} \bar{\omega}^{2-d/2}} \int_0^\infty \frac{\xi^{d-1} d\xi}{\xi^4 + 1}, \quad (\text{F.3})$$

and therefore we find

$$\frac{1}{\tau_\phi}(\omega) = C_d \int_{\Omega} \frac{d\bar{\omega}}{\bar{\omega}^{2-d/2}} W(T, \omega, \bar{\omega}), \quad (\text{F.4})$$

where we have defined the parameter  $C_d$  as follows:

$$C_d = \frac{2S_d \xi_d}{(2\pi)^{d+1} \nu D^{d/2}}, \quad (\text{F.5})$$

## 84 F. Integration over internal momenta in infinite system size approximation

where  $\xi_d$  is given by the following integral

$$\xi_d = \int_0^\infty \frac{\xi^{d-1} d\xi}{\xi^4 + 1}, \quad (\text{F.6})$$

with the results  $\xi_1 = \xi_3 = \pi/(2\sqrt{2})$  and  $\xi_2 = \pi/4$ . We will give the expressions for  $C_d$  for  $d = 1, 2, 3$  in terms of the dimensionless conductance in  $d$  space dimensions,  $g_d$ , and the Thouless energy,  $E_{\text{th}} \equiv D/L^2$ . From the Einstein relation  $\sigma = e^2\nu D$  and from Ohm's law for the conductance,  $G_d = \sigma L^{d-2}$ , we have the following relation [5]:

$$g_d = 2\pi\nu DL^{d-2}. \quad (\text{F.7})$$

By use of Eq.(F.7), we obtain from Eq.(F.5):

$$C_d = \left\{ \begin{array}{l} \frac{c_1\sqrt{E_{\text{th}}}}{g_1}, \quad d = 1 \\ \frac{c_2}{g_2}, \quad d = 2 \\ \frac{c_3}{g_3\sqrt{E_{\text{th}}}}, \quad d = 3 \end{array} \right\}, \quad (\text{F.8})$$

where  $c_1 = 1/(2\sqrt{2}\pi)$ ,  $c_2 = 1/(8\pi^2)$  and  $c_3 = 1/(8\sqrt{2}\pi^3)$ . This finally yields from Eq.(F.4):

$$\frac{1}{\tau_\phi}(\omega) = \frac{c_d(E_{\text{th}})^{1-d/2}}{g_d} \int_\Omega^\infty \frac{d\bar{\omega}}{\bar{\omega}^{2-d/2}} W(T, \omega, \bar{\omega}). \quad (\text{F.9})$$

# Appendix G

## Asymptotic analysis in the high-temperature regime

We derive Eq.(5.5) of the main text from Eq.(5.4). The latter equation reads:

$$\frac{1}{\tau_\phi}(\theta) = \frac{c_d E_{\text{th}}}{2g_d} \left( \frac{2T}{E_{\text{th}}} \right)^{d/2} \left[ \left( 1 + \frac{\theta^2}{3} \right) \int_{\Delta}^{\infty} \frac{\xi^{d/2} d\xi}{\sinh^2 \xi} + \theta^2 \int_{\Delta}^{\infty} \frac{\xi^{d/2} d\xi}{\sinh^2 \xi} \left( \coth^2 \xi - \frac{1}{\xi^2} - \frac{2}{3} \right) \right]. \quad (\text{G.1})$$

Consider the first integral in Eq.(G.1). In the one-dimensional case, we rewrite the integral by adding and subtracting  $1/\xi^2$  in the integrand, to find

$$\int_{\Delta}^{\infty} \frac{\xi^{1/2} d\xi}{\sinh^2 \xi} = \int_{\Delta}^{\infty} \frac{d\xi}{\xi^{3/2}} + \int_0^{\infty} d\xi \xi^{1/2} \left[ \frac{1}{\sinh^2 \xi} - \frac{1}{\xi^2} \right] - \int_0^{\Delta} d\xi \xi^{1/2} \left[ \frac{1}{\sinh^2 \xi} - \frac{1}{\xi^2} \right], \quad (\text{G.2})$$

The second integral on the r.h.s. of Eq.(G.2) is evaluated numerically,

$$\int_0^{\infty} d\xi \xi^{1/2} \left[ \frac{1}{\sinh^2 \xi} - \frac{1}{\xi^2} \right] = -1.830, \quad (\text{G.3})$$

and from the first and third integral we obtain the following leading and subleading contributions in  $\Delta$ :

$$\int_{\Delta}^{\infty} \frac{d\xi}{\xi^{3/2}} - \int_0^{\Delta} d\xi \xi^{1/2} \left[ \frac{1}{\sinh^2 \xi} - \frac{1}{\xi^2} \right] = \frac{2}{\sqrt{\Delta}} + \frac{2}{9} \Delta^{3/2} + \mathcal{O}(\Delta^{7/2}). \quad (\text{G.4})$$

For  $d = 2$ , the integral can be done analytically,

$$\int_{\Delta}^{\infty} \frac{\xi d\xi}{\sinh^2 \xi} = \Delta \coth \Delta + \ln \sinh \Delta = \ln \frac{1}{\Delta} + 1 - \ln 2 + \frac{\Delta^2}{6} + \mathcal{O}(\Delta^4). \quad (\text{G.5})$$

For  $d = 3$ , the integral is convergent in the limit  $\Delta \rightarrow 0$ . We write

$$\int_{\Delta}^{\infty} \frac{\xi^{3/2} d\xi}{\sinh^2 \xi} = \int_0^{\infty} \frac{\xi^{3/2} d\xi}{\sinh^2 \xi} - \int_0^{\Delta} \frac{\xi^{3/2} d\xi}{\sinh^2 \xi}, \quad (\text{G.6})$$

where the first integral is done numerically and the integrand of the second integral can be expanded in powers of  $\Delta$ . We find

$$\int_0^{\infty} \frac{\xi^{3/2} d\xi}{\sinh^2 \xi} = 2.456, \quad (\text{G.7})$$

and

$$\int_0^{\Delta} \frac{\xi^{3/2} d\xi}{\sinh^2 \xi} = 2\Delta^{1/2} + \mathcal{O}(\Delta^{5/2}). \quad (\text{G.8})$$

Now we turn to the second integral in Eq.(G.1) and write this integral as

$$\int_{\Delta}^{\infty} \frac{\xi^{d/2} d\xi}{\sinh^2 \xi} \left( \coth^2 \xi - \frac{1}{\xi^2} - \frac{2}{3} \right) = \Gamma_d - \int_0^{\Delta} \frac{\xi^{d/2} d\xi}{\sinh^2 \xi} \left( \coth^2 \xi - \frac{1}{\xi^2} - \frac{2}{3} \right) \quad (\text{G.9})$$

where  $\Gamma_d$  is calculated numerically

$$\Gamma_d \equiv \int_0^{\infty} \frac{\xi^{d/2} d\xi}{\sinh^2 \xi} \left( \coth^2 \xi - \frac{1}{\xi^2} - \frac{2}{3} \right) = \begin{cases} 0.078 & , d = 1 \\ 0.080 & , d = 2 \\ 0.093 & , d = 3 \end{cases}, \quad (\text{G.10})$$

For the remaining integral in Eq.(G.9), we find to leading order in  $\Delta \ll 1$ :

$$\int_0^{\Delta} \frac{\xi^{d/2} d\xi}{\sinh^2 \xi} \left( \coth^2 \xi - \frac{1}{\xi^2} - \frac{2}{3} \right) = \begin{cases} \frac{2}{45} \Delta^{3/2} + \mathcal{O}(\Delta^{7/2}) & , d = 1 \\ \frac{1}{30} \Delta^2 + \mathcal{O}(\Delta^4) & , d = 2 \\ \frac{2}{75} \Delta^{5/2} + \mathcal{O}(\Delta^{9/2}) & , d = 3 \end{cases}. \quad (\text{G.11})$$

Putting all pieces together in Eq.(G.1), and keeping only leading terms in  $\Delta$  and  $\theta$ , we finally find

$$\frac{1}{\tau_{\phi}}(\theta) = \begin{cases} \frac{c_1}{g_1} \sqrt{\frac{2TE_{\text{th}}}{\Delta}} \left( 1 - 0.915\sqrt{\Delta} + \frac{\theta^2}{3} \right) & , d = 1 \\ \frac{c_2 T}{g_2} \left[ \ln \frac{1}{\Delta} \left( 1 + \frac{\theta^2}{3} \right) + 1 - \ln 2 + \frac{\Delta^2}{6} \right] & , d = 2 \\ \frac{2.456c_3 T}{g_3} \sqrt{\frac{2T}{E_{\text{th}}}} [1 - 0.814\Delta^{1/2} + 0.174\theta^2] & , d = 3 \end{cases}, \quad (\text{G.12})$$

which is Eq.(5.5) of the main text.

# Appendix H

## Hikami calculus

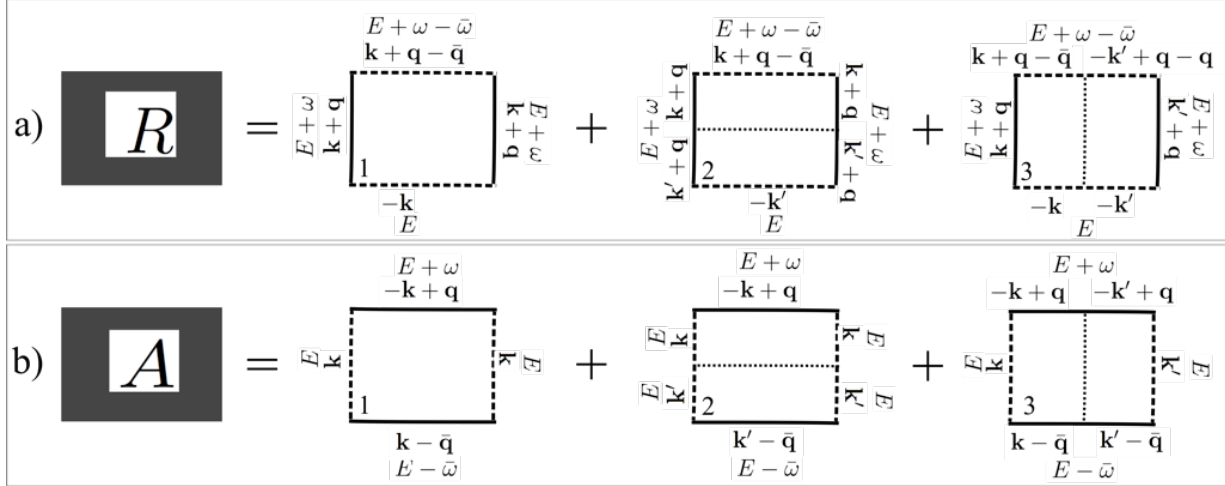


Figure H.1: Definition of the Hikami box.

In this appendix, we calculate the Hikami boxes which appear in the self-energy diagrams for the Cooperon. The impurity-dressed Hikami box corresponds to the diagrams in Fig.H.1. We consider first the  $R$ -Hikami box in Fig.H.1a), which translates into the

following expression:

$$\begin{aligned}
H^R &= H_1^R + H_2^R + H_3^R, \\
H_1^R &= \frac{1}{V} \sum_{\mathbf{k}} [\bar{G}_{E+\omega}^R(\mathbf{k} + \mathbf{q})]^2 \bar{G}_{E+\omega-\bar{\omega}}^A(\mathbf{k} + \mathbf{q} - \bar{\mathbf{q}}) \bar{G}_E^A(-\mathbf{k}) \\
H_2^R &= \frac{\gamma}{V^2} \left[ \sum_{\mathbf{k}} [\bar{G}_{E+\omega}^R(\mathbf{k} + \mathbf{q})]^2 \bar{G}_{E+\omega-\bar{\omega}}^A(\mathbf{k} + \mathbf{q} - \bar{\mathbf{q}}) \right] \times \left[ \sum_{\mathbf{k}'} [\bar{G}_{E+\omega}^R(\mathbf{k}' + \mathbf{q})]^2 \bar{G}_E^A(-\mathbf{k}') \right] \\
H_3^R &= \frac{\gamma}{V^2} \left[ \sum_{\mathbf{k}} \bar{G}_{E+\omega}^R(\mathbf{k} + \mathbf{q}) \bar{G}_{E+\omega-\bar{\omega}}^A(\mathbf{k} + \mathbf{q} - \bar{\mathbf{q}}) \bar{G}_E^A(-\mathbf{k}) \right]^2.
\end{aligned} \tag{H.1}$$

In the diffusive limit, we expand the Green's functions in Eq.(H.1):

$$\bar{G}_{E+\omega}^{R/A}(\mathbf{k} + \mathbf{q}) \approx \bar{G}_E^{R/A}(\mathbf{k}) - (\omega - \mathbf{v} \cdot \mathbf{q}) \left[ \bar{G}_E^{R/A}(\mathbf{k}) \right]^2 + q^2 v^2 \left[ \bar{G}_E^{R/A}(\mathbf{k}) \right]^3, \tag{H.2}$$

where  $\mathbf{v} = \nabla_{\mathbf{k}} \epsilon(\mathbf{k})$ . We substitute the expansion Eq.(H.2) for the Green's functions in Eq.(H.1). To evaluate sums of the type

$$f^{m,n} \equiv \frac{\gamma}{V} \sum_{\mathbf{k}} \left[ \bar{G}_E^R(\mathbf{k}) \right]^m \left[ \bar{G}_E^A(\mathbf{k}) \right]^n, \tag{H.3}$$

we use [5, Table 3.2] and note that the calculation is straightforward using the residual calculus. Using the angular average  $\langle \mathbf{v} \cdot \mathbf{q} (\mathbf{v} \cdot \bar{\mathbf{q}}) \rangle = v^2 q \bar{q} = Dq\bar{q}/\tau d$  [5] and thus arrive at the following result, to leading order in  $\omega\tau, \mathbf{q}l_e$ :

$$H_{\mathbf{q},\bar{\mathbf{q}}}^R(\omega, \bar{\omega}) = (2\pi\rho\tau^4) \left[ D(\mathbf{q} - \bar{\mathbf{q}})^2 - i(\omega + \bar{\omega}) \right]. \tag{H.4}$$

We repeat similar steps for the  $A$ -Hikami box in Fig.H.1a). The expression

$$\begin{aligned}
H^A &= H_1^A + H_2^A + H_3^A, \\
H_1^A &= \frac{1}{V} \sum_{\mathbf{k}} [\bar{G}_E^A(\mathbf{k})]^2 \bar{G}_{E+\omega}^R(-\mathbf{k} + \mathbf{q}) \bar{G}_{E-\bar{\omega}}^R(\mathbf{k} - \bar{\mathbf{q}}) \\
H_2^A &= \frac{\gamma}{V^2} \left[ \sum_{\mathbf{k}} [\bar{G}_E^A(\mathbf{k})]^2 \bar{G}_{E+\omega}^R(-\mathbf{k} + \mathbf{q}) \right] \times \left[ \sum_{\mathbf{k}'} [\bar{G}_E^A(\mathbf{k}')]^2 \bar{G}_{E-\bar{\omega}}^R(\mathbf{k}' - \bar{\mathbf{q}}) \right] \\
H_3^A &= \frac{\gamma}{V^2} \left[ \sum_{\mathbf{k}} \bar{G}_E^A(\mathbf{k}) \bar{G}_{E+\omega}^R(-\mathbf{k} + \mathbf{q}) \bar{G}_{E-\bar{\omega}}^R(\mathbf{k} - \bar{\mathbf{q}}) \right]^2.
\end{aligned} \tag{H.5}$$

leads to the result:

$$H_{\mathbf{q},\bar{\mathbf{q}}}^A(\omega, \bar{\omega}) = (2\pi\rho\tau^4) \left[ D(\mathbf{q} - \bar{\mathbf{q}})^2 - i(\omega - \bar{\omega}) \right]. \tag{H.6}$$

# Bibliography

- [1] A. Zagoskin : *Quantum Theory of Many-Body Systems*. Springer, New York, 1998.
- [2] A.A. Abrikosov, L.P. Gorkov, I.E. Dzyaloshinski: *Quantum Field Theoretical Methods in Statistical Physics, 2nd ed.* Pergamon, New York, 1965.
- [3] B.L.Altshuler, A.G. Aronov, D.E. Khmel'nitskii, *J. Phys. C* **15** (1982), 7367.
- [4] E. Abrahams, P. W. Anderson, D. C. Licciardello, T. V. Ramakrishnan, *Phys. Rev. Lett.* **42** (1979), 673.
- [5] E. Akkermans, G. Montambaux: *Mesoscopic Physics of Electrons and Photons*. Princeton University Press, Princeton, 1974.
- [6] G. Bergmann , *Phys. Rep.* **107** (1984), 1.
- [7] H. Bruus, K. Flensberg : *Many-body Quantum Theory In Condensed Matter Physics*. Oxford University Press, Oxford, 2004.
- [8] I.L. Aleiner, B.L. Altshuler, M.E. Gershenson, *Waves Random Media* **9** (1999), 201.
- [9] J. Rammer, H. Smith, *Reviews of Modern Physics* **58** (1986), 323.
- [10] J. von Delft, F. Marquardt, R.A. Smith, V. Ambegaokar , *Physical Review B* **76** (2007), 195331.
- [11] J. von Delft, F.Marquardt, R.Smith, V. Ambegaokar, *Phys. Rev. B* **76** (2007), 195332.
- [12] J.S. Langer, T.Neal, *Phys. Rev. Lett.* **16** (1966), 984.
- [13] L.P. Gorkov, A. I. Larkin, D. E. Khmel'nitskii, *JETP Letters* **30** (1979), 228.
- [14] M. Treiber, C.Textier, O. M.Yevtushenko, J. von Delft, I.V. Lerner, *Phys. Rev. B* **84** (2011), 054204.
- [15] M. Treiber, O.M. Yevtushenko, F. Marquardt, J. von Delft, I.V. Lerner, *World Scientific, Singapore* **Ch.20** (2010).
- [16] M.E. Peskin, D.V. Schroeder: *An Introduction to Quantum Field Theory*. Westview, Boulder, 1967.

- [17] S. Chakravarty, A. Schmid, *Phys. Rep.* **140** (1986), 193.
- [18] S. Doniach, E. Sondheimer : *Green's Functions for Solid State Physicists*. Frontiers in Physics, New York, 1974.

# Acknowledgements

Foremost, I want to express my special gratitude to my supervisor Jan von Delft for the great opportunity to work in his group. I owe earnest thankfulness to my close advisor Oleg Yevtushenko, who supported me with numerous patient and very instructive discussions. Many thanks go to Maximilian Treiber, who supported me with neat explanations and worthy daily advice. I would like to thank all members of von Delft group for creating an excellent working atmosphere. Last but not least I would like to thank my beloved family for their love and patience, especially in the final period of this work.



# Statutory declaration

I herewith declare that I have completed the present thesis independently making use only of the specified literature and aids. Sentences or parts of sentences quoted literally are marked as quotations; identification of other references with regard to the statement and scope of the work is quoted. The thesis in this form or in any other form has not been submitted to an examination body and has not been published.